Vítor Hugo Pessoa Oliveira

Modelação Acoplada dos Estuários do Minho e do Lima: Resposta Bioquímica a Eventos Extremos e Interação de Plumas Estuarinas

Coupled Modelling of the Minho and Lima Estuaries: Biochemical Response to Extreme Events and Interaction of Plumes Estuarine

Universidade de Aveiro Departamento de Física
2018

Vítor Hugo Pessoa Oliveira

Modelação Acoplada dos Estuários do Minho e do Lima: Resposta Bioquímica a Eventos Extremos e Interação de Plumas Estuarinas

Coupled Modelling of the Minho and Lima Estuaries: Biochemical Response to Extreme Events and Interaction of Plumes Estuarine

Dissertação apresentada à Universidade de Aveiro para cumprimento dos requisitos necessários à obtenção do grau de Mestre em Ciências do Mar e da Atmosfera, realizada sob a orientação científica do Doutor João Miguel Sequeira Silva Dias, Professor Associado com Agregação do Departamento de Física da Universidade de Aveiro, e co-orientação do Doutor Fernando Manuel Raposo Morgado, Professor Associado com Agregação do Departamento de Biologia da Universidade de Aveiro.

O júri

Presidente	Prof. Doutor José Manuel Henriques Castanheira Professor Auxiliar do Departamento de Física da Universidade de Aveiro
Arguente	Doutor Luís Miguel dos Santos Russo Vieira Investigador Auxiliar do Centro Interdisciplinar de Investigação Marinha e Ambiental
Orientadores	Prof. Doutor João Miguel Sequeira Silva Dias Professor Associado com Agregação do Departamento de Física da Universidade de Aveiro

agradecimentos /
acknowledgements

Este espaço é dedicado àqueles que deram a sua contribuição para que esta tese fosse realizada. Peço desde já desculpa àqueles que tenha omitido. A todos eles deixo aqui o meu agradecimento sincero.

Em primeiro lugar, um especial e sentido obrigado à minha família e em especial aos meus pais, Victor Pessoa e Cristina Oliveira, por, ao longo deste período, me terem apoiado nos momentos mais difíceis e me darem esta oportunidade de alcançar o grau de Mestre, pois sem a ajuda deles o caminho seria muito mais difícil.

De seguida, agradeço ao Prof. Dr. João Miguel Dias, pela forma como orientou o meu trabalho, dando sempre o seu apoio, conselhos valiosos e disponibilidade inquestionável.

Agradeço também ao Prof. Dr. Fernando Morgado por todas as sugestões e ajudas dadas durante este processo.

Fica também aqui uma nota de apreço a todos os colegas da NMEC (Núcleo de Modelação Estuarina e Costeira) por compartilharem os seus conhecimentos comigo. Particularmente à Dra. Magda Sousa, quero agradecer por toda a paciência, ajuda e apoio que me deu no desenvolvimento do modelo numérico e no esclarecimento de dúvidas.

Por fim, quero também agradecer a todos os meus amigos e colegas, destacando o André Silva, a Beatriz Gomes, o João Oliveira, o Rui Alpuim e o Válter Cró, por todo o apoio fundamental, ajuda, companhia, camaradagem e por todos os momentos que me proporcionaram durante todo o meu trajeto académico.

Mais uma vez agradeço a todos.

Palavras Chave

Delft3D, Dinâmica Estuarina, Minho, Lima, Pluma Estuarina, Traçador, Nutrientes, Cenários

Resumo

Nos últimos anos, devido à atividade do Homem, à litoralização e às alterações climáticas, os estuários passaram por grandes transformações, tanto na dinâmica estuarina como na qualidade da água. Os estuários do Minho e do Lima estão separados apenas 20 km, possuem grande valor ecológico e estão sob a dependência de barragens que controlam o aporte de água doce. Neste contexto, emerge a necessidade e interesse em estudar a dinâmica e interação entre as plumas estuarinas do Minho e do Lima, bem como o impacto de eventos extremos de descargas fluviais na dinâmica de nutrientes de ambos os estuários, assim como o tempo de resposta do estuário do Minho a uma descarga pontual de poluentes através do tributário rio Coura. Para efetuar estes estudos foi desenvolvida uma aplicação numérica incluindo simultaneamente os dois estuários referidos. Esta engloba o módulo hidrodinâmico e de qualidade de água do modelo numérico Delft3D, que foram calibrados através da realização de um conjunto alargado de simulações e do recurso a um vasto conjunto de dados monitorizados *in situ*. Posteriormente foram definidos e simulados vários cenários tendo em vista a concretização dos objetivos deste trabalho, e analisados os respetivos resultados de forma comparativa. Para o estudo da dinâmica e interação entre as plumas estuarinas simularam-se as trajetórias de traçadores passivos emitidos em cada estuário. Para estudar o impacto de eventos extremos de descargas fluviais na dinâmica dos nutrientes efetuaram-se 3 simulações numéricas, caraterizadas pela variação dos caudais fluviais afluentes aos estuários (1ª simulação: *baseline*; 2ª simulação: cenário de cheias, com descargas fluviais duplas relativamente ao *baseline*; 3ª simulação: descarga de caudais ecológicos (período de seca)). Para estudar o tempo de resposta do estuário do Minho a uma descarga pontual de poluentes efetuaram-se duas simulações adicionais, considerando uma descarga de poluentes em maré morta (10/08/2012) e em maré viva (19/08/2012). Da análise dos resultados verificou-se: 1) existe interação entre os estuários em estudo, tanto durante o verão como durante o inverno; 2) o movimento das plumas estuarinas depende da direção e intensidade do vento e da intensidade das descargas fluviais (na estação de verão ambas as plumas tendem a deslocar-se para sul sob a ação de vento predominante de norte e no inverno observa-se o padrão oposto); 3) em períodos de grande descarga fluvial não existirá um grande impacto para a biota estuarina, tanto no verão como no inverno, dado que existirão maiores concentrações de nutrientes e não existirá grandes variações nas concentrações de oxigénio dissolvido; 4) a descarga de caudais ecológicos por parte de barragens causará grande impacto na biota estuarina, principalmente no estuário do Lima, uma vez que se verifica uma diminuição média de 2 mg O_2/L (estuário mais anóxico, podendo resultar na morte ou migração de espécies biológicas); e 5) em maré morta o estuário tem um tempo de resposta mais longo do que em maré viva. Em síntese, neste trabalho foi desenvolvido com sucesso um modelo conjunto para os estuários do Minho e do Lima, que contribuiu para: 1) aumentar o conhecimento da interação e dinâmica das plumas estuarinas; 2) compreender o impacto direto que as barragens poderão ter nos estuários em estudo (dado que as descargas fluviais são controladas por elas); e 3) determinar o tempo que estuário do Minho demora o a reagir a uma descarga pontual.

Keywords Delft3D, Estuarine Dynamics, Minho, Lima, Estuarine Plume, Tracer, Nutrients, Scenarios

Abstract In the last years, due to human activity, increase in the number of inhabitants in the coastal areas and climate change, estuaries have undergone major changes, both in dynamics and in water quality. The Minho and Lima estuaries are separated only by 20 km, have great ecological value and are under the dependence of dams that control the freshwater input. In this context, arises the need and interest to study the dynamics and interaction between the Minho and Lima estuarine plumes, as well as the impact of extreme river discharges events on the nutrient dynamics in both estuaries, as well as the response time of the Minho estuary to a point discharge of pollutants by a tributary (river Coura). To carry out these studies, a numerical application including simultaneously the two estuaries mentioned was developed. This includes the hydrodynamic and water quality module of the Delft3D numerical model, which were calibrated through a large set of simulations and using a vast set of data monitored in situ. Subsequently, several scenarios were defined and simulated in order to achieve the objectives of this work, and the respective results were analysed in a comparative way. To study the intrusion and dynamics of the estuarine plumes, the trajectories of passive tracers emitted in each estuary were simulated. In order to study the impact of extreme river discharge events on nutrient dynamics, three numerical simulations were carried out, characterized by the variation of the river flows to the estuaries (1st simulation: baseline; 2nd simulation: flood scenario, with double fluvial discharges comparing to the baseline; 3rd simulation: discharge of ecological flows (dry season). To study the response time of the Minho estuary to a punctual discharge of pollutants, two additional simulations were carried out, considering a discharge in neap tide (10/08/2012) and in spring tide (19/08/2012). From the analysis of the results it was verified: 1) there is interaction between estuaries under study, both during the summer and the winter seasons; 2) the movement of estuarine plumes depends on the direction and intensity of the wind and the intensity of the river discharge (in the summer season both plumes tend to move southward in response to the predominant north wind, while in winter the opposite is observed); 3) during periods of higher river discharge there will be no major impact on estuarine biota, both in summer and winter, because there will be higher concentrations of nutrients and the variation in the concentrations of dissolved oxygen is insignificant; 4) the discharge of ecological flows by dams will have a major impact on the estuarine biota, mainly in the Lima estuary, since the estuary suffers an average decrease of 2 mg O_2/ L (more anoxic estuary, which may result in the death or migration of biological species); and (5) in neap tide, the estuary has a longer response time than in a spring tide. In summary, the model developed in this work contributed to: 1) increase the knowledge about the interaction and dynamics of the plumes; 2) perceive the direct impact that dams may have on estuaries under study (since river discharges are controlled by them); and 3) understand the response time it takes for the Minho estuary to react to a point discharge.

Contents

List of Figures

List of Tables

1 Introduction

An estuary is a body of semi-enclosed water with connection to the sea, extending to the limit of the tide propagation or salt intrusion, and where may or may not occur permanent fluvial discharges [Wolanski, 2007].

These systems are highly dynamic since they are constantly changing their physical form (processes of erosion and sedimentation) and their physicochemical properties. These physicochemical changes are strongly influenced by atmospheric conditions, wind, river discharges and tidal wave, making the estuaries very productive systems, as they are places where there are large concentrations of nutrients, leading to the development and growth of all the organisms that inhabit these coastal systems [Miranda et al., 2002]. For this reason, there is a particular interest in these ecosystems, both ecologically and economically (e.g. aquaculture).

Since these systems are very important, there is a need for their preservation, however, currently, the world population is growing and is concentrated predominantly in coastal areas and near estuaries. According to the Instituto Nacional de Estatisticas (INE), in the last edition of the Retrato Territorial de Portugal [RTP, 2017], it has been verified that over the years there has been a trend to increase the number of inhabitants in the coastal zone in Portugal, since coastal areas have favourable characteristics for human beings to have a better quality of life, both economically and socially.

The increase in population density on the coastal zone substantially rises the concern for the conservation, preservation and sustainability of estuarine and oceanic ecosystems, as these become the final receptors of most of the pollutants released by humans. Pollutants that reach these ecosystems can come from point sources [e.g.: domestic effluents (cooking oils, cleaning products, domestic sewage) and industrial effluents (detergents, chemicals with heavy metals, paints, petroleum)] or from non-point sources (action of rainfall, freshwater inflow, infiltration, winds and atmospheric movements). Generally, point sources introduce potentially toxic elements (mercury, cadmium, lead, arsenic, etc.) in riverbeds or in the ocean, since they don't have any previous treatment. However non-point sources also introduce toxic waste from fertilizers used in agriculture, combustion of raw materials, dredging, mining, among others. These discharges can harm human health and totally destroy existing ecosystems.

In Portuguese estuaries (e.g.: Minho and Lima estuaries) it is possible to observe these effluent discharges exporadically [Santos et al., 2013].

The idea of preserving these areas naturally arises, and currently, there are two issues of great concern. One of the issues of high importance are climate changes and in turn the occurrence of extreme events. According to Doney et al. [2002], it is expected that there will be an increase in water temperature of 1.8 °C - 4 °C by the end of the 21st century and this increase brings with it some problems, one of them being the decrease of dissolved oxygen inside the estuaries, which can cause serious problems for the existing biota. The second issue is mainly to understand what impact humans have on these systems, as well as to see if these impacts can spread to other estuaries by analysing the interaction between different estuaries.

1.1 Motivation

In the last 50 years, due to the human activity, the planet has undergone great transformations, some of which have already been documented. However, this century has witnessed major changes in marine systems, green cover of the planet and air quality.

As mentioned previously, there is currently a desertification of many areas in the interior of the country, as there is a great mobility of people to the coast, with the corresponding population growth, providing greater social needs (e.g. agricultural products and mining production). The fact that these needs exist leads to high industrial development. In most

cases, these industries use old-fashioned technologies, which can lead to serious problems in the estuaries, as much of their waste is excreted into these systems without any treatments, which may create unfavourable conditions for the existing biota.

Given that in the last decade there has been a rapid expansion of aquaculture, and events occurred in the past had caused serious problems to the biota, leading to the appearance of serious diseases, as happened in Japan in 1956 in the city of Minamata (neurological syndrome caused by mercury poisoning), there is a need to conduct hydrodynamic and biogeochemical studies in estuaries to preserve and protect estuarine ecosystems and human health.

In estuaries, hydrodynamic processes (waves, tides, wind stress, freshwater discharges by rivers and exchanges with the atmosphere) play a very important role in the biogeochemical cycles, as these will influence the sedimentation rate, zonation and species productivity, water temperature and salinity of each zone. These very complex features of the estuaries make them very valuable, since they serve as a shelter for fish and have a high primary production, due to nutrients availability coming from the rivers and coastal upwelling.

In this way, it is easily understood that there are a large number of scientific and practical reasons (e.g.: aquaculture production, in order to reduce human demand for fish), which justify the interest in protecting and understanding the dynamics of these ecosystems to different forces.

To explain the existing biogeochemical processes in estuaries over the years and throughout the world, numerical models are being currently widely used [Mateus et al. [2012]; Pan et al. [2017]; Mattern et al. [2017]], considering their capacity of approximately reproducing one or several real phenomena.

The numerical models are used nowadays with this purpose, since they show many important advantages. The first consists in the possibility of generating data with high spatial and temporal coverage with a very low economic cost, complementary to *in situ* monitoring, which presents high costs and limited spatial coverage, thus reducing costs in equipment and laboratory tests and increasing the data availability. Their second advantage is the capacity to make predictions and in addition to isolate processes (e.g.: wind, tide, erosion and sediment accretion), generating conditions to study and assess their importance in the system. Another advantage is the possibility of performing sensitivity studies (e.g.: how the study area reacts to increased river discharge, dredging, construction of coastal defence works and port construction) and hypothetical scenarios [Sousa, 2013]. The final advantage is that the model results can serve as a predictive or decision support tool [Neves, 2007].

Therefore, the present work intends to use the numerical model Delft3D to research the impact of extreme events (flood periods and periods of drought) on the physical-chemical variables of the Minho and Lima estuaries and to verify if there are interaction and exchanges of properties between them (since they are separated by only 20 km and it is probable that there may be a connection between the water masses coming from the two estuaries) and finally study the response time that the Minho estuary has to a point discharge of pollutants.

1.2 Aims

As the biochemical processes in the Minho and Lima estuaries have not been studied in detail, also the lack of numerical models designed for this purpose, the main objective of this study is to couple hydrodynamic and biochemical models to study the intrusion and dynamics of estuarine plumes in the two estuaries (using a single numerical application), the impact of extreme river discharge events on the nutrient dynamics and the response time of the Minho estuary to a discharge point of pollutants (nitrates and orthophosphates) by a tributary (Coura river).

To achieve this goal, some specific objectives have been established:

- Characterize the Minho and Lima estuaries;
- To develop 2D hydrodynamic and biochemical models in which the two estuaries were included in a single numerical application to reproduce the main biochemical processes in estuaries under study and their interaction. To achieve this objective, model predictions will be compared with observed data;
- Define two passive conservative tracers (one for the Minho estuary and another for the Lima estuary) to study the intrusion and dynamics of estuarine plumes;
- Define two distinct river discharge scenarios with the purpose of verifying nutrient dynamics and then analyse model predictions to verify the time/space patterns of nutrients (ammonium, nitrate, orthophosphate) and dissolved oxygen during the winter and summer seasons;
- Define a possible contaminant discharge (period of occurrence, concentration) to analyse the response time of the Minho estuary to a point discharge of pollutants (nitrates and orthophosphates).

1.3 Literature review

1.3.1 Hydrodynamic and biochemical studies in estuarine systems

An estuarine system is an area where freshwater coming from the rivers meets the ocean, resulting in brackish water. These coastal zones of interaction between salt water and freshwater can be defined in various ways (lagoons, estuaries, barrier islands).

For most scientists, these areas are considered as zones of interaction between freshwater and salt water, however, over the years several definitions have occurred. Since the 60s there have been numerous definitions of estuaries [Cameron and Pritchard [1963]; Pritchard [1967]; Fairbridge [1980]; Day et al. [1989]], until the most recent definition of Wolanski [2007]: semi-enclosed body of water connected to the sea as far as the tidal limit or the salt intrusion limit and receiving freshwater runoff; however the freshwater inflow may not be perennial, the connection to the sea may be closed for part of the year and tidal influence may be negligible.

Through this diversity of definitions referred previously, it is easy to understand that coastal systems are very dynamic and complex, since they have many oceanographic processes to operate simultaneously. Because these systems are complex, they make them interesting systems to study, since the estuaries serve as shelter to a large biological community and are also of great economic and social importance, considering the cultivation of fish and marine algae, the use for recreation and tourism activities and finally the protected conditions to harbor maritime ports.

When studying the hydrodynamics of an estuary or even studying some biogeochemical processes, it is important to know which are the determining oceanic processes in each estuary. In general, the main determinant processes that influence the estuarine circulation and all the biogeochemical processes that occur there are:

- River discharges, as they transport fine sediments, nutrients and organic matter from the earth to the ocean [Sousa, 2013], changing the rates of the biogeochemical processes and the coastal sediment budget [Garvine [1984]; Kourafalou [1999]], depending on the concentrations and intensity of these variables;
- Tide, because through its cycles can cause the water column to mix (making the estuary with a completely homogeneous water column), transports sediments and changes the

topography of the bottom, providing the generation of sandbanks between the flood and ebb channels, leading to changes in the hydrodynamics and in addition to the aforementioned, this process is important because it exposes beaches and muddy flats and can alter the properties of water (e.g. water temperature and salinity), due to the existing exchanges between the ocean and the estuary and between adjacent estuaries;

- Wind stress, since this during short periods can force local circulations and contribute to a greater vertical mixture and can also contribute to the emergence of Coastal Upwelling, the latter being a very important process, since there is the resuspension of nutrients for the surface layers, which may cause the existing biota to increase and grow;

- Waves, providing the sedimentary transport and mixing by the surface waves;

- Sea level variation induced by meteorological forcing and in the long-term its rise way migrate the estuary to another location.

Briefly, all the processes referred to above will influence the estuarine circulation patterns and morphology [Hayes [1975]; Fairbridge [1980]; Walker and James [1992]] as well as estuarine plumes generation [Garvine [1974]; Fong and Geyer [2002]; Berdeal et al. [2002]].

Given that in recent years there has been a huge technological evolution and an increase in scientific knowledge in the oceanic area, the scientific community has shown an increasing interest in studying the estuaries, in order to understand the importance of the processes mentioned above, as well as the impact of these processes on the economic level, given that currently these systems harbor a large set of economic and tourist activities.

During the last century, many hydrodynamic studies were carried out in several estuaries, many of them studies based on observations, however, due to the technological evolution, numerical and laboratory studies were started, in order to answer real problems. Some examples of such hydrodynamic studies are:

- Alvarez-Salgado et al. [1993] studied the hydrographic variability of the Rias Baixas (ESP) during the upwelling period (1989), concluding that the thermohaline properties of the upwelling waters tend to increase with time;

- Ashizawa and Cole [1994] studied different long-term datasets in the Hudson river region (USA) and analysed possible temperature trends, concluding that the long-term heating rate is in line with global trends;

- Dias et al. [1999] studied the properties of tides and currents, as well as characterizing the horizontal and vertical variations of salinity and water temperature in the Ria de Aveiro (POR) during an early summer period and concluded that the hydrology of the Ria de Aveiro is essentially dominated by tidal forcing, causing a strong mixture between water masses;

- DeCastro et al. [2000] performed hydrodynamic and thermohaline measurements in the Ria de Pontevedra (1998) (ESP), these measurements being used to describe current patterns;

- Ruiz-Villarreal et al. [2002] used a numerical model to study the influence of the hydrodynamic characteristics of the Ria de Pontevedra on the nutrient cycle and consequently on the Ria productivity and concluded that hydrodynamic characteristics are important in nutrient cycles and productivity;

- Preston [2004] carried out a study in the Chesapeake Bay estuary (USA) to identify temporal patterns of estuarine surface temperature anomalies (<1m) and subsurface temperature anomalies (> 15m) between 1949 and 2002 and found that there is a trend for water heating;

- Villar et al. [2009] analysed the variability of regional extremes in the Amazon basin (BRA) and found that changes in discharge extremes are related to the multiannual variability of regional precipitation and associated atmospheric circulation, as well as to large-scale tropical climate indicators , thus showing the importance of atmospheric processes in estuaries;

- Sousa [2013] implemented and developed the three-dimensional model (MOHID) to analyse the influence of plume intrusion of the Minho river (POR) in the Rias Baixas (ESP) and concluded that in periods when the wind blows from south to north, the plume of the Minho river can change the physical parameters of the Rias Baixas;

- Mendes et al. [2017] carried out a study on the Douro river (POR), in which he used regional climate indexes [Eastern Atlantic (EA) and North Atlantic Oscillation (NAO)] to identify the influence of atmospheric variability on the generation of anomalous turbid river plume patterns and concluded that there is a strong link between river flow and turbidity levels in the river plume, as well as a strong link between precipitation and turbidity of the plume.

Although the hydrodynamic perspective is important, as well as the study of estuarine plumes and their exchange of properties with adjacent estuaries, the biological and chemical perspective has also been widely studied, since the hydrodynamic processes interfere greatly in the biogeochemical processes, as mentioned previously and in addition, it is increasingly intended to gain more knowledge about the impacts of human actions on estuarine biota as well as on the planktonic and benthic biodiversity existing in estuaries. To obtain a better perspective of the reality, over the years, periodic measurements have been made in coastal estuaries and numerical models have been used to try to explain and reproduce the different biogeochemical processes. Some examples of these studies are:

- Carbonel and Valentin [1999] studied the phenomenon of phytoplankton bloom during upwelling events in the coastal region of Cabo Frio (BRA), using a ocean model including the physics of coastal waters and the biological changes of the marine primary biomass and concluded that changes in wind direction and duration affect the temporal response of biological components, altering the instant of maximum concentration of nutrients, but keeping the maximum instant of phytoplankton unchanged;

- Edwards et al. [2000] studied the biological response to upwelling conditions, based on a simple nutrient–phytoplankton–zooplankton (NPZ) pelagic ecosystem model and concluded that with the upwelling, the phytoplankton and zooplankton maxima have more limited zonal extent, are more independent of the duration of wind forcing, and near-surface nutrient levels remain high over most of the domain and also verified that the longer the duration of this wind, the greater the rate of growth of the phytoplankton, since greater concentrations of nutrients were resuspended;

- Kemp et al. [2001] developed simple numerical models of plankton dynamics to explore how nutrient enrichment and habitat variability can influence the efficiency by which phytoplankton production is transferred to the growth of zooplankton consumers in coastal ecosystems and have concluded that despite an increase in zooplankton also

showed a higher mortality rate, resulting in more pronounced declines in zooplankton growth per unit phytoplankton production with increasing nutrients;

- Wang et al. [2014] investigated a non-linear model of the interaction between nutrients and plankton, which was approached using a pair of reaction-advection-diffusion equations and found that nutrients have a very large impact on phytoplankton density, since with the increase of nutrients, an increase of phytoplankton is observed.

Given that many of these works are current, a brief historical evolution of water quality models will be presented below. This historical development will only serve as supplementary information for the reader, since much of this development was due to the fact that it sought a rapid response to real problems that had occurred over the years.

One of the first models of water quality was developed by Streeter and Phelps [1925] and related the domestic sewage with the amount of dissolved oxygen in lakes and rivers. As science and technology evolved, new biogeochemical studies were performed, such as O'Connor [1961, 1967], where a model was developed to calculate the dissolved oxygen balance at steady state. The O'Connor model used analytical solutions for the partial differential equations of mass conservation and motion, however, when applied to estuarine and river systems, constant geometry and steady state had to be considered.

At the same time, Thomann [1963] began to develop finite difference models with the objective of evaluating the various water quality problems, leading to a better representation of the physical characteristics of the systems being studied.

At the 70s, importance start to be given to modelling nutrients dynamics (nitrogen and phosphorus) since it stimulate the rapid growth of phytoplankton, which can generate eutrophication in the estuarine waters. The rapid growth of phytoplankton will cause rapid oxygen uptake, causing the low levels of dissolved oxygen in waters, thus leading to fish mortality. Due to this problem, the mathematical models began to relate the nutrients with eutrophication and in turn the oxygen dissolved in the water [Fitzpatrick and Imhoff, 2001].

At the end of the 20th century, due to some environmental disasters (e.g.: Minamata disaster), environmentalists began to recognize the threat that potentially toxic elements (cadmium, lead, arsenic, mercury) could cause in the world population. This concern has led to the development of more complex water quality models [Delft3D-WAQ, AESOP (Advanced Ecological System Modelling Program), BFWASP (Boundary Fitted Eutrophication Modelling System)] that are being presently applied to coastal environments.

All the publications listed above, both in the area of physics and in the area of biology and chemistry, contributed in a way to expand the scientific knowledge about the area and topics under study, helping to select the most important processes and substances to be studied and helped in the concretization of the present research work.

1.3.2 Minho estuary

The Minho river is located in Northern Portugal. It is bordered by Spain and is very important because its discharge influences the coastal density gradients and the salinity in the other estuaries, located to the north (e.g.: Rias Baixas) [Fiedler and Laurs [1990]; Sousa [2013]]. The freshwater discharges from this river contribute to the generation of an extensive buoyant plume [Otero et al. [2008, 2013]; Mendes et al. [2016]], known as the Western Iberian Buoyant Plume (WIBP). The fact that this river influences the coastal gradients of density, salinity and even water temperature turns very interesting to carry out hydrodynamic and biogeochemical studies, since these parameters will impact the local biological community.

One of the most recent attempts to characterize the Minho river estuary hydrodynamics was performed by Pereira [2016], who studied some physical parameters, such as water

temperature and salinity, using 3D numerical modelling (Delft3D model).

Through this study, the distribution of these parameters in the summer and winter season, both longitudinally, laterally and vertically, as well as the estuarine plume and the hydrological response of the Minho estuary to climatic changes were determined and analysed.

Regarding the longitudinal gradients of the water temperature in the summer season, Pereira [2016] through his model observed that the Minho estuary presents higher water temperature upstream and colder near the mouth. With respect to the lateral gradients, the Minho estuary has a higher water temperature in the South margin and lower in the North margin, thus showing that the flood current flows through the North side, and the ebb current flows predominantly through the South side. In terms of vertical gradients, this estuary presents a discrete stratification, with the water temperature decreasing from the surface to the bottom.

In relation to salinity, the longitudinal structure presented higher values near the mouth and less saline water upstream. It is also verified that there is more freshwater on the south margin, and in the vertical structure, verified a stratification similar to that presented for water temperature.

During winter conditions, the different patterns are observed, since an inversion of the longitudinal, lateral and vertical structures of the estuary was found. According to Pereira [2016], this inversion is due to the decrease of the water temperature of the river and to the increase of the river flow in the winter season. Regarding salinity, a similar pattern was found both in summer and winter. Concerning climate change, it is expected that this estuary in the future will present a higher saline intrusion and an increase in the mean water temperature, because the river discharges will be lower.

Finally, Pereira [2016] carried out the study on the generation and propagation of estuarine plumes and verified that in the summer season the estuarine plume of the Minho is small, while in the winter season it observed a robust estuarine plume, being able to propagate to the north and integrate in the WIBP [Mendes et al., 2016].

Over the years other hydrodynamic studies have been carried out, such as: Santos et al. [2006], who studied the dependence of hydrography on tidal amplitude under low freshwater inflow, concluding that the estuary is vertically homogeneous during the spring tide and highly stratified during the neap tide. Zacarias [2007] studied the effect of bathymetry and river flow on tidal propagation and concluded that the bottom morphology influences the progression of tidal waves; Sousa et al. [2014b,a] studied the influence of the Minho estuary plume in the Rias Baixas and concluded that under large river discharges of the Minho river, the low salinity waters are advected to the right due to the Coriolis effect, leading the plume to deviate to the north, thus causing changes in the standard circulation of the Rias Baixas.

Currently, with the introduction of the Water Framework Directive, the discharge of contaminants into transitional ecosystems has been largely reduced and constantly monitored, as is the case of lagoons and estuaries of great ecological and landscape importance.

Since this estuary was subject to constant monitoring, it was possible to find water quality data, adequate to calibrate numerical models and in turn to perform more detailed biogeochemical studies. Some examples of studies are: Elumalai et al. [2007], who studied enzymatic biomarkers in *Carcinus maenas* crabs exposed to zinc and mercury and concluded that these metallic elements induce adverse effects on the biota of this region, since they will interfere with neurotransmitters, as happened with the study crabs; De la Rosa et al. [2012] carried out a study on the origin, pathways of dispersion and accumulation of organic matter over the years in the Minho estuary and concluded that the main sources of organic matter have terrestrial origin and were maximum during the small ice age and in turn, in the periods between 1960-1985 obtained higher values of the $\delta 13C$ isotope at the entrance of the estuary,

which can be explained by the drastic reduction of the discharges of the Minho river due to the construction of several dams; Vieira et al. [2015], who studied the effects of multi-stressors in the estuarine zooplankton communities, concluded that the main factors affecting the micro and meso-zooplankton pelagic organisms are salinity and water quality; and finally, Caetano et al. [2016] recently carried out a study that aimed to evaluate physicochemical parameters supporting the biological quality elements. To carry out this assessment, water samples were collected in several estuaries and the nutrient concentrations (nitrates, nitrites, ammonium, phosphate and silicates) were quantified to meet the requirements of the Water Framework Directive. After analysing the data, it was concluded that the Minho estuary presents values lower than the benchmark values and therefore a classification of High was given.

Although the studies previously mentioned have possible achieved a characterization of the Minho estuary, several issues were not addressed, such as biological and chemical interactions with Lima estuary. In addition, none of these studies carried out a water quality study using a 2D / 3D numerical models, these models being a very important tool because they can generate data with high spatial and temporal coverage, with low economic costs (there is no need to carry out *in situ* monitoring, and laboratory tests), provide a large number of data with a large spatial coverage, and in addition, this tool can isolate processes and can serve as a predictive support tool (e.g.: predicting environmental quality).

1.3.3 Lima estuary

The Lima river, is located south of the Minho river and has also equal biological and chemical importance.

During the 21st century, several hydrodynamic studies have been carried out about the Lima estuary. Some of these studies are: Pinho and Vieira [2007], who applied a hydrodynamic model (2D) to analyse the saltwater intrusion in the estuary, noting that saline intrusion can extend up to 12 km upstream of the river mouth (in the worst-case scenario - spring tides and low river discharge); Rebordão and Trigo-Teixeira [2009] studied the propagation of the tide and its role in the estuarine circulation and mixing processes; Vieira and Pinho [2010] studied the salt distribution in the Lima estuary for different hydrodynamic regimes and verified that under fluvial discharges and wind blowing from the south, the estuarine plume moves to the north; Vale and Dias [2011] investigated the effect of the tidal regime and river inflow in the estuarine circulation, and verified how the salinity varied and concluded that the estuary has a well-mixed or partially stratified water column, varying according to the inflow rate allowed by the upstream power generation dams; and Araújo et al. [2011] studied the ability of the ADCIRC model to model storm events in the region, concluding that astronomical effects and meteorology interact non-linearly.

As previously mentioned, with the introduction of the Water Framework Directive, it is usually easier to carry out studies about the chemical and biological components of estuaries, however this estuary has not been subject to major biogeochemical studies. The most relevant studies on water quality were carried out by Lopes et al. [2004], in which used the ADCIRC model, to study the impact that water temperature and dissolved oxygen have on aquatic fauna. This study was carried out on a stretch of the Lima river, downstream of the Touvedo dam, including Lima estuary and the authors found that different freshwater discharges by the dam (quantity and duration of water) brought impacts to hydrodynamics and water quality, resulting in a negative impact on the aquatic fauna under study [brown trout (*Salmo trutta*), Iberian nase (*Chondrostoma polylepis*) and chub (*Leuciscus carolitertii*)]; Cardoso et al. [2006, 2008] characterized various estuaries environments geochemically, including the Lima, concluding that the highest concentrations of metals are observed in marshes; and Almeida et al. [2011] carried out a study about the role that the various marsh plants in

the Lima estuary have in the retention of metals and have concluded that the presence of invasive and exotic plants in some areas of marshes can considerably affect the distribution and retention of metals in the estuarine region.

1.4 Structure of this work

To improve the comprehension and reading of this dissertation, it is presented below the structure of this work.

This dissertation was divided into 8 chapters. Chapter 1 presents the Introduction, which describes the motivations, general objectives, a general review of the literature and the structure of the work. This is followed by Chapter 2, where a description of the area under study is made. A detailed description of the Delft3D-FLOW and Delft3D-WAQ numerical model is presented in Chapter 3. Chapter 4 presents the description of the inputs used in the Delft3D numerical model, Chapter 5 describes the implementation of the model, the calibration process and its application and Chapter 6 describes the results of model calibration. Chapter 7 presents a discussion of the case studies mentioned in the objectives of the work, and finally Chapter 8 presents the conclusions of the dissertation and gives some suggestions for future work.

2 Description of the study area

Once the objectives of this work is to study the Minho and Lima estuaries [Figure 1], which are between 41° 36' and 42° 2' N latitude and between 8° 24' and 8° 54' W longitude. In this section will be initially presented a general description of the estuarine and oceanic circulation, followed by the morphological, hydrographic and hydrological characterization of the Minho and the Lima estuaries and finally a general description of the Minho and Lima river basins [Figure 1], which will address the region's climate, geology, geomorphology, among other subjects. To carry out this detailed characterization of the study area, the Technical Report of the Plano de Gestão de Região Hidrográfica do Minho e Lima [PGRH1, 2012] was analysed, which provided all the information found below.

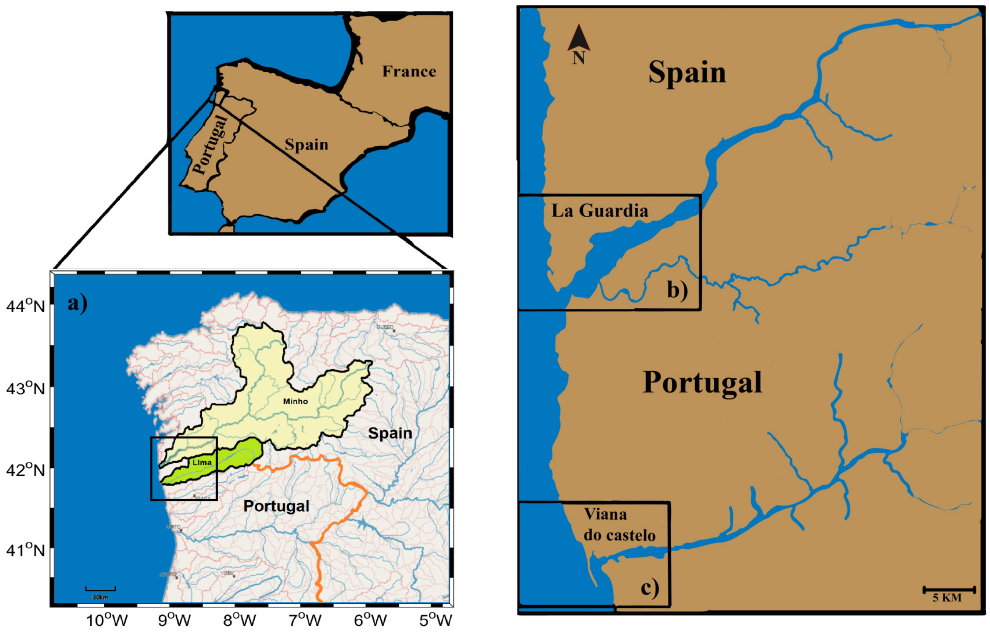

Figure 1: Study area: a) hydrographic basin of the Minho and Lima rivers, b) Minho estuary and c) Lima estuary.

2.1 Estuarine and oceanic circulation

To understand the estuarine circulation within the two estuaries under study, it is necessary to study the adjacent area, more specifically the ocean circulation near these estuaries.

In the North Atlantic Ocean there are two systems that transport surface water masses from West to East across the Atlantic. One is the North Atlantic Current and the other is the Azores Current. The North Atlantic Current extending to the north of the Iberian Peninsula (48 °N to 53 °N) and the Azores Current south of Iberia centered around 34-35 °N [Pollard and Pu, 1985; Peliz et al., 2005].

In the Portuguese coast there is the Portugal Current System, which is composed by two main currents and a seasonal current. The two main currents are predominantly North-South direction and are called the Portugal Current (slow and far from the coast) and the Portugal Coastal Current (fast and closer to the shelf break), while the seasonal current is the Portugal Coastal Counter Current, which is formed mainly when there is a weakening of north winds, coming from the Gulf of Cadiz with a South-North direction [Peliz et al., 2005; Dias, 2015]. According to Mazé et al. [1997] and Pollard and Pu [1985], Portugal Current has an average

speed of 1.6 cm/s, extend about 300 km beyond the shelf and can transport around 2.0 ± 1.2 Sv. Regarding to Portugal Coastal Current, during the summer, it has a maximum speed of 40 cm/s, a width of 30 to 40 km and a depth of 50 to 100 m [Peliz et al., 2002], while in the winter season it practically disappears [Álvarez-Salgado et al., 2003]. This Portugal Coastal Current is also of great importance on the Iberian Coast because when there is a north wind there is the transport of this water mass to offshore, providing the resuspension of the Eastern North Atlantic Central Water that comes from the subpolar region (> 45 °N), which is cold and rich in nutrients.

In addition to the currents mentioned above, there is another current flowing South-North along the northwest coast of the Iberian Peninsula, which is called the Iberian Poleward Current. This current is important because it transports hot and salt water, towards the poles and reaches speeds of the order of 20 cm/s [Dias, 2015].

According to Sousa [2013], in the coastal region, the surface circulation is also influenced by freshwater plumes resulting from the discharge from local rivers (Verdugo-Oitab´en, L´erez, Ulla, Umia, Tambre and to the south by the Minho and Douro), generating a persistent buoyant plume, the Western Iberian Buoyant Plume [Peliz et al., 2002]. This buoyant plume normally has salinity levels below 35.7 and an average depth of 20 m, however, as it approaches the coast, this thickness decreases [Varela et al., 2005]. According to Otero et al. [2008], in the winter season, the Western Iberian Buoyant Plume is located near the coast because the winds are from the south.

Although these surface currents are of great importance, it should be keep in mind that beneath these currents, there are other water bodies that contribute to all the dynamics of this study area.

In relation to the estuarine circulation, as mentioned in Section 1.3.1, the processes that determine the estuarine circulation are the wave regime, as well as wind stress, interaction with atmospheric processes, river discharges and tidal currents, being the latter process the main driver of the dynamics in the estuaries under study. These processes influence the distribution of physical-chemical variables (e.g.: salinity, water temperature, nutrients), both horizontally and vertically.

2.2 Morphological, hydrographical and hydrological characteristics

2.2.1 Minho estuary

The Minho river [Figure 2 a)] is born in Spain (Serra de Meira), at an altitude of 750 m and flows into the Atlantic Ocean, between La Guardia (Spain) and Caminha (Portugal). This river serves as a northern border between Portugal and Spain and has an approximate length of 300 km, of which 230 km are in Spanish territory and the remaining 70 km are crossed in Portugal [Pereira, 2016].

The total area of the hydrographic basin of the Minho river is 17080 km^2 [Figure 1 a)], of which 5% (798 km^2) is located in Portuguese territory, between the coordinates 41° 45' N and 43° 40' N latitude and 6° 10' W and 8° 55′ W longitude.

The main Portuguese tributaries are the rivers Trancoso, Mouro, Gadanha and Coura, while the main Spanish tributaries are the rivers Támoga, Ladra, Ferreira, Avia, Tea, Louro, Neira, Sil and Arnoya [Delgado, 2011]. This river presents an average annual discharge of 305 m^3/s, and the average monthly discharged varies between 121 during the summer and 692 m^3/s in the winter [Sousa, 2013], depending heavily on the discharges made by the hydroelectric dam existing throughout its extension.

The Minho estuary has an average length of 35 km and is characterized as a mesotidal system (astronomical tide varies between 2 m, during the neap tides and almost 4 m in the

spring tides) and partially mixed. However, during periods of high river flow, it tends to be a salt wedge estuary [Sousa et al., 2005]. This estuary presents an average depth of 2.6 m [Freitas et al., 2009].

It is important to mention that next to the mouth of the Minho estuary there is an island that will have an impact on the estuarine circulation. This Portuguese island is called Ínsua.

2.2.2 Lima estuary

The Lima river [Figure 2 b)] is also an international river, since it is born in Spain (Sierra S. Mamede), at an altitude of 950 m and flows into Viana do Castelo (Portugal). This river is located between the coordinates 41° 35' N and 41° 45' N latitude and 7° 50' W and 8° 55' W longitude.

The Lima river is about 108 km length, of which 41 km are in Spanish territory and the remaining 67 km are crossed in Portugal [Pereira, 2016]. The rivers Vez and Castro Laboreiro are the main Portuguese tributaries.

The total area of the hydrographic basin of the Lima river is 2470 km^2 [Bettencourt et al., 2003] [Figure 1 a)], of which 49% (1213 km^2) is in Portuguese territory.

This river has an average discharge of 30 m^3/s in the summer and 130 m^3/s in the winter season (SNIRH, www.snirh.apambiente.pt), depending heavily on the discharges made by the dams in the region (Touvedo and Alto Lindoso dams).

As in the Minho estuary, the Lima estuary is characterized as a semi-diurnal, mesotidal and partially mixed system. It has a length of 22 km [Pereira, 2016] and an average depth of 3 m, while the greatest depths of 10 m are observed in the navigation channels [Vale, 2008].

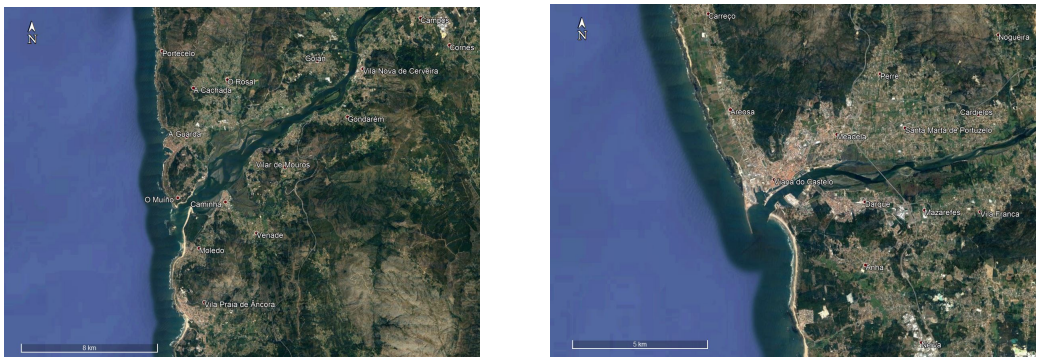

(a) (b)

Figure 2: Satellite image of a) Minho estuary and b) Lima estuary (©Google).

2.3 General characteristics of the hydrographic region of Minho and Lima

Due to the fact that the hydrographic basin of Minho and Lima is international, it was divided into two areas of jurisdiction. The Portuguese area is under the jurisdiction of the regional department of the North APA (Agência Portuguesa do Ambiente) and is delimited by the Spanish territory to the East and North, by the Atlantic Ocean to the West, by the Douro river basin to the Southwest and by the Cávado sub-basin to the South. The Spanish part of the river basin is under the jurisdiction of the Confederación Hidrográfica Miño Sil.

The hydrographic basins of these two estuaries have approximately an area of 20000 km^2, in which 2400 km^2 are in national territory, representing about 12% of the total. In Spanish territory, this hydrographic region has about 858,000 inhabitants, although the population

density is relatively low (49 inhab./km^2), while in Portuguese territory reside approximately 276000 inhabitants, representing a higher density population per km^2.

According to Plano de Gestão de Região Hidrográfica do Minho e Lima [PGRH1, 2012], this hydrographic region in the Portuguese part presents 2 bodies of groundwater and 71 surface water bodies, of which 56 are rivers, 3 are reservoirs (dams), 10 are transitional waters and 2 are coastal waters.

Regarding the availability of surface water resources, the hydrographic region of Minho and Lima has a total annual average flow of 17091 hm^3, of which 13648 are generated in the part of the Spanish watershed and the remain in Portuguese territory. The fact that there is a great availability of water resources, resulted in the construction of 3 hydroelectric dams in Portugal, with a storage capacity of 223 hm^3/year.

2.3.1 Climatology

The hydrographical region under study has a temperate climate, with well-defined winter and summer seasons. This climate varies according to the seasons of the year because it is influenced by the evolution and the seasonal movement of the two major atmospheric systems found in the North Atlantic Ocean. These are the Azores Anticyclone (high pressure centre) and the Icelandic cyclone (low pressure centre).

In the summer season, the climate is generally dry and with low humidity, because the Azores anticyclone moves north towards the Iberian Peninsula, while in the winter season the anticyclone moves southwards, allowing other cyclonic systems to invade the Iberian Peninsula, provoking a more humid and rainier climate.

Due to this fact, the hydrographic region under study has a mean monthly precipitation of about 162 mm, being the maximum value observed in December, presenting a mean monthly precipitation of 283 mm and the minimum value observed in July, with a monthly mean precipitation of 33 mm.

In terms of average annual relative humidity, this region presents an average humidity of 79%, that varies according to the basins (the Lima basin between 72% and 87% and the Minho basin between 71% and 86%).

Regarding the average annual temperature, the hydrographic region presents an average temperature of 14 °C, however in the coastal zones are always observes lower temperatures, that way reach 8 °C in the winter months and 20 °C in the summer months.

Finally, the average annual wind velocity in the Minho and Lima hydrographic region is 7.1 km/h, however, in general, there are always higher speeds in the Lima basin, reaching 13 km/h in the winter months.

For information purposes, due to the annual migration of the Azores anticyclone in latitude, the wind regime on the western coast of the Iberian Peninsula has a predominant direction towards the equator (north wind), mainly in the spring and summer seasons, creating favourable conditions to the development of transport of surface waters to offshore, causing the Coastal Upwelling. However sometimes in the winter and autumn seasons these events may also be observed. These upwelling bring a number of benefits to the estuaries, as nutrient rich waters masses arise, providing the growth of the estuarine species.

2.3.2 Geomorphology and Geology

Regarding the geomorphology of the hydrographic region of Minho and Lima, it is verified that this region is topographically uneven, since it presents accentuated reliefs, which cause discontinuous plateaus preserved in the top of individual blocks between deep and broad valleys and flat bottom.

Regarding the international section of the Minho river, the valley coincides with an important seismotectonic zone, being possible to identify 3 different sectors. The upstream sector is a rocky zone characterized by wide bottom depressions alternating with abrupt cliffs covered with weeds and rocky outcrops, and also by small alluvial depositions. In the intermediate sector (between Monção and Valença) is beginning to deposit material in suspension, since the currents are slow, giving rise to the appearance of islands and beaches in the margins. In the last sector, downstream, the slopes are smooth and the valley is very wide and open, observing very slow currents, giving rise to the deposition of sands with formation of banks, being of note the Boega Island, near Vila Nova de Cerveira, and, further downstream, Morraceira das Varandas, Morraceira do Grilo and Canossa, near the Spanish margin [Delgado, 2011].

Regarding the Lima river, it presents a geomorphology characterized by high slopes along its path, but along the coastal strip it is possible to observe a coastal plain carved in rock, with occasional dune cover north of the Lima river.

In geological terms, this region presents a diversity of geological units. The region can be divided into three main domains: the eastern domain is characterized by a large granite area; the central domain is constituted by metasedimentary rocks; and finally the western domain is constituted by granitoids and very fractured metasedimentary rocks (of the Xisto-Grauváquico Complex), quartzite and shale rocks (of the Palaeozoic).

2.3.3 Ecological and chemical state of the hydrographic region

According to the Water Framework Directive, to study the state of water bodies, it is important to carry out a study of the ecological status and chemical status and for this the North APA [PGRH1, 2012] has divided water bodies into "Rivers", "Lakes (reservoirs)", "Transitional waters" and "Coastal waters".

According to PGRH1 [2012], the hydrographic region of Minho and Lima has a high ecological value (Table 1), since 77% of the natural water bodies (rivers) are in a "good" ecological state, presenting only 15% of these masses in the "reasonable" state and 8% in the "mediocre" state. Regarding transitional waters, 33% of water bodies have a "good" state and 67% presents less than "good" state. Finally, in the coastal waters, one presented "good" ecological status and the other was not classified due to lack of information about the quality of the same.

Table 1: Number of water bodies in the Lima and Minho hydrographic region by Ecological State class [PGRH1, 2012].

Quality Class	Rivers	Transitional waters	Coastal waters
	Nº of water bodies	Nº of water bodies	Nº of water bodies
Excellent	—	—	—
Good	41	2	1
Reasonable	8	2	—
Mediocre	4	1	—
Bad	—	1	—
Without classification	—	—	1
Total	53	6	2

In addition to the water bodies, this hydrographic region has a high value, since it has a great diversity of habitats, such as marshes, reeds and sandbanks and in addition, it presents 2 Protected Areas for Birds, 6 Sites of Community Importance and 4 Protected

Areas [PGRH1, 2012], thus conferring on these two estuaries important protection statutes such as the Rede Natura 2000, Special Protection Area for Birds (SPA), Important Bird Area (IBA) and Biotope CORINE.

Regarding the chemical state (Table 2 and Figure 3), there is only a mass of transitional water, which is classified as "insufficient" due to the substance nonylphenol and the remain are in a "good" state. It is important to mention that there are many unclassified water bodies since PGRH1 did not have enough monitoring data in order to carry out this evaluation of the chemical status.

Table 2: Number of water bodies in the Lima and Minho hydrographic region by Chemical State class [PGRH1, 2012].

Quality Class	Rivers	Transitional waters	Lakes (reservoirs)	Coastal waters
Good	15	8	1	1
Insufficient	—	1	—	—
Without classification	41	1	2	1
Total	56	10	3	2

In general, the hydrographic region under study has a good water quality, however, pollution sources are still sometimes observed along these rivers, mainly of industrial, domestic or agricultural origin.

In a general evaluation of the quality of surface water, it can be concluded that the Lima river does not present significant level of pollution that prevents most of its uses, however there are some sections where there is a strong bacteriological contamination [Barbosa et al., 2004], which may impair water uses, since there is an increase in CBO_5, NH_4 and Fecal Coliforms [Hidroprojecto, 1992]. This contamination is more noticeable during periods of drought (August and September), as river flows are reduced. These sources of pollution are due to domestic and industrial effluent discharges [Barbosa et al., 2004].

Regarding the Minho river, it also has a good water quality. According to Fidalgo [2000], this river presents values of dissolved oxygen content above the minimum value recommended for waters of class A1 (Annex I of Decree-Law no. 236/98 of the Diário da República [Portugal]), presents values of organic matter that are included in the classification of waters not polluted, has ammoniacal nitrogen contents very close to zero or even below the limit of detection of the analytical method adopted and the observed nitrate values were always lower than the recommended maximum value for water destined for human consumption. Finally, phosphate levels are also very close to zero. Although this river presents a good quality of water, in the Spanish part of the watershed of the Minho river there is sometimes pollution of industrial origin. This industrial pollution is relatively high, mainly due to the industries in Porriño (Tui city) [Santos et al., 2013], which illegally discharge into the Louro river [Filgueiras et al., 2004], introducing large amounts of nutrients in the Minho river. Although the factories discharge wastewater into the Minho river and supply large quantities of nutrients, there is also diffuse pollution related to agriculture and the use of fertilizers [PBH, 2001].

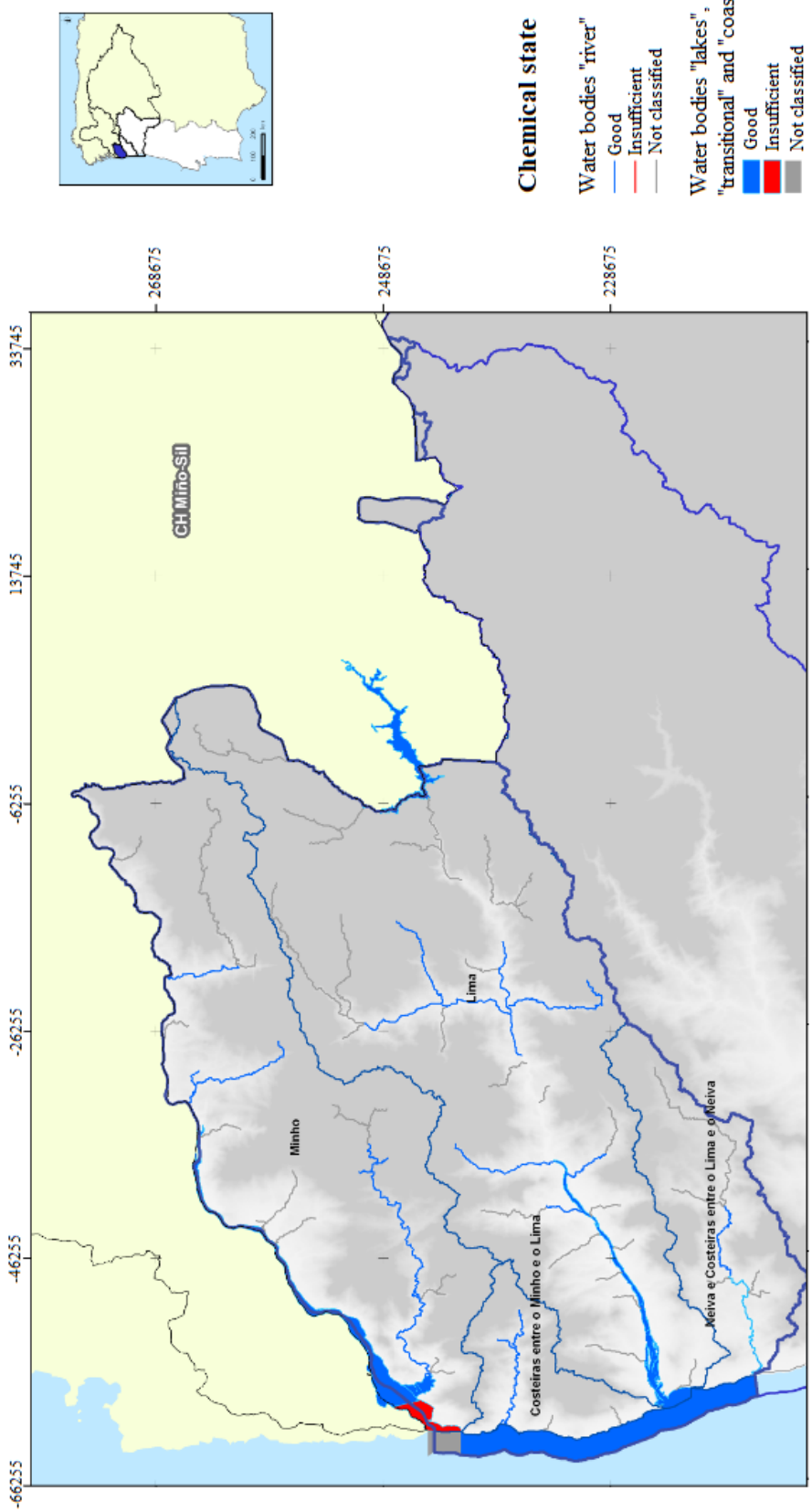

Figure 3: Chemical status of surface water (adapted from PGRH1 [2012]).

3 The numerical model: Delft3D

To accomplish the objectives of this work, it is indispensable to use a numerical model. The model suite chosen was Delft3D, which is a package of models for aquatic environments, that enables interaction between the available modules.

Delft3D allow any user to perform flow simulations (Delft3D-FLOW), waves (Delft3D-WAVE), water quality (Delft3D-WAQ and Delft3D-PART), ecology (Delft3D-ECO) and transport of sediments (Delft3D-SED).

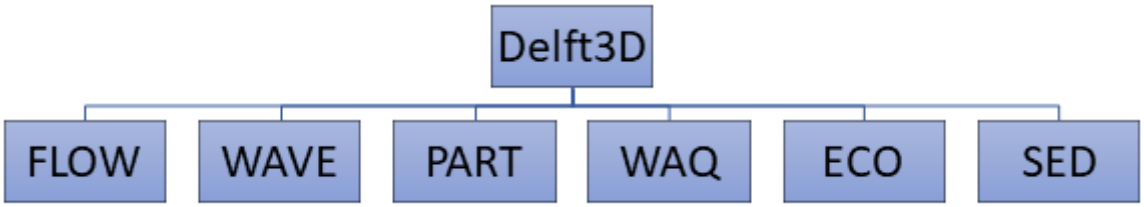

Figure 4: Main modules in Delft3D.

In addition to the six modules, Delft3D also includes several programs developed to facilitate treatment of raw data, such as Delft3D-RGFGRID and Delft3D-QUICKIN. The main purpose of Delft3D-RFGRID is to generate and modify curvilinear or orthogonal grids, which is very useful since it meets the Delft3D-FLOW requirements of grid smoothness and orthogonality, while Delft3D-QUICKIN allows to create, edit and view bathymetric data used as input to the Delft3D-FLOW and Delft3D-WAVE modules.

Also, Delft3D has a post-processing tool (Delft3D-QUICKPLOT), that can be used to visualize and animate numerical results.

Since this work will only make use of Delft3D-FLOW and Delft3D-WAQ modules, then the main characteristics of these modules will be presented, based on the information available in the Deltares [2016b] and Deltares [2016c] manuals.

3.1 The Delft3D-FLOW module

The hydrodynamic module, Delft3D-FLOW, allows working in 2 or 3 dimensions. This module solves the shallow water equations based on the finite difference method, obtained through the Navier-Stokes three-dimensional equations and continuity equation. In addition, the model simulates transport phenomena resulting from tidal and/or meteorological forcing, including the effect of density differences due to a non-uniform water temperature and salinity distribution (density-driven flow) [Deltares, 2016b].

To carry out the present study, it was decided to work in 2D model, since the use of three-dimensionality was not justified, since the studied estuaries can be considered vertically homogeneous [Sousa et al., 2005], and the time simulation as well as the size of the data generated would be very large if used the 3D option, aggravating these factors when coupled to the WAQ module.

Some of the possible applications for this FLOW module are: predicting flow in coastal areas, estuaries, lagoons, rivers and lakes; salt intrusion into estuaries; discharge of rivers in bays; thermal stratification in estuaries; astronomical tides; meteorological tides; and river flows [Deltares, 2016b].

3.1.1 Numerical aspects

As previously mentioned, the FLOW module solves shallow water equations in 2D (depth-averaged) or in 3D, in incompressible fluids, resulting in a system of three equations that express conservation of momentum and mass [Deltares, 2016b].

To solve the equations in the horizontal direction, the Delft3D-FLOW can use orthogonal curvilinear co-ordinates (free surface level and bathymetry are related with the horizontal plane of reference) or spherical co-ordinates on the globe (reference plane follows the curvature of the Earth). In the vertical direction, the model has two co-ordinate systems, the sigma co-ordinate system (model σ) and the Cartesian co-ordinate system (model Z).

In the present work was chosen the orthogonal curvilinear co-ordinate system, because it presents a staggered grid (Arakawa C grid), where the pressure points are defined in the centre of the cell and the velocity components are defined perpendicular to the cell faces of the grid (Figure 5).

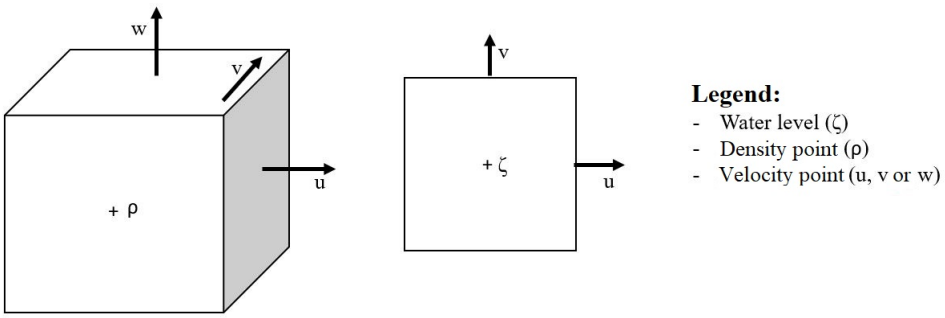

Figure 5: Staggered grid.

3.1.2 Governing equations

Once estuaries under study are considered vertically homogeneous (vertical gradient of density is negligible), it is possible to make some approximations. These approximations will cause a reduction in the number of equations required.

As previously mentioned, 2D models can be used to determine the horizontal components of the mean velocity along the vertical, through 3 equations: continuity equation and the horizontal equations of motion. These equations represent the fundamental principles of mass conservation and linear momentum in Newtonian fluids.

To calculate these equations, this model makes some approximations, such as: the hydrostatic approximation; the Boussinesq approximation; and Newtonian fluid (constant shear stress).

The hydrostatic approximation consists of the balance between the gravitational force and the pressure gradient term, once vertical accelerations are considered negligible. This balance is given by:

$$\frac{\partial P}{\partial z} = -g\rho H \tag{1}$$

Where, P is the pressure; H is the total depth of water ($H = d+\zeta$); g is the gravitational acceleration; ρ is the *in-situ* density and z is the depth below the reference level.

Considering that the density variations are relatively small, their effect on the mass of the fluid can be neglected, but should be considered in the weight. Although the density of water is considered constant (Boussinesq approximation), there are small variations in density, resulting in a new term in the equation of motion, which describes the forces of impulsion.

By vertically integrating the hydrostatic equation between the depth (z) and the free surface of the water (atmospheric pressure equal to the pressure of the free surface of the water), is obtained the following equation:

$$P = P_{atm} + gH \int_z^0 \rho(x, y, z', t) dz' \tag{2}$$

Where, P_{atm} is the atmospheric pressure.

Although in most estuaries these spatial variations of atmospheric pressure can be neglected because the medium is relatively small, this approximation is inserted into the system of equations for horizontal motion.

After making these approximations, the model vertically integrates the horizontal equations, thus eliminating the terms affected by the vertical velocities, resulting in a system of equations that can be solved by knowing the horizontal speeds and the free surface level.

Taking into account all the approximations referred to above and after integrating the vertical continuity equation, is obtained the following continuity equation for vertical mean flows:

$$\frac{\partial \zeta}{\partial t} + \frac{1}{\sqrt{G_{xx}}\sqrt{G_{yy}}} \frac{\partial (HU\sqrt{G_{yy}})}{\partial x} + \frac{1}{\sqrt{G_{xx}}\sqrt{G_{yy}}} \frac{\partial (HV\sqrt{G_{xx}})}{\partial y} = HQ \tag{3}$$

Where, t is the time; ζ is the free-surface water elevation; $\sqrt{G_{xx}}$ and $\sqrt{G_{yy}}$ are the coefficients used to transform curvilinear to rectangular co-ordinates; U and V is the depth averaged velocities; and Q represent the contributions per unit area due to the input or output of water through discharge or withdrawal, precipitation and evaporation.

To obtain the conservation equations of the linear momentum in the 2 directions (x and y), the model takes into account the approximations referred above, the stress that the wind causes on the free surface of the water, the roughness coefficient, the integration of the terms of pressure, the Coriolis term, among others. All simplifications and deductions can be followed in detail in the respective manual [Deltares, 2016b]. These approximations result in the following equations:

$$\begin{aligned} \frac{\partial u}{\partial t} + \frac{u}{\sqrt{G_{xx}}} \frac{\partial u}{\partial x} + \frac{v}{\sqrt{G_{yy}}} \frac{\partial u}{\partial y} + \frac{\omega}{(d+\zeta)} \frac{\partial u}{\partial z} - \frac{v^2}{\sqrt{G_{xx}}\sqrt{G_{yy}}} \frac{\partial \sqrt{G_{yy}}}{\partial x} + \frac{uv}{\sqrt{G_{xx}}\sqrt{G_{yy}}} \frac{\partial \sqrt{G_{xx}}}{\partial y} - fv \\ = -\frac{1}{\rho_0 \sqrt{G_{xx}}} P_x + F_x + \frac{1}{(d+\zeta)^2} \frac{\partial}{\partial z} \left(\nu_V \frac{\partial u}{\partial z} \right) + M_x \end{aligned} \tag{4}$$

$$\begin{aligned} \frac{\partial v}{\partial t} + \frac{u}{\sqrt{G_{xx}}} \frac{\partial v}{\partial x} + \frac{v}{\sqrt{G_{yy}}} \frac{\partial v}{\partial y} + \frac{\omega}{(d+\zeta)} \frac{\partial v}{\partial z} + \frac{uv}{\sqrt{G_{xx}}\sqrt{G_{yy}}} \frac{\partial \sqrt{G_{yy}}}{\partial x} - \frac{u^2}{\sqrt{G_{xx}}\sqrt{G_{yy}}} \frac{\partial \sqrt{G_{xx}}}{\partial y} + fu \\ = -\frac{1}{\rho_0 \sqrt{G_{xx}}} P_y + F_y + \frac{1}{(d+\zeta)^2} \frac{\partial}{\partial z} \left(\nu_V \frac{\partial v}{\partial z} \right) + M_y \end{aligned} \tag{5}$$

Where, u and v are the components of the horizontal velocity, integrated in the x and y directions; w is the velocity component in the vertical direction; d is the depth relative to the reference z=0; ρ_0 is the reference density of water; $f(= 2\Omega \sin\theta)$ is the Coriolis parameter; v_v is the vertical eddy diffusivity; the forces F_x and F_y represent the unbalance of horizontal

Reynold's stresses; P_x and P_y are the gradient hydrostatic pressure and the forces for the unbalance of horizontal Reynold's stresses; and M_x and M_y represents the discharge of water.

Once this model computes the flow of rivers, estuaries and tides, it is important to consider the transport of dissolved substances, salinity and heat. From the knowledge of the horizontal velocity fields, the model can determine this transport, using an advection-diffusion equation. This advection-diffusion equation is given by:

$$\begin{aligned}&\frac{\partial(d+\zeta)c}{\partial t}+\frac{1}{\sqrt{G_{xx}}\sqrt{G_{yy}}}\left(\frac{\partial\left[\sqrt{G_{xx}}(d+\zeta)\right]uc}{\partial x}+\frac{\partial\left[\sqrt{G_{xx}}(d+\zeta)\right]vc}{\partial y}\right)+\frac{\partial wc}{\partial z}=\\&=\frac{d+\zeta}{\sqrt{G_{xx}}\sqrt{G_{yy}}}*\left(\frac{\partial}{\partial x}\left[D_H\frac{\sqrt{G_{xx}}}{\sqrt{G_{yy}}}\frac{\partial c}{\partial x}\right]+\frac{\partial}{\partial y}\left[D_H\frac{\sqrt{G_{xx}}}{\sqrt{G_{yy}}}\frac{\partial c}{\partial y}\right]\right)+\\&+\frac{1}{d+\zeta}\frac{\partial}{\partial z}\left(D_v\frac{\partial c}{\partial z}\right)-\lambda_d(d+\zeta)c+S\end{aligned} \tag{6}$$

Where, D_H and D_v are the horizontal and vertical diffusion coefficient respectively; λ_d represents the first order decay process; and S is the source and sink terms per unit area due to discharge Q_{in} or withdrawal Q_{out} of water and/or the exchange of heat through the free surface Q_{tot}:

$$S=(d+\zeta)(Q_{in}C_{in}-Q_{out}c)+Q_{tot} \tag{7}$$

3.1.3 Boundary conditions

Given that there is not possible or desirable to simulate the entire globe, the Delft3D model has two boundary conditions that can be implemented. The two conditions are called open boundary condition and closed boundary condition.

The open boundary condition (also called the water-water boundary) aims to reduce computational time and restrict the study area, while the closed boundary condition aims to delimit the coastline and riverbanks.

In addition to these boundary conditions mentioned above, there is also a need to take account of vertical boundary conditions.

- Open boundary condition

In open boundary conditions, virtual boundaries are locations where the model is connected to open ocean or freshwater areas. The data imposed on these sites are obtained by measurements of river discharge, tidal data or a larger model.

Depending on the purpose of the work, the model presents several boundary conditions that can be selected [Deltares, 2016b]. Only the most important boundary conditions will be presented below (for detailed information see Section 9.4.1 in Delft3D FLOW_User_Manual).

Water level boundary:

$$\zeta=F_\zeta(t)+\delta_{atm} \tag{8}$$

Where:

$$F_\zeta(t)=\zeta+\alpha\frac{\partial}{\partial t}\left(U\pm2\sqrt{gH}\right)\qquad\qquad\alpha=T_d\sqrt{\frac{H}{g}} \tag{9}$$

$$\delta_{atm} = \frac{P_{average} - P_{atm}}{\rho g} \tag{10}$$

Velocity boundary:

$$U = F_u(t) \tag{11}$$

Where:

$$F_u(t) = U + \alpha \frac{\partial}{\partial t}\left(U \pm 2\sqrt{gH}\right) \qquad \alpha = T_d \tag{12}$$

Discharge:

$$Q = F_Q(t) \tag{13}$$

Where T_d is the time that a free surface wave takes to travel from the left boundary to the right boundary of the model domain; $U \pm 2\sqrt{gH}$ represents the Riemann invariants (avoid the reflections of the outgoing waves into the model area); α is the reflection coefficient; $P_{average}$ is average pressure; and Q represents the contributions per unit area due to the discharge or withdrawal of water, precipitation and evaporation.

- Closed boundary condition

Regarding the closed boundary condition, it is located in the transition between land and water, so there is no flow crossing the boundary, however, there is shear stress along the boundary.

This shear stress can be described by two conditions (zero tangential shear-stress and partial slip) and its use depends on whether the study is large scale or small scale (laboratory scale). If the study is large scale, the influence of shear stresses along the closed boundary can be neglected.

- Vertical boundary condition

In the vertical boundary conditions, the model takes into account the kinematic boundary conditions, bed boundary condition and surface boundary condition.

Kinematic boundary conditions

In the z co-ordinate system, the free surface (z = 0) and the bottom (z = -1) are z co-ordinate surfaces and w is the vertical velocity relative to the z-plane. The impermeability of the surface and the bottom is defined by:

$$W|_{z=-1} = 0 \tag{14}$$

$$W|_{z=0} = 0 \tag{15}$$

Bed boundary condition

At the seabed, the boundary conditions for the momentum equations along the x and y directions are:

$$\frac{v_v}{H}\frac{\partial u}{\partial z}|_{z=-1} = \frac{1}{\rho_0}\tau_{bx} \tag{16}$$

$$\frac{v_v}{H}\frac{\partial v}{\partial z}|_{z=-1} = \frac{1}{\rho_0}\tau_{by} \tag{17}$$

Where τ_{bx} and τ_{by} represent the bed stress.

Since the model used in this study is 2D, the shear-stress at the bed induced by a turbulent flow is given by a quadratic friction law:

$$\overrightarrow{\tau_b} = \frac{\rho_0 g \overrightarrow{U} \overrightarrow{|U|}}{C_{2D}^2} \tag{18}$$

Where $\overrightarrow{|U|}$ is the magnitude of the depth-averaged horizontal velocity and C_{2D} is the 2D-Chézy coefficient, which can be determined according to the Manning formulation (formulation used at work):

$$C_{2D}^2 = \frac{\sqrt[6]{H}}{\eta} \tag{19}$$

Where η is the Manning coefficient.

Surface boundary condition

At the free surface, the boundary conditions for the momentum equations are:

$$\frac{v_v}{H}\frac{\partial u}{\partial z}|_{z=0} = \frac{1}{\rho_0}\overrightarrow{|\tau_{s|}}\cos(\theta) \tag{20}$$

$$\frac{v_v}{H}\frac{\partial v}{\partial z}|_{z=0} = \frac{1}{\rho_0}\overrightarrow{|\tau_{s|}}\sin(\theta) \tag{21}$$

Where θ is the angle between the wind stress vector and the local direction of the grid-line. Without wind, the stress at the free surface is zero. The magnitude of the wind shear-stress is determined by the following quadratic expression:

$$\overrightarrow{|\tau_{s|}} = \rho_a C_d U_{10}^2 \tag{22}$$

Where, ρ_a is the density of air; C_d is the wind drag coefficient (dependent on U_{10}) and U_{10} is the wind speed at 10 meters above the free surface (time and space dependent).

3.1.4 Heat Flux

The radiative balance is the difference between the input and the output of elements of a system. The main components for the radiation balance in the terrestrial system are: surface, atmosphere and clouds.

When solar radiation enters the terrestrial system, one part is absorbed by the earth's surface or clouds and another part is reflected back into space (due to clouds and particles), thus maintaining the earth's thermal equilibrium.

In Delft3D-FLOW the heat exchange at the free surface is modelled by taking into account the separate effects of solar (short wave) and atmospheric (long wave) radiation, and heat loss due to back radiation, evaporation and convection [Ribeiro, 2015].

Although the Delft3D-FLOW has several heat flux models, the model used was the heat flux model 2 (absolute flux, net solar radiation), which uses the combined net solar radiation (Equation 23) and net atmospheric radiation (Equation 24).

The net solar radiation (short wave) is given by the following expression:

$$Q_{sr} = \sigma T^4 \tag{23}$$

Where, σ is the Stefan-Boltzmann's constant and T is the absolute temperature of a black-body in Kelvin.

The Net atmospheric radiation (long wave) is given by the following expression:

$$Q_{ar} = (1 - r)\varepsilon\sigma T_a^4 g(F_c) \tag{24}$$

Where, r is the reflection coefficient ($r = 0.03$); ε is the emissivity factor; T_a is the air temperature in Kelvin; and $g(F_c)$ is the cloud function.

3.2 The Delft3D-WAQ module

The water quality module, Delft3D-WAQ, also allows working in 2 or 3 dimensions, depending on the choice made in the Delft3D-FLOW module.

It solves the advection-diffusion-reaction equation on a predefined computational grid and for a wide range of model substances.

This module allows to model a wide range of substances as well as processes. As Delft3D-WAQ is not a hydrodynamic model, it will seek hydrodynamic information from the Delft3D-FLOW module, through the Coupling process. This process (Coupling) will seek hydrodynamic information from the final hydrodynamic simulation file and extracts from the file the velocities, water elevations, density, salinity, water temperature, vertical eddy viscosity and vertical eddy diffusivity, which may be useful for studying the processes and substances in study, in the Delft3D-WAQ module. The water quality module provides a wide range of physical (bio) chemical and biological substances and processes that can be used. Some of the substances that can be modelled are:

- Conservative substances (e.g.: salinity);
- Suspended sediment;
- Water temperature;
- Nutrients (ammonia, nitrate, phosphate, adsorbed P);
- Organic matter (subdivided in carbon, nitrogen, phosphorus and sulphur components);
- Dissolved oxygen;
- Phytoplankton biomass (algae species);
- Heavy metals.

Regarding the processes, the following processes can be modelled in Delft3D-WAQ:

- Sedimentation and resuspension;
- Reaeration of oxygen;
- Algae growth and mortality;
- (De)nitrification;
- Phosphate adsorption and precipitation.

With this, the model in use shows that it is possible to carry out a great diversity of studies, since it presents a wide applicability (e.g.: study of eutrophication in lakes, reservoirs, estuaries; study of dissolved oxygen depletion in stratified systems; study of sediment transport and heavy metals; among others).

3.2.1 Governing equations

Delft3D-WAQ solves the equations for transport and physical, (bio)chemical and biological processes. Below are displayed the mass balance and the mathematical advection-diffusion-reaction equation that forms the basis of Delft3D-WAQ module.

Mass balances

In each computational cell, the Delft3D-WAQ module administrates the mass balance of selected state variables, such as dissolved oxygen and nitrate. Mass transported by flowing water from one cell to the next serves as a negative term in the mass balance in the first computational cell and as a positive term in the second computational cell. When is taken into account that within a computational cell substance can be converted to other substances, water quality processes have to be included. For example, nitrification converts ammonium $\left[NH_4^+\right]$ to nitrate $\left[NO_3^-\right]$, resulting in a negative term in the ammonium mass balance of that computational cell and a positive term in the nitrate mass balance [Deltares, 2016c].

To solve each state variable, at any time interval, the Delft3D-WAQ module solves the following advection-diffusion-reaction equation:

$$M_i^{t+\Delta t} = M_i^t + \Delta t \left(\frac{\Delta M}{\Delta t}\right)_{Tr} + \Delta t \left(\frac{\Delta M}{\Delta t}\right)_{P} + \Delta t \left(\frac{\Delta M}{\Delta t}\right)_{S} \tag{25}$$

Where, Δt is the time step; M_i^t is the mass at the beginning of a time step; $M_i^{t+\Delta t}$ is the mass at the end of a time step; $\left(\frac{\Delta M}{\Delta t}\right)_{Tr}$ are the changes by transport; $\left(\frac{\Delta M}{\Delta t}\right)_{P}$ are the changes by physical, (bio)chemical or biological processes; and $\left(\frac{\Delta M}{\Delta t}\right)_{S}$ are the changes by sources (e.g.: waste loads, river discharges). This equation is a simplified representation of the advection-diffusion-reaction equation which will be discussed next.

Advection-diffusion-reaction equation

As previously mentioned, the Delft3D-WAQ module solves the advection-diffusion-reaction equation. This equation is in fact a mass balance for the pollutants or state variables necessary to describe the problem at hand [Deltares, 2016c]. In a simplified way this equation can be written as follows:

$$\frac{\partial M}{\partial t} = advection + dispersion + source \tag{26}$$

- Advective transport

The advective transport is given by:

$$T_{x_0}^A = v_{x_0} A C_{x_0} \tag{27}$$

Where, $T_{x_0}^A$ is the advective transport at $x = x_0$; v_{x_0} is the velocity at $x = x_0$; A is the surface area at $x = x_0$; and C_{x_0} is the concentration at $x = x_0$.

It is important to mention that the model assumes velocities and concentrations as a representative average value for the whole surface, so the smaller the cross section, the better this assumption.

- Dispersive transport

The dispersive transport across an exchange is assumed to be proportional to the concentration gradient and to the surface area.

The dispersive transport is based on the Fick diffusion law. This law describes several cases of diffusion of matter or energy in a medium in which there is initially no chemical or thermal equilibrium. In situations where there are concentration gradients of a substance, or

temperature, there is a flow of particles or heat that tends to homogenize the dissolution and to standardize the concentration or the temperature. The homogenizing flow is a statistical consequence of the random motion of the particles giving rise to the second principle of thermodynamics, also known as random thermal movement of the particles and this flow will go in the opposite direction of the gradient.

Thus, the proportionality constant D_{x_0} is called the dispersion (or diffusion) coefficient and the minus $(-)$ signal means that the liquid transport of concentrations takes place from the highest concentrations to the lowest concentrations (opposite direction to the concentration gradient). With this, the dispersive transport is given by the following equation:

$$T_{x_0}^D = -D_{x_0} A \frac{\partial C}{\partial x}|_{x=x_0} \tag{28}$$

Where, $T_{x_0}^D$ is the dispersive transport at $x = x_0$; D_{x_0} is the dispersion coefficient at $x = x_0$; A is the surface area at $x = x_0$; and $\frac{\partial C}{\partial x}|_{x=x_0}$ is the concentration gradient at $x = x_0$.

- Transport from sources

The transport of pollutants by sources (e.g.: river discharges) is given by:

$$T_{src} = Q_{src} C_{src} \qquad Q_{src} > 0 \tag{29}$$

Where, T_{src} is the transport from sources, Q_{src} is the flow at $x = x_0$ and C_{src} is the concentration at $x = x_0$.

However, if the discharge flow Q_{src} is negative (withdrawal), the model uses the following expression:

$$T_{src} = Q_{src} C_i \qquad Q_{src} < 0 \tag{30}$$

Where, C_i represents the concentration in the receiving Water Quality-segment. It is important to note that if the source concentrations provided by the user are negative, they are neglected.

- Mass transport by advection and dispersion

When it is add to the one-dimensional equation (Equation 25) the mass transport by advection and dispersion and the terms of a second surface (left and right sides of a volume), new terms have to be added to the equation. Delft3D-WAQ uses the following equation:

$$M_i^{t+\Delta t} = M_i^t + \Delta t (Q_{x_0} C_{x_0} - Q_{x_0+\Delta x} C_{x_0+\Delta x} - D_{x_0} A_{x_0} \frac{\partial C}{\partial x}|_{x_0} + D_{x_0+\Delta x} A_{x_0+\Delta x} \frac{\partial C}{\partial x}|_{x_0+\Delta x}) \tag{31}$$

Where, A_{x_0} is the surface area at $x = x_0$; Q_{x_0} is the flow at $x = x_0$; and C_{x_0} is the concentration at $x = x_0$.

Taking the asymptotic limit $\Delta t \to 0$ and $\Delta x \to 0$, the advection-diffusion equation for one dimension results:

$$\frac{\partial C}{\partial t} + \frac{\partial}{\partial x}(vC) - \frac{\partial}{\partial x}(D \frac{\partial C}{\partial t}) = 0 \tag{32}$$

Where, v is the velocity;C is the concentration; and D is the dispersion coefficient.

Thus, the Delft3D-WAQ module to solve the advection-diffusion equation uses the finite volume method for transport. The accuracy of the method will be related to the size of Δx, $A(= \Delta y * \Delta z)$ and Δt.

3.2.2 Boundary conditions

As mentioned in Section 3, it is not possible to simulate the whole globe and for this there is the possibility of limiting the area of study, implementing boundaries. As in the Delft3D-FLOW module, there are also two boundaries conditions in the Delft3D-WAQ: the open and the closed boundaries.

The open boundaries in the Delft3D-WAQ are necessary for the solution of the advection-diffusion equation, while the closed boundaries are those that have zero flow and dispersion for all time steps, so no transport is associated with these exchange surfaces.

In the case of the open limits of the Delft3D-WAQ module, all substances and dispersion coefficients must be specified for all time intervals.

Although Delft3D-WAQ works in the same way as the Delft3D-FLOW module, the following problems must be taken into account:

- If the advection term is computed by a "central method", the concentration at the interface between the last model segment and the downstream boundary is computed as the average between the concentration in the last segment and the downstream boundary concentration, thus affecting downstream advective transport.

- For the computation of the dispersive term, the concentration gradient at the interface between the last model segment and the downstream boundary is computed as the difference between the concentration in the last segment and the downstream boundary concentration divided by the distance between the two. Therefore, the downstream boundary concentration affects the dispersive transport.

These problems are due to the mathematics behind the Water Quality model, since the concentrations in the downstream boundaries do have an effect on the solution of the Water Quality model.

Although these effects do occur, Delft3D-WAQ presents solutions to solve these effects, one of which uses an upwind advection scheme locally at the model boundaries, and the other suppress the dispersive transport locally at the model boundaries.

It is important to note that concentrations outside the model area are influenced by the previous outputs, that is if the flow changes sign and inflow takes place again (as in tidal estuaries), it can be assumed that part of the water flowing previously enter again. This is a very important boundary conditions, because in the case of water quality it allows the entry of nutrients and substances again.

This so-called Thatcher-Harleman time lag uses the inner concentration if outflow takes place and starts with the latest outflow concentration to reach the specified boundary concentration within the user specified time lag.

This equation is given by:

$$C(t_0 + t) = C(t_0)(0.5 + 0.5\cos(\frac{\pi t}{2T})) + C_B(t)(0.5 - 0.5\cos(\frac{\pi t}{2T})) \tag{33}$$

Where, t_0 is the time that outflow changes to inflow; t is the time after t_0; C simulated boundary concentration; C_B is tuser-specified boundary concentration (may be time-dependent as well); and T is the Thatcher-Harleman time lag.

4 Data Presentation

This section aims to describe the data used in this work. It presents the data that were used to generate the numerical bathymetry applied on the model's grid, the data that were used in the limits of the model (oceanic, fluvial and atmospheric boundary conditions), and the field data used to calibrate the water level and the transport module.

4.1 Bathymetric data

To implement a numerical model for the Minho and Lima estuaries, bathymetric data were required, to interpolate the numerical grid.

The bathymetric data used in the present study is the same used by Pereira [2016]. These data were obtained from General Bathymetric Chart of the Oceans (GEBCO), Direção Geral do Território (DGT) and Hidrodata company (HC) and all of them are referenced to the WGS 1984 Datum (work done by Pereira [2016] with the support of ArcGis software).

GEBCO provided bathymetric data from the coastal region, the DGT provided bathymetric data from the Minho river estuary (collected in 2011 through the LIDAR system, with a spatial resolution of 2 meters), and HC provided bathymetric data from the Lima river estuary (collected between October 2002 and December 2003, with a spatial resolution of 5 meters).

4.2 Boundaries conditions

To force the Delft3D-FLOW and Delft3D-WAQ models, the harmonic constituents (to force the tide), water temperature, salinity, ammonia, nitrate, orthophosphate, dissolved oxygen, phytoplankton and total net primary production data were used at the ocean-ocean interface, while in the interface ocean-atmosphere data of "irradiation", wind and heat flux were used. Finally in river boundary, river discharges, water temperature, ammonia, nitrate, orthophosphate and dissolved oxygen were imposed.

4.2.1 Oceanic boundary

The tide data was obtained from TOPEX / Poseidon (www.jpl.nasa.gov) [Macmillan et al., 2004] for the period under study (referred to in Section 5.2.1). The TOPEX / Poseidon is based on a global oceanic tide model (model NAO.99b), which provides the 13 tidal solution main constituents (M_2, S_2, N_2, K_2, K_1, O_1, P_1, Q_1, M_f, M_m, M_4, MS_4 and MN_4) with a spatial resolution of 0.25°. These harmonic constituents are estimated from 5 years of data from the TOPEX / Poseidon altimeter [Pereira, 2016].

Regarding the values of water temperature, salinity, orthophosphates, ammonia, nitrates, dissolved oxygen, phytoplankton and total net primary production imposed at the ocean-ocean interface, these were taken from the Copernicus Marine Environment Monitoring Service database (CMEMS, www.marine.copernicus.eu).

From the CMEMS, daily data were extracted for the study period (referred to in Sections 5.2.2 and 5.2.3). The water temperature and salinity data, were taken from the Atlantic-European North West Shelf-Ocean Physics Reanalysis from METOFFICE (1985-2014), since this model was the only that covered the period under study. The biochemical data (dissolved oxygen, nitrates, orthophosphates, phytoplankton and total net primary production) were taken from Atlantic - European North West Shelf - Ocean Biogeochemistry Analysis and Forecast.

Both models mentioned above are based upon the Forecasting Ocean Assimilation Model 7 km Atlantic Margin Model (FOAM AMM7). These are forced at the surface by ERA-interim

winds, precipitation fluxes and atmospheric temperature, with a horizontal resolution of 7×12 km (CMEMS, www.marine.copernicus.eu).

According to the short description of this model, on the CMEMS website, the Forecasting Ocean Assimilation Model 7 km Atlantic Margin model (FOAM AMM7) is a coupled hydrodynamic-ecosystem model, nested in a series of one-way nests to the Met Office global ocean model. The hydrodynamics are supplied by the Nucleus for European Modelling of the Ocean (NEMO) with the 3DVar NEMOVAR system used for the assimilation of sea surface temperature data. This is coupled to the European Regional Seas Ecosystem Model (ERSEM), developed at Plymouth Marine Laboratory (PML) (CMEMS, www.marine.copernicus.eu).

4.2.2 River boundary

The daily series of freshwater discharges (m^3/s) and water temperature (°C) for the Minho and Lima rivers were obtained from the Confederacion Hidrográfica del Miño-Sil (www.chminosil.es) and the Sistema Nacional de Informação de Recursos Hídricos (SNIRH, snirh.apambiente.pt), respectively. For the Minho river, data were obtained from the Salvaterra do Minho station (N015), while for the Lima river, data were obtained from the Touvedo dam (03G / 01A) automatic data network (turbinated flow data).

Due to the scarcity of biochemical data for the river discharges input into the estuaries under study, data from the HypeWeb model (www.hypeweb.smhi.se) were used. Since the data period of the HypeWeb model doesn't include the year under study (2012/13), a monthly average of all the years existing in the HypeWeb was made, for the soluble phosphorus and inorganic nitrogen (variables simulated by the HypeWeb model).

Since Delft3D does not contain the substances soluble phosphorus and inorganic nitrogen, these data had to be converted to obtain the concentration of ammonia, nitrates and orthophosphates. To carry out the conversion, the methods described in the following articles EPA [2007] and Kacikoc and Beyhan [2014] were considered, in which 80% of the inorganic nitrogen was assumed as nitrates and 20% was ammonium. Regarding soluble phosphorus, it was considered that all of it would be in the form of orthophosphates.

4.2.3 Atmospheric boundary

Daily atmospheric data from the European Center for Medium-Range Weather Forecasts (ECMWF, www.ecmwf.int) were used on the water surface. The ECMWF provides a global atmospheric reanalysis (ERA-Interim) model, which is updated daily.

From ERA-Interim data were extracted relative humidity (%), air temperature (°C) and net radiation ($J/m^2/s$). These data have a time resolution of 3 hours and were used to force the Heat Flux model.

Regarding the atmospheric pressure and the wind data (u and v components near the surface), these were taken from the Thredds Server of MeteoGalicia (www.mandeo.meteogalicia.es). This server has historical data predicted by the WRF model. In this server, it is possible to choose 3 domains, each domain having a different spatial resolution. Domain 1 has a resolution of 36 km, Domain 2 of 12 km and Domain 3 of 4 km. The domain chosen for this work was Domain 3 (D03), since it presented higher resolution.

Finally, irradiation data were also taken from Meteogalicia. These data were taken from the weather station "As Eiras", every 10 minutes.

4.3 Model Calibration

To perform the calibration of the Delft3D-FLOW and Delft3D-WAQ models, data of harmonic constituents, water temperature, salinity, ammonia, nitrates, orthophosphates and dissolved oxygen, measured in the field, were used.

The harmonic constituents data in the Minho estuary were collected by Zacarias [2007] between February 20 and March 19, 2006 (this campaign took place during high fluvial discharges), while in the Lima estuary these data were taken from the Portuguese Hydrographic Institute, in the Viana do Castelo station. The six locations where the tidal surveys were done are represented in Figure 6.

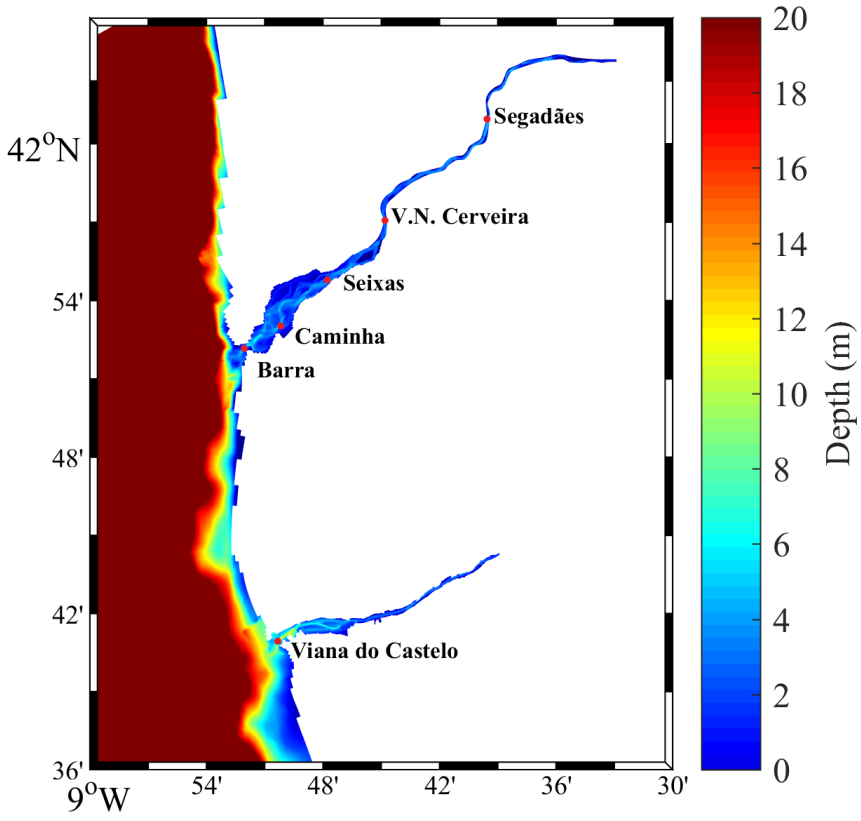

Figure 6: Tide gauge stations used for the extraction of the sea surface elevation.

Regarding the water temperature, salinity, ammonia, nitrates, orthophosphates and dissolved oxygen data, these were collected by Vieira et al. [2015] during the period between February 2012 and February 2013. These measurements were collected one day a month along the Minho and Lima estuaries (the date and sampling period is depicted in Tables 13, 14, 15 and 16, in Appendix). To make these collections in the same location and at the same depth, Vieira et al. [2015] defined seven transepts in each estuary (Figure 7), in which they measured the coordinates of the sampling sites, as well as the depth of the site, using a GPS (HP IPAQ GPSMAP) and a depth gauge (Hondex PS-7) (Table 3).

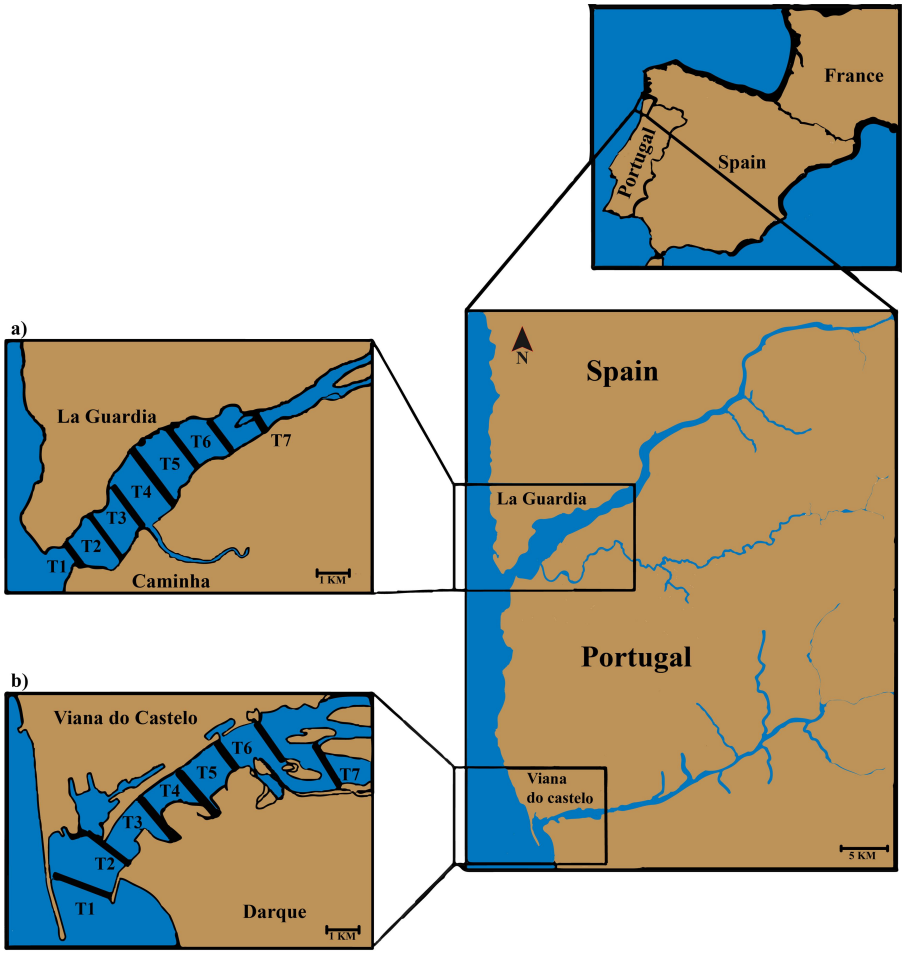

Figure 7: Estuaries under study [a) Minho estuary and b) Lima estuary] with sampling transects (T1-T7) in both estuaries (adapted from Vieira et al. [2015]).

In each transept was collected water and were made measurements *in situ* (water temperature, salinity and dissolved oxygen), with a multi-parameter probe (VWR SP90M5), in 3 regions (south margin of the river, middle of the river and north margin of the river). In each region, three replicates were made, to obtain a better representation of the study area and to minimize errors. The water samples were collected with polyethylene-terephthalate bottles and stored at -20 °C for nutrient analysis [Vieira et al., 2015] and was measured the nutrients concentrations (ammonium, nitrates and orthophosphate), using commercial photometer kits (Photometer 7000, Palintest, Kingsway, England).

Table 3: Coordinates and average depths of each site for all the transects. Site 1 is located on the south margin, the Site 2 on the middle margin and the Site 3 on the north margin.

		Transect						
Estuary		**T1**	**T2**	**T3**	**T4**	**T5**	**T6**	**T7**
Minho	**Site 1**	41° 52' 02" N	41° 52' 23" N	41° 52' 47" N	41° 53' 06" N	41° 53' 28" N	41° 53' 55" N	41° 54' 12" N
		08° 51' 11" W	08° 50' 42" W	08° 50' 23" W	08° 49' 58" W	08° 49' 35" W	08° 49' 11" W	08° 48' 44" W
	Depth (m)	1.5	1.0	1.5	1.0	1.0	1.5	2.0
	Site 2	41° 52' 10" N	41° 52' 32" N	41° 52' 52" N	41° 53' 16" N	41° 53' 37" N	41° 53' 58" N	41° 54' 15" N
		08° 51' 35" W	08° 51' 03" W	08° 50' 44" W	08° 50' 23" W	08° 49' 59" W	08° 49' 26" W	08° 48' 57" W
	Depth (m)	2.0	1.5	2.0	1.5	1.5	2.5	2.5
	Site 3	41° 52' 24" N	41° 52' 43" N	41° 53' 01" N	41° 53' 32" N	41° 53' 51" N	41° 54' 06" N	41° 54' 26" N
		08° 51' 52" W	08° 51' 28" W	08° 51' 07" W	08° 50' 52" W	08° 50' 20" W	08° 49' 42" W	08° 49' 17" W
	Depth (m)	3.0	1.5	2.0	1.0	2.0	1.5	1.5
Lima	**Site 1**	41° 40' 48" N	41° 40' 59" N	41° 41' 09" N	41° 41' 22" N	41° 41' 23" N	41° 41' 24" N	41° 41' 22" N
		08° 50' 15" W	08° 49' 43" W	08° 49' 26" W	08° 49' 14" W	08° 48' 44" W	08° 08' 14" W	08° 47' 35" W
	Depth (m)	4.0	4.0	4.0	1.5	2.0	2.0	1.5
	Site 2	41° 40' 50" N	41° 41' 07" N	41° 41' 17" N	41° 41' 26" N	41° 41' 33" N	41° 41' 36" N	41° 41' 29" N
		08° 50' 25" W	08° 49' 58" W	08° 49' 37" W	08° 49' 20" W	08° 48' 54" W	08° 48' 26" W	08° 47' 38" W
	Depth (m)	6.0	5.0	5.0	3.0	2.5	3.0	2.0
	Site 3	41° 40' 58" N	41° 41' 09" N	41° 41' 21" N	41° 41' 30" N	41° 41' 40" N	41° 41' 44" N	41° 41' 36" N
		08° 50' 35" W	08° 50' 08" W	08° 49' 47" W	08° 49' 28" W	08° 49' 02" W	08° 48' 35" W	08° 47' 50" W
	Depth (m)	5.0	4.0	4.0	3.0	2.5	2.5	2.0

5 Methodology

This section aims to describe the procedures followed in this work. In this way, it will be described in detail all the steps performed (e.g.: variables used, initial and boundary conditions imposed in the model, calibration process of the model, application of the model, among others), in order to achieve the objectives of this work.

5.1 Implementation of the model

To study the intrusion and dynamics of estuarine plumes in the two estuaries under research, the impact of extreme river discharge events on the nutrient dynamics and the response time of the Minho estuary to a point of discharge of pollutants, the Delft3D model was used. As mentioned in Section 3.1, this model allows to calculate flows and the transport of properties in 2D and 3D.

Since the water quality module requires large information storage capacity, a two-dimensional (2D) model was used in the hydrodynamic and water quality module.

5.1.1 Hydrodynamic model

To develop the hydrodynamic model, first step was to develop the numerical grid. The numerical grid developed started from that build by Pereira [2016]. This grid considered both estuaries under study in a single domain, however this grid had some limitations in the oceanic part, concerning the objective of this work (e.g.: generation of jet streams). To overcome these limitations, the numerical grid was readjusted, changing the oceanic boundary to a circular shape (Figure 8), maintaining the same resolution in the interior areas of the two estuaries.

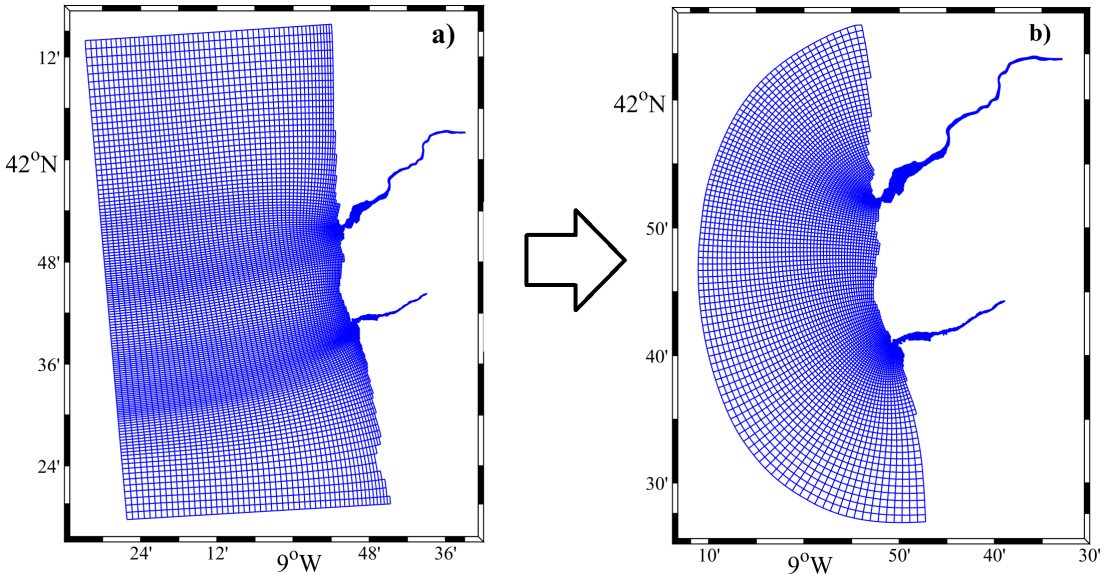

Figure 8: Numerical grid used by Pereira [2016] (a), and new numerical grid (b).

The new grid has a maximum distance from the coastline to the open sea of 25 km, a total size of 835 cells in the M (longitude) direction and 170 in the N (latitude) direction and a total grid elements of 28844.

The size of the cells decrease upstream in each estuary, with cells of 900×800 m in offshore, 300×200 m near the coast and inside the estuaries, 50×70 m in the Minho estuary and

20×30 m in the Lima estuary. Within the estuaries, there is a higher resolution to better represent the processes occurring in these regions.

This new grid has an orthogonality lower than 0.02, which is a good value, as it meets the recommended range by Deltares [2016a]. The time step used was 15 seconds, aiming to obtain a number of Courant-Friedrichs-Lewy lower than 10 in the entire grid, since the smaller this number, the greater the stability and accuracy of the numerical results. The Courant-Friedrichs-Lewy number equation (CFL - Equation 34) depends on the time step $[\triangle t]$ (minutes), the gravitational acceleration $[g]$ (m/s^2), the water column depth $[H]$ and of the grid dimensions ($\triangle x = \sqrt{G_{xx}}$ and $\triangle y = \sqrt{G_{yy}}$).

$$CFL = 2\triangle t\sqrt{gH}\sqrt{\frac{1}{\triangle x^2} + \frac{1}{\triangle y^2}} < 1 \tag{34}$$

After generating the grid, the bathymetric data were implemented for each grid element. To perform this implementation, it was necessary to convert the bathymetric data (referred to in Section 4.1) to .xyz format (format used by Delft3D) and then interpolate the result in the numerical grid, using tools and mechanisms available in Delft3D-QUICKIN. This bathymetry is represented in Figure 9.

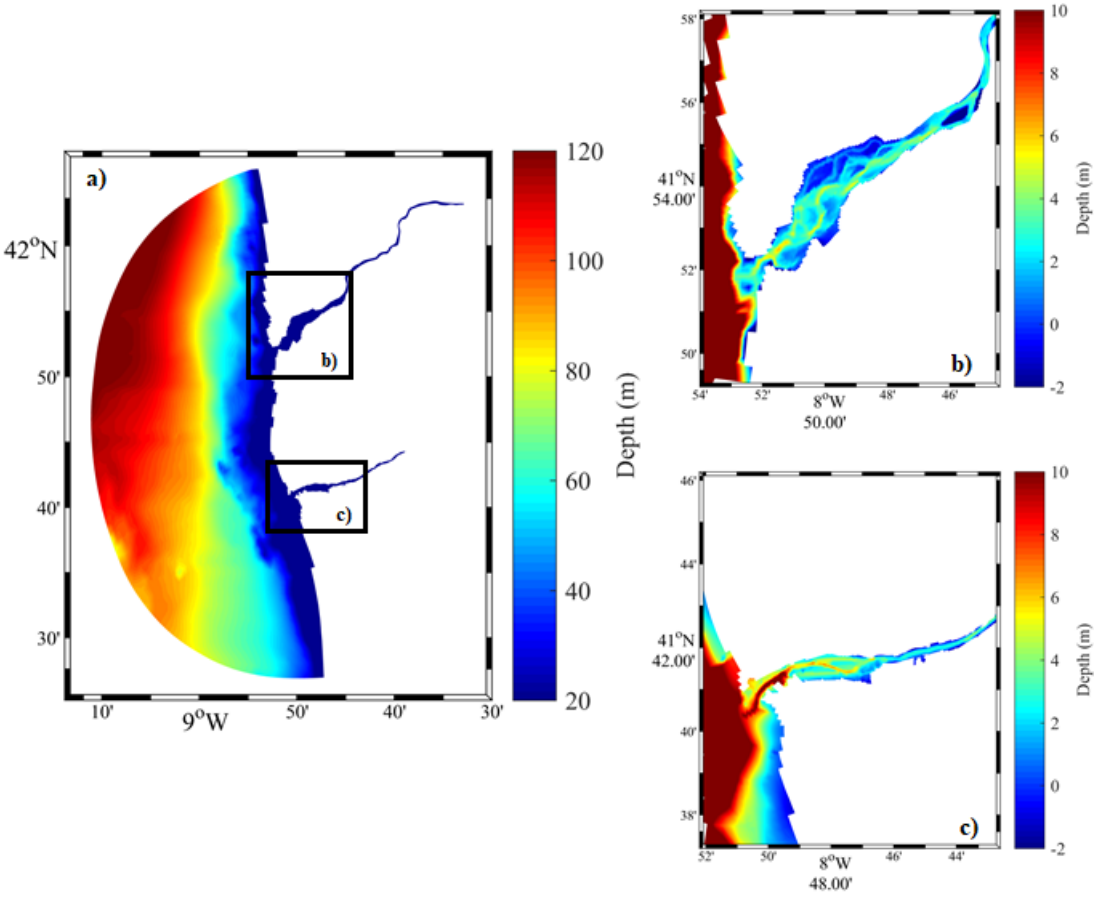

Figure 9: Bathymetry of the: a) study area; b) Minho estuary; and c) Lima estuary.

After constructing the numerical bathymetry, it was necessary to define some physical parameters required to run the model. The physical parameters used in the hydrodynamic model were: gravity of 9.81 m/s^2; water density of 1024 kg/m^3; and air density of 1.225

kg/m^3. Similarly, the horizontal background viscosity and the diffusivity used were standard, 1 m^2/s and 10 m^2/s, respectively.

Concerning ocean boundary conditions, the harmonic constituents (referred to in Section 4.2.1) were imposed in order to force the model and simulate the tidal propagation.

The period of simulation for the propagation of the tidal wave was from 20 February 2006 to 19 March 2006, since this period corresponds to that in which observational data of the harmonic constituents were obtained (data presented in Section 4.3).

After adding all the necessary inputs to force the hydrodynamic model, it was performed the model calibration (methodology presented in Section 5.2.1 and results in Section 6.1).

5.1.2 Salt and heat transport model

After the calibration of the tidal propagation, three new processes (water temperature, salinity and wind) were added to the FLOW module.

To verify if the salt and heat transport model represented well the water temperature and the salinity inside the estuaries, a new simulation period was defined (1 January 2012 to 1 March 2013). This period was chosen because it corresponds to the observed data period of water temperature and salinity (Section 4.3) that will be used later to compare model predictions with observations. The model predictions will only be used at the end of the first 30 days of simulation, called warm-up period, in order to attenuate the initial perturbations of the model and make the results independent of the initial conditions.

After defining the simulation period, time series of water temperature and salinity (referred in Section 4.2.1) at the oceanic boundary and data on river flows and freshwater temperature (referred in Section 4.2.2) at river boundary were imposed. In relation to the ocean-atmosphere interface, wind direction, atmospheric pressure near the surface, relative humidity, air temperature and net radiation (referred in Section 4.2.3) were imposed in the model.

Since there was a large data set to be implemented in the boundary conditions, it was decided to use Matlab scripts to create all the files that will serve as inputs for boundaries conditions and initial conditions (.amu, .amv,. amp and .tem files for the ocean-atmosphere interface; .dis file for the fluvial boundary, and .bca and .bcc files for the oceanic boundary). With respect to the .ini file of the initial conditions, null velocities and a water level of 0 m were used, and salinity values and water temperature were varied throughout the computational domain (values taken from Copernicus for the first day of simulation - 1 January 2012).

After adding all the inputs to force the salt and heat transport model, it was calibrated (methodology presented in Section 5.2.2 and results in Section 6.2).

5.1.3 Water quality model

After implementing and calibrating the hydrodynamic module (hydrodynamic model and the salt and heat transport model), the water quality model was also implemented.

The first step was to define the simulation period. The period chosen for the water quality model was the same used in the salt and heat transport model (1 January 2012 to 1 March 2013), because it corresponds to the period of observed data of ammonia, nitrates, orthophosphates and dissolved oxygen (presented in Section 4.3). This data will serve to compare model predictions with observed water quality data.

After defining the simulation period, the same numerical grid that was used in the Delft3D-FLOW module was implemented in the water quality model and was defined a time step 1 minute, to ensure the model stability.

The vertical and horizontal dispersion coefficients used for both directions were 1 m^2/s.

As mentioned in Section 3.2, the Delft3D-WAQ is not a hydrodynamic model, so it is necessary to seek hydrodynamic information from the Delft3D-FLOW module (e.g.: velocity of currents, water temperature, salinity, among other variables) and for that, it was used the COUPLE tool provided by Delft3D. After coupling, the file resulting from this process was inserted into the water quality module.

Given that in the water quality module there are several numerical discretization schemes available, the integration method 15 (Iterative solver, backward differences) was chosen for the present work. This choice was based on its accuracy, stability, positivity and efficiency, since this method is efficient if large time intervals are used, it has always positive positivity (there are no negative concentrations in the calculus cells) and allows to perform simulations with a large number of substances [Deltares, 2016c].

Since Delft3D-WAQ presents many processes and substances to be modelled, several numerical simulations were made aiming to select the most relevant processes and substances in estuaries under study and to verify if the model approached the reality, comparing data predicted by the model with the observed data, at the end of each new simulation. Given this, the best numerical simulation presented the processes and substances mentioned in Table 4.

Table 4: Processes and substances selected.

Substances	Processes
Algae [non-Diatoms]	Potential minimum dissolved oxygen [OXYMin]
	Nett primary production and mortality [GroMrt_Gre]
Dissolved Oxygen [OXY]	Potential minimum dissolved oxygen [OXYMin]
	Uptake of nutrients by growth of alga [NutUpt_alg]
	Variation of primary production within day [VAROXY]
	Horizontal dispersion velocity depend [HDisperVel]
	Denitrification in water column [Denwat_NO3]
	Nitrification of ammonium [Nitrif_NH4]
	Reaeration of oxygen [RearOXY]
	Composition [Compos]
Ammonium [NH4]	Uptake of nutrients by growth of alga [NutUpt_alg]
	Nitrification of ammonium [Nitrif_NH4]
	Composition [Compos]
Nitrate [NO3]	Uptake of nutrients by growth of alga [NutUpt_alg]
	Denitrification in water column [DenWat_NO3]
	Nitrification of ammonium [Nitrif_NH4]
	Composition [Compos]
Orthophosphate [PO4]	Uptake of nutrients by growth of alga [NutUpt_alg]
	Ad[De]Sorption ortho phosphorus to inorg. matter
	Composition [Compos]

These processes were chosen because: [Compos] calculates the stoichiometric ratios of nutrients; [Nitrif_NH4] takes into account bacteria and fungi degrade ammonium (NH_4^+) and it is converted to nitrite (NO_2^-) and subsequently into nitrate (NO_3^{2-}); [DenWat_NO3] takes into account the denitrification of nitrates [the denitrifying bacteria decompose the nitrate and release to the atmosphere N_2; [NutUpt_alg] takes into account the limitation of primary production, since it depends on nutrients, light and water temperature; [RearOXY] takes into account the exchange of oxygen between the atmosphere and water; [HDisperVel] relates the horizontal dispersion to the flow velocity (e.g.: in river systems or if the horizontal grid cells are too large to resolve important variations in the flow field); [VAROXY] takes into account the

intensity of the light, the average daily solar radiation and the duration of the day; [OXYMin] computes the minimal DO-concentration that may occur during the day, when daily averaged forcing is used; and [GroMrt_Gre] takes into account the growth and mortality of algae.

It is important to note that as new processes and substances were added to the numerical simulations, new boundary conditions had to be inserted and sometimes significant processes had to be eliminated, because there was no data available to force the model (e.g.: particulate matter concentration). Thus, in the last numerical simulation, time series of ammonia, nitrates, orthophosphates, dissolved oxygen, phytoplankton and total net primary production (data taken from Copernicus) were imposed at the oceanic boundary, dissolved oxygen, ammonia, nitrates and orthophosphates (mentioned in Section 4.2.2) at the fluvial boundaries and irradiation data at the ocean-atmosphere interface. In the initial conditions, a fixed value of dissolved oxygen (6.7035 g/m^3), ammonia (0.2 gN/m^3), nitrate (0.1107 gN/m^3), orthophosphates (0.0232 gP/m^3) and phytoplankton (0.0281 gC/m^3) was considered. These values were included in the initial conditions resulting from the average of the Copernicus values obtained for the first day of simulation (1 January 2012).

After adding all the necessary inputs, this model was calibrated (methodology presented in Section 5.2.3 and results in Section 6.3).

5.2 Model calibration

To ensure the best reproduction of the hydrodynamic and biochemical processes within the study estuaries, several numerical simulations were carried out to achieve the best model accuracy in predicting the local estuarine processes (results presented in Sections 6.1, 6.2 and 6.3). For each numerical simulation performed, its accuracy was quantified.

5.2.1 Hydrodynamic model

The period used to calibrate the hydrodynamic model was from 20 February 2006 to 19 March 2006, as referred in Section 5.1.1.

Based on the background roughness values proposed by Dias et al. [2001] and Picado et al. [2010] for the Ria de Aveiro, as a starting point, several simulations were performed in which the Manning coefficient (Equation 19) was varied with the objective of improving the adjustment of the tidal propagation between predicted and observed data.

To perform the model calibration, three steps were performed at the end of each numerical simulation: the first step comprises a visual comparison between predicted and observed free surface elevation at the six sites (Barra, Caminha, Seixas, Vila Nova de Cerveira, Segadães and Viana do Castelo), mentioned in Section 4.3; the second step consisted in quantifying the differences between the observed and predicted amplitudes and phases of the main harmonic constituents M_2, S_2, K_1 and O_1 (only these harmonic constituents were analysed because they are the main local constituents); and the third step consisted in quantifying the accuracy of the model predictions, using adequate parameters. These harmonic constituents are determined by harmonic analysis, made using a package of Matlab routines called T_TIDE [Pawlowicz et al., 2002]. This package has an important characteristic: calculates the amplitude and phase with a 95% confidence interval.

This quantification was performed through the Root Mean Square Error (RMSE) [Atwater and Ball, 1978] and SKILL [Willmott, 1981]. The expressions of RMSE and SKILL are the following:

$$RMSE = \sqrt{\frac{\sum_{i=1}^{N} ([\zeta_P(t_i) - \zeta_h(t_i)]^2}{N}} \tag{35}$$

$$SKILL = 1 - \frac{\sum_{i=1}^{N} |\zeta_P(t_i) - \zeta_h(t_i)|^2}{\sum_{i=1}^{N} \left[\left|\zeta_P(t_i) - \zeta_h\bar{(t_i)}\right| + \left|\zeta_h(t_i) - \bar{\zeta_P}(t_i)\right|\right]^2} \tag{36}$$

Where $\zeta_p(t_i)$ is the predicted water level and $\zeta_h(t_i)$ is the observed water level, both at t_i time and N is the number of time steps.

After obtaining the best adjustment between the predicted and observed data (calibration results in Section 6.1), the salt and heat transport model was implemented and calibrated.

5.2.2 Salt and heat transport model

For the calibration of the salt and heat transport model, the data from Vieira et al. [2015] were used (referred in Section 4.3). Since sampling was performed in the period from February 2012 to February 2013 (one sampling per month), the calibration of the model was also performed in this period, in order to make a direct comparison between model predictions and observed data.

Since there were 21 sampling sites for each estuary (7 transepts and in each of them there were 3 sampling sites), only the sampling sites in the middle of the transept were considered, thus reducing to 7 sampling sites per estuary. Only this data will be used to carry out the calibration. After selecting the sampling sites, the mean of the replicas was done for these sites, since at each sampling site 3 water samples (3 replicates) were collected. In the calibration results (Section 6.2), only Transepts 1, 3, 5 and 7 of each estuary will be presented.

It is important to note that the data observed have uncertainties in the collection time (approximately 1 hour) and thus, it was chosen to make an error bar which comprises all the values of salinity and water temperature within that time period (e.g.: if the sample was collected at 5:00 p.m., the time period in the error bar is between 4.30 and 5.30 p.m.).

Finally, to assess the accuracy in predicting salinity and water temperature, RMSE (Equation 35) was calculated again for each transept (transects shown in Figure 7) and a temporal analysis was made between the water temperature and salinity data predicted by the model and observed data.

The results of this calibration can be found in Section 6.2.

5.2.3 Water quality model

Once the water temperature and salinity data were collected at the same time as the ammonia, nitrate, orthophosphate and dissolved oxygen data, the water quality model calibration was also performed for the same period (1 February 2012 to 1 February 2013).

Once the biochemical data (ammonia, nitrates, orthophosphates and dissolved oxygen) were collected at the same sampling sites (21 sampling sites) as the hydrodynamic data, the same methodology used in the salt and heat transport model was applied to the water quality model. This methodology consists of only considering the sampling sites that are in the middle of the channel, resulting in only one value in the 7 transepts (per estuary). It is important to note that in the calibration results (Section 6.3) only Transepts 1, 3, 5 and 7 of each estuary will be analysed.

After defining the processes to be modelled (referred in Section 5.1.3), new numerical simulations were carried out, in order to improve the adjustment between model predictions and the data observed. To improve this setting the parameter total respiration flux was used. This parameter was used to calibrate the model because in this work only algae were considered as producers of oxygen (biota that make photosynthesis) and were not considered oxygen consumers (e.g.: zooplankton). Although this parameter has the greatest impact on dissolved oxygen concentration in estuaries, it will also have an impact on nutrients, since biota need nutrients to grow.

It is important to note that this adjustment was based on the theoretical foundations and standards found in reality (e.g.: the concentration of dissolved oxygen in winter is high because there is a higher rate of production than respiration and in summer there is more consumption than oxygen production and in addition to that previously mentioned, the higher the water temperature and the salinity, the lower the concentration of dissolved oxygen in the water).

After this adjustment, the accuracy of the model was again assessed, using the Root Mean Square Error (RMSE). Once this type of models have lower accuracy and more deviations than the hydrodynamic modulus (since all biogeochemical processes occurring within the estuaries and their interactions between processes and substances were not considered), it is also calculated the Cost Function (CF). The CF quantifies the difference between the observed data and predictions, giving a non-dimensional value, which is indicative of the "goodness of fit" between two sets of data. CF is given by:

$$CF = \frac{1}{N} \sum_{i=1}^{N} \frac{|\zeta_h(t_i) - \zeta(t_i)|}{\sigma_D(t_i)} \tag{37}$$

Where σ_D is the standard deviation of the data. According to Radach and Moll [2006], the performance levels are categorised as follows: CF $<$ 1 very good; 1–2 good; 2–3 reasonable; and CF $>$ 3 poor.

The results of this calibration can be found in Section 6.3.

After the models calibration (hydrodynamic model, salt and heat transport model and water quality model), different case studies were defined and explored using these models.

5.3 Application of the model

After the models were calibrated, different scenarios and case studies were developed, aiming to achieve the objectives of this work, described in Section 1.2.

5.3.1 Intrusion and dynamics of estuarine plumes of Minho and Lima estuaries

To research a possible interaction and exchange between the two estuaries under study, the paths of two passive conservative tracers were simulated with the hydrodynamic module (previously calibrated), one released in Minho estuary [Figure 10a)] and another in Lima estuary [Figure 10b)]. The concentration used for these tracers was 100 kg/m^3, and the same concentration was applied to the river discharges to maintain a source of the tracer in each estuary.

This method was used because it has higher reliability than analysing salinity fields, since estuarine plumes and water masses vary their properties from estuary to estuary and have different spatial scales, thinning, spreading and buoyancy [Ribeiro, 2015].

To research possible intrusions of the Minho plume in the Lima estuary and vice versa, as well as to study the dynamics of estuarine plumes, several transepts were defined along

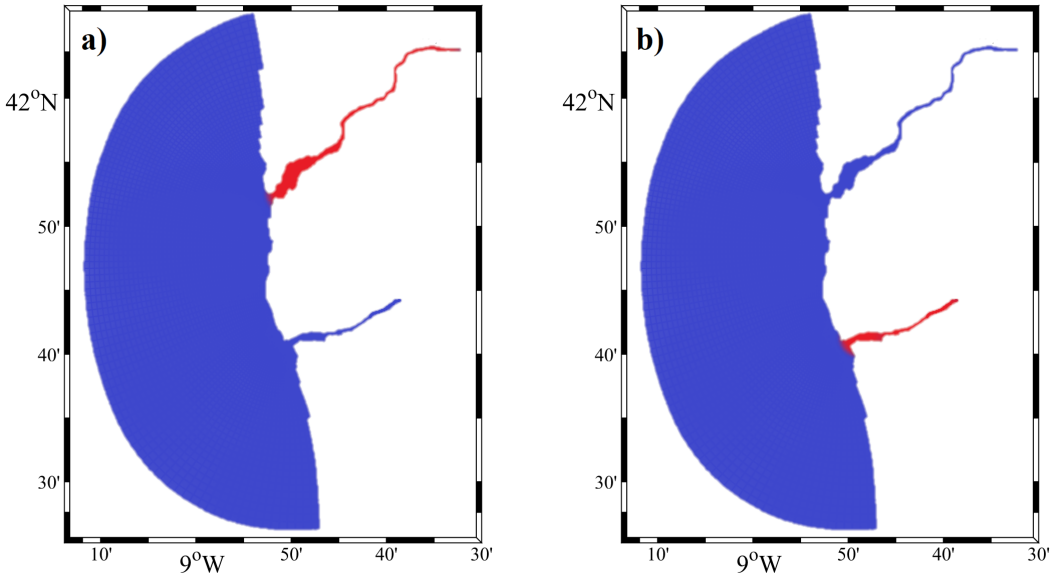

Figure 10: Mask applied to the grid area to calculate the propagation of the estuary plume of a) Minho and b) Lima. The red and blue colour are the tracer concentration of 100 and 0 kg/m^3, respectively.

the study area (Figure 11). These transepts were located at the entrance of both estuaries and perpendicular to the coast. The studied period was winter and summer seasons. These periods were chosen considering that estuarine plumes in the winter are more perceptible and there is a higher probability of interactions and exchanges of properties between the estuaries, while in the summer season they are less likely, due to the reduced fluvial discharges.

In the results section (Section 7.1) figures of the cumulative advection transport of the tracers in Transepts 1 and 2 (transepts shown in Figure 11) will be presented. In the Transept 1 will be measured the cumulative advection transport of Lima tracer and in Transept 2 the cumulative advection transport of Minho tracer. Since river discharge and wind are important processes in scattering an estuarine plume [Sousa, 2013], figures of these variables will be made for the same period (wind intensity and direction were retrieved for the point "P" shown in Figure 11).

It is important to mention that only cumulative advection transport was taken into account during the study period, so all cumulative advective transport registered until the beginning of the respective season was extracted from the time series. Due to this fact sometimes negative cumulative advective transport is observed.

Finally, to study the dynamics of both plumes, figures of tracer concentration and tracer transport (Transept 1 at the mouth of the Minho estuary; Transept 2 at the mouth of the Lima estuary; Transept 3 between the Minho and Lima estuary; Transept 4 south of the Lima estuary; and Transept 5 north of the Minho estuary) will be made.

All results can be found in Section 7.1.

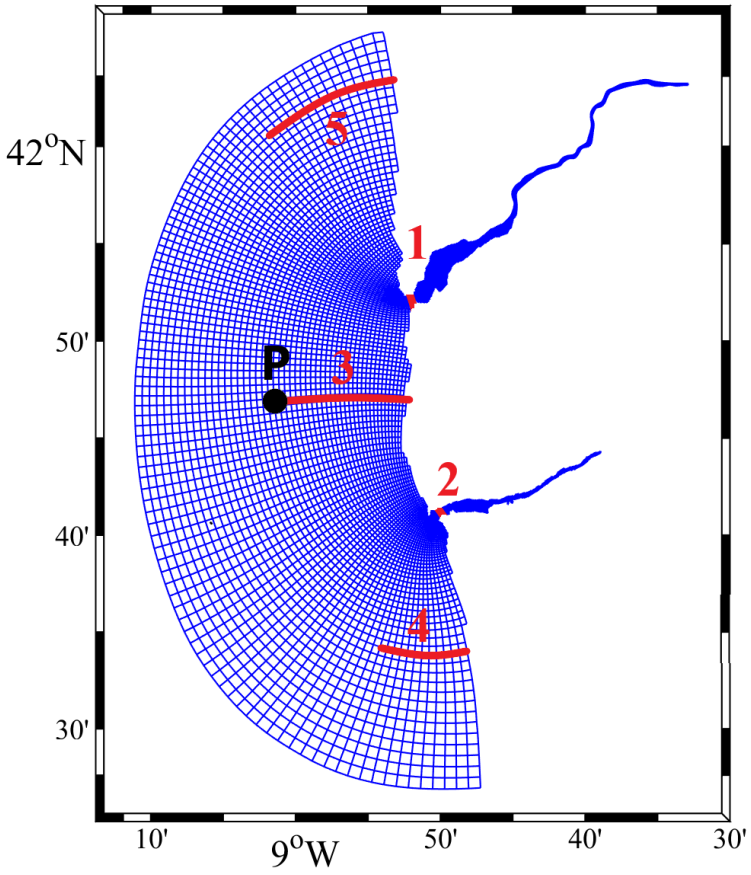

Figure 11: Transepts used to study the intrusion and dynamics of plumes, and point (P) where the wind direction and intensity were retrieved.

5.3.2 Impact of extreme events on the nutrient dynamics in Minho and Lima estuaries

To understand the nutrients dynamics (ammonia, nitrate, orthophosphate) and dissolved oxygen, as well as to understand the impact of extreme inflow conditions during summer (21 June 2012 to 20 September 2012) and winter (21 December 2012 to 1 March 2013) seasons in both studied estuaries (extreme events mainly caused by climate change impact), three simulations were made in the period from 1 January 2012 to 1 March 2013.

The first simulation corresponds to the case of the numerical simulation used for model calibration, serving as baseline (hereinafter referred as SCEN 0) and the remaining two correspond to a flood scenario (SCEN 1) and a drought scenario (SCEN 2). In SCEN 1, river discharges were considered to have twice the discharges from the calibration simulation (SCEN 0) and in SCEN 2 only the ecological discharges (minimum flows released by dams in the event of drought) were considered. These scenarios were chosen because under climate changes the extreme events are predicted to be more frequent and intense (e.g.: very cold or very hot weather; heavy rains or severe droughts).

Ecological flow data at the river boundary, in the second scenario (SCEN 2), was based on reports from the Região Hidrográfica do Minho e Lima of the Agência Portuguesa do Ambiente [APA, 2015] and in the Boletín Oficial Del Estado [BOE, 2009], of the Plan Hidrológico de la parte española de la DH del Miño-Sil. The ecological flows values for estuaries under study

are presented in Table 5.

Table 5: Ecological flow values (m^3/s).

	Minho	Lima			Minho	Lima
Jan	109.42	6.8		Jul	51.16	0.8
Feb	109.42	7.6		Aug	51.16	0.5
Mar	109.42	6.8		Set	51.16	0.7
Apr	79.64	4.1		Oct	70.34	1.5
May	79.64	2.9		Nov	70.34	3.5
Jun	79.64	1.6		Dez	70.34	5.3

It is important to mention that the only factor changing between these scenarios was the river discharges, keeping the remaining inputs of the model unchanged.

The results of this case study can be found in Section 7.2.

5.3.3 Response time of the Minho estuary to a point discharge of pollutants

Finally, given that the present work has the objective of analysing the response time of the Minho estuary to a point discharge of pollutants, a new river discharge was considerered in the reference simulation (SCEN 0). This river discharge simulates a tributary of the Minho river, called the Coura river.

This tributary is very close to the mouth of the Minho estuary ($\sim$ 3 km) [Figure 12 a)] and since the flow rates in most Portuguese tributaries are not monitored, an average annual discharge of 10 m^3/s was considered for the Coura river. Usually, this tributary presents a good water quality [Santos et al., 2013].

For this study, two numerical simulations were performed, the first being representative of the point discharge of pollutants on August 10 (corresponding to neap tide) and the second on August 19 (corresponding to spring tide), representing the most critical tidal conditions [Figure 12 b)]. In both cases, there was a discharge of 17 gN/m^3 of nitrates and 0.44 gP/m^3 of orthophosphate (on the remaining days the discharges of nutrients were always considered null). This period was chosen since the Minho river discharge is usually very low (ranging between 2 and 10 m^3/s).

The concentrations of nitrates and orthophosphates discharged by the Coura river were based on the mean concentration of nutrients on August 10 (0.17 gN/m^3 and 0.0044 gP/m^3), considering that the point discharge of pollutants had a concentration 100 times higher than the nutrients in the estuary.

The results of this case study can be found in Section 7.3.

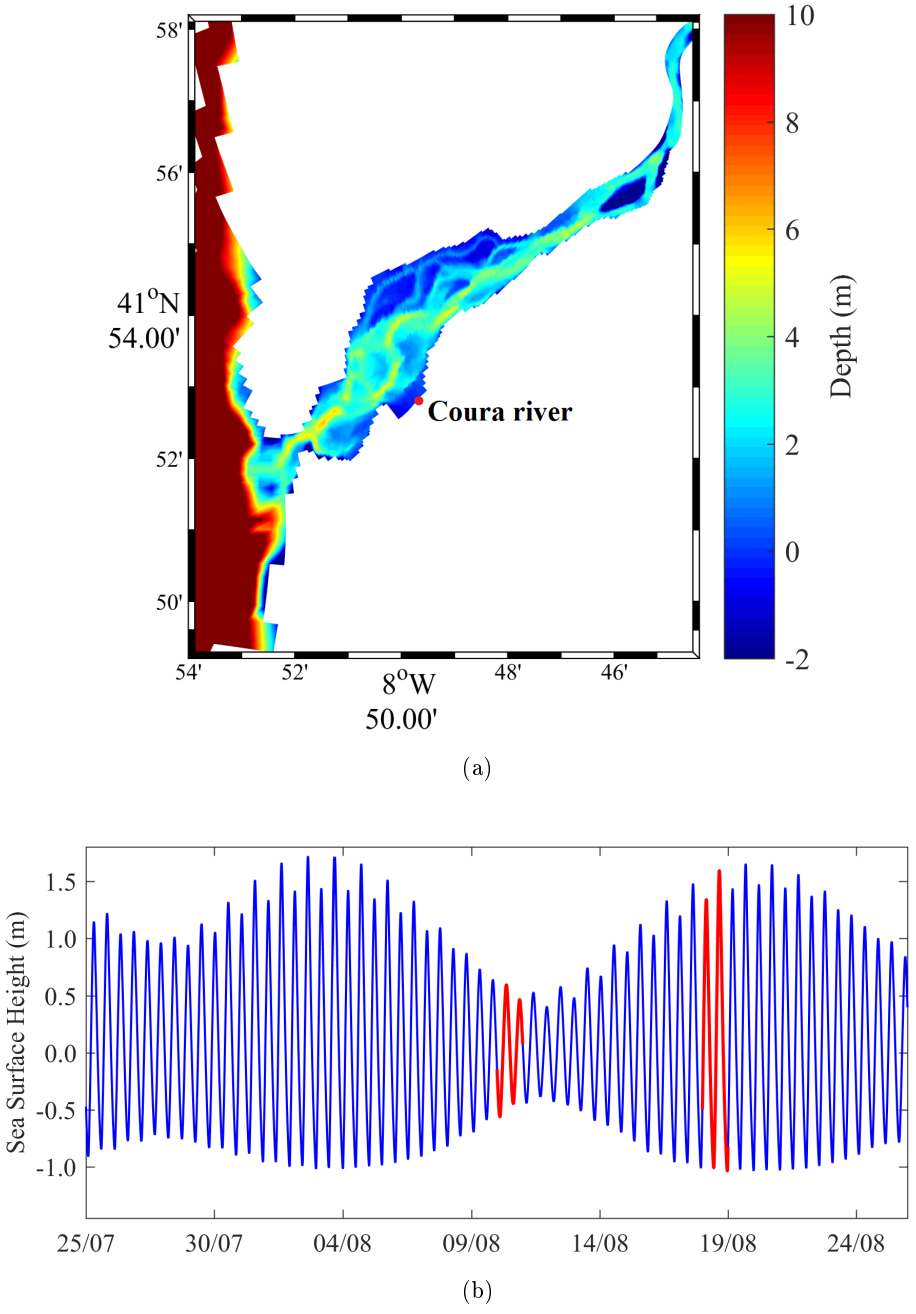

Figure 12: Location of the Coura river (a) and sea surface height for the period in which the point discharge of pollutants occurred (b) (red line represents the periods of points discharges of pollutants).

6 Model calibration results

This section aims to present the calibration results of the hydrodynamic model, the salt and heat transport model and the water quality model.

6.1 Hydrodynamic model calibration results

In the process of water level calibration several figures were made. Figure 13 represents the best comparison between the sea surface height predicted by the model and the observed data, in the six sampling sites shown in Figure 6.

To achieve these results, several simulations (as referred in Section 5.2.1) were made to improve the fit between predictions and observations and for this, the background friction was varied. The best results were obtained with the set of Manning values presented in Table 6.

Table 6: Bottom friction coefficients.

Depth (m)	Manning's n values
-20 $\leq$ h $<$ -2.5	0.025
-2.5 $\leq$ h $<$ -2	0.024
-2 $\leq$ h $<$ -1.5	0.023
-1.5 $\leq$ h $<$ -1	0.022
-1 $\leq$ h $<$ 0	0.021
0 $\leq$ h $<$ 0.5	0.020
0.5 $\leq$ h $<$ 1	0.019
1 $\leq$ h $<$ 3	0.017
3 $\leq$ h $<$ 10	0.016
10 $\leq$ h $<$ 5000	0.015

From the visual comparison between predictions and observations, it is verified that the values predicted by the numerical model closely follow the observed records, revealing that the numerical model reproduces exactly the propagation of the tide inside the two estuaries, with the exception of Barra and Seixas stations. In the Barra station, it is observed that the model presents a lower level than the data observed at the low tide, while in the Seixas station the opposite is observed (the predicted data present a relatively larger level than the observed in the periods of low tide). These differences in the two sites may result from constant changes in the bathymetry along these areas, since they have great sediment dynamics and accumulation (due to the flow and reflux currents near the mouth and the widening of the channel near Seixas [Reis et al., 2009]). Another fact that may explain these differences is that the bathymetric data used are from 2011 and this comparison is carried out with data measured in 2006, which can also cause small changes in the tidal amplitude.

As previously mentioned, the second step in model calibration consists of verifying phase and amplitude differences between the harmonic constituents (M_2, S_2, K_1 and O_1) for all six sites.

The results of this harmonic analysis can be found in Figures 14 (semidiurnal constituents) and 15 (diurnal constituents).

From Figures 14 and 15, it is verified that the differences of amplitude and phase between the predictions and observations are minimum, proving again that the model is reproducing well the tidal propagation within the estuaries.

The M_2 constituent has the largest amplitude difference in Seixas (24 cm) and the lowest one is observed in Vila Nova de Cerveira (1 cm). Regarding the phase difference, the largest

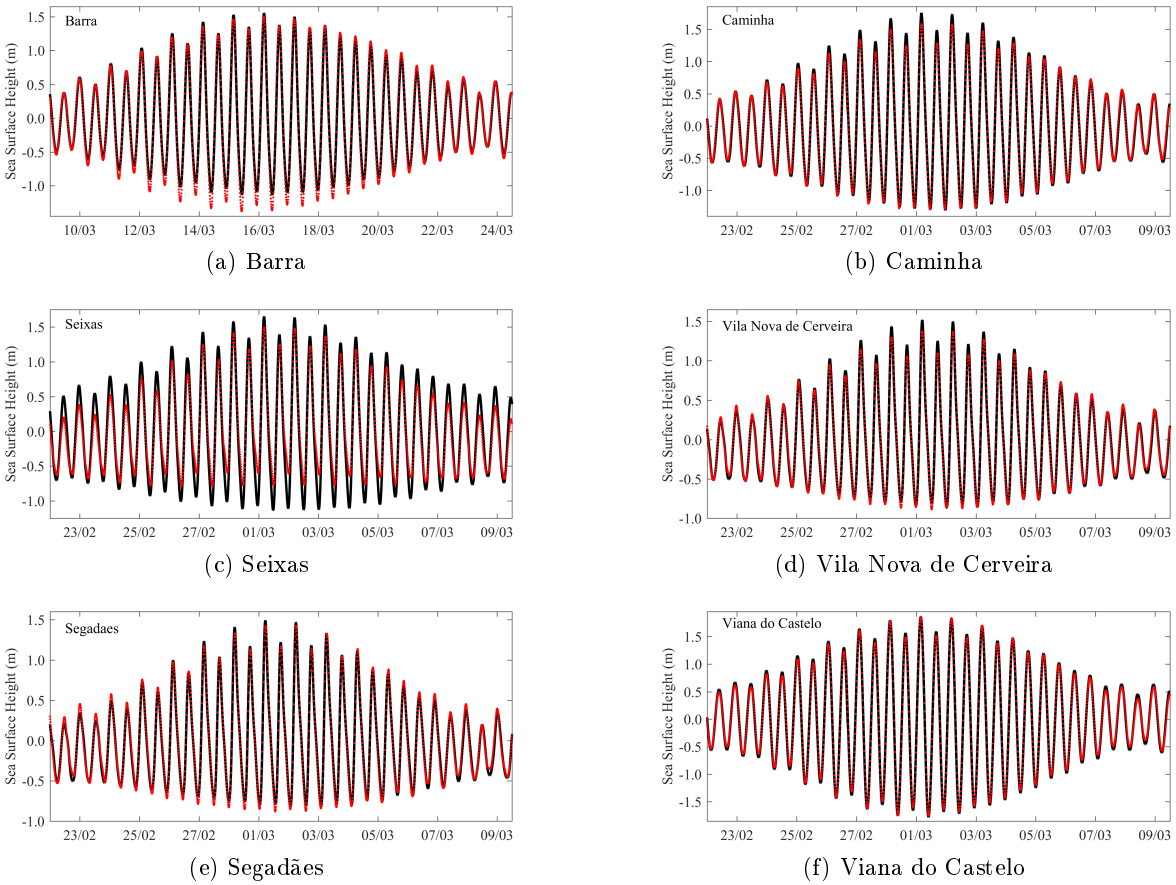

(a) Barra (b) Caminha

(c) Seixas (d) Vila Nova de Cerveira

(e) Segadães (f) Viana do Castelo

Figure 13: Comparison between predicted (black colour) and observed (red colour) sea surface height over a period of 15 days at the six sampling sites.

one was observed in Barra (10.35 min) and the lowest was observed in Segadães (2.49 min).

In the two estuaries, the smallest difference of amplitude for the S_2 constituent is observed in Cerveira, while the maximum amplitude difference for this constituent is observed in Barra (6 cm). The smallest phase difference in this constituent is observed in Caminha (0.83 min) and the highest difference is in Seixas (12.61 min).

Regarding the diurnal constituents, the constituent O_1 presents a smaller difference of amplitude in Barra and a larger one in Seixas (2 cm), whereas the constituent K_1 presents a smaller amplitude difference in Barra and in Caminha and a higher difference in Seixas (4 cm).

In general, the smallest errors are in the semidiurnal constituents, M_2 and S_2, whereas the largest errors are in the diurnal constituents, K_1 and O_1. These results show there is a suitable representation of the amplitude and phase of the main harmonic constituents by the numerical model.

As referred in Section 5.2.1, it was calculated the RMSE and SKILL for the 6 sampling sites. The results are presented in Table 7. From this table, is verified that the best results were obtained for Viana do Castelo, Caminha, Vila Nova de Cerveira and Segadães, and the worst results were found in Barra and Seixas, with an RMSE of 0.111 m and 0.201 m, respectively.

According to Dias et al. [2009], a SKILL greater than 0.99 indicates an excellent correlation between model predictions and observations. Thus, from the analysis of Table 7 is found that

Table 7: Error values for tidal water levels.

Estuary	Site	RMSE (m)	SKILL
Minho	Barra	0.111	0.994
	Caminha	0.072	0.997
	Seixas	0.201	0.974
	Vila Nova de Cerveira	0.048	0.998
	Segadães	0.056	0.997
Lima	Viana do Castelo	0.046	0.999

in all places, except Seixas, the SKILL is higher than 0.99, which again shows that model predictions and observations have an excellent agreement.

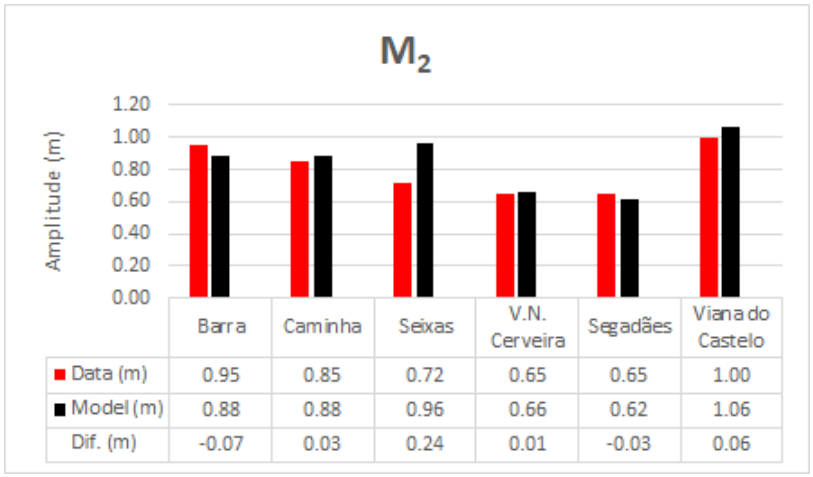

	Barra	Caminha	Seixas	V.N. Cerveira	Segadães	Viana do Castelo
Data (m)	0.95	0.85	0.72	0.65	0.65	1.00
Model (m)	0.88	0.88	0.96	0.66	0.62	1.06
Dif. (m)	-0.07	0.03	0.24	0.01	-0.03	0.06

(a) Constituent M_2 - Amplitude (m)

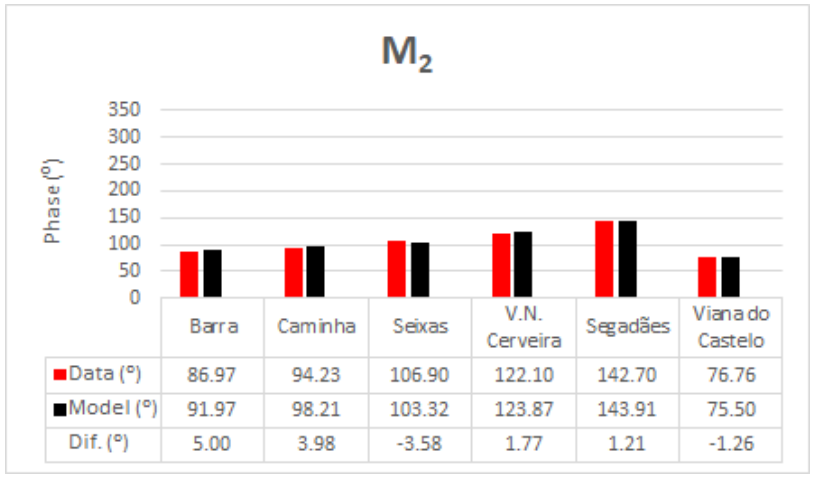

	Barra	Caminha	Seixas	V.N. Cerveira	Segadães	Viana do Castelo
Data (°)	86.97	94.23	106.90	122.10	142.70	76.76
Model (°)	91.97	98.21	103.32	123.87	143.91	75.50
Dif. (°)	5.00	3.98	-3.58	1.77	1.21	-1.26

(b) Constituent M_2 - Phase (°)

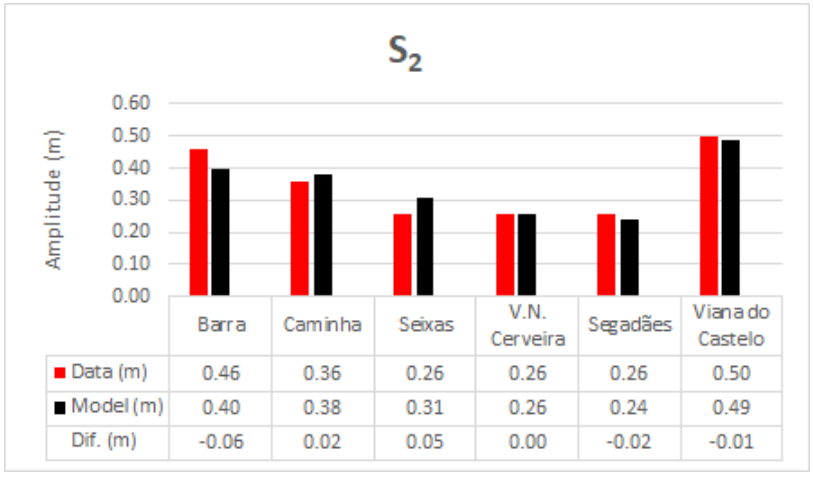

	Barra	Caminha	Seixas	V.N. Cerveira	Segadães	Viana do Castelo
Data (m)	0.46	0.36	0.26	0.26	0.26	0.50
Model (m)	0.40	0.38	0.31	0.26	0.24	0.49
Dif. (m)	-0.06	0.02	0.05	0.00	-0.02	-0.01

(c) Constituent S_2 - Amplitude (m)

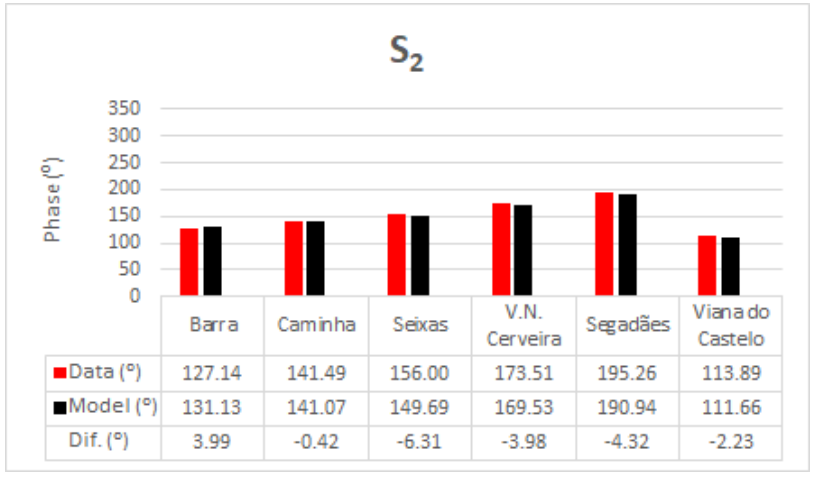

	Barra	Caminha	Seixas	V.N. Cerveira	Segadães	Viana do Castelo
Data (°)	127.14	141.49	156.00	173.51	195.26	113.89
Model (°)	131.13	141.07	149.69	169.53	190.94	111.66
Dif. (°)	3.99	-0.42	-6.31	-3.98	-4.32	-2.23

(d) Constituent S_2 - Phase (°)

Figure 14: Harmonic comparison between predicted and observed semidiurnal constituents (M_2 and S_2) for six tidal stations spatially distributed in the Minho and Lima estuaries and differences between model predictions and observations.

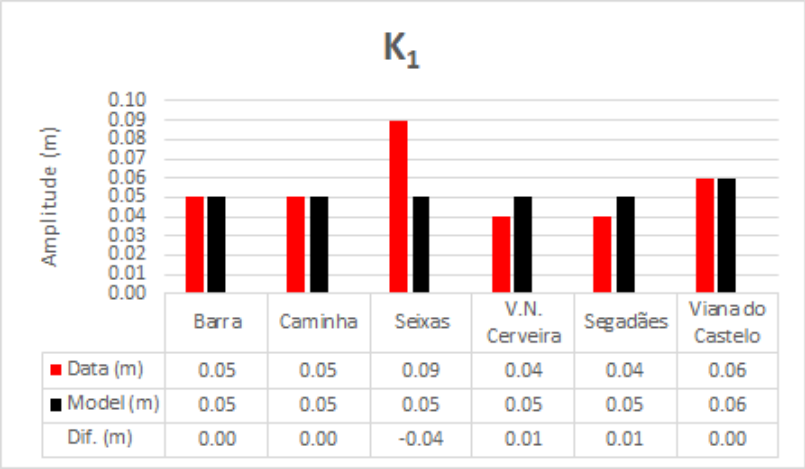

	Barra	Caminha	Seixas	V.N. Cerveira	Segadães	Viana do Castelo
Data (m)	0.05	0.05	0.09	0.04	0.04	0.06
Model (m)	0.05	0.05	0.05	0.05	0.05	0.06
Dif. (m)	0.00	0.00	-0.04	0.01	0.01	0.00

(a) Constituent K_1 - Amplitude (m)

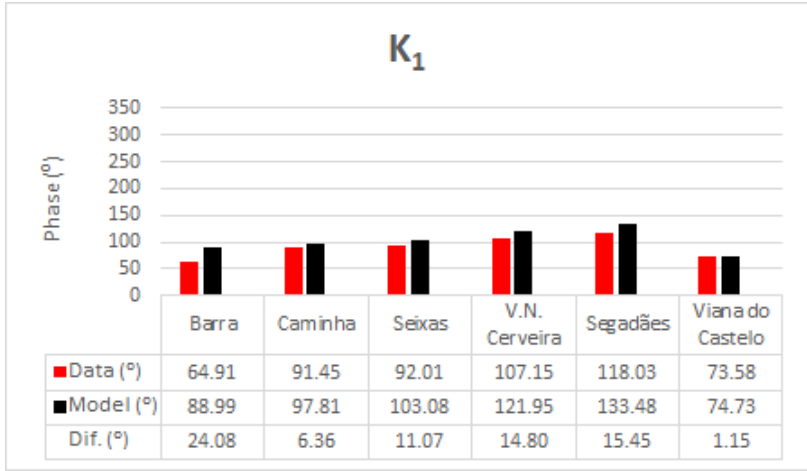

	Barra	Caminha	Seixas	V.N. Cerveira	Segadães	Viana do Castelo
Data (°)	64.91	91.45	92.01	107.15	118.03	73.58
Model (°)	88.99	97.81	103.08	121.95	133.48	74.73
Dif. (°)	24.08	6.36	11.07	14.80	15.45	1.15

(b) Constituent K_1 - Phase (°)

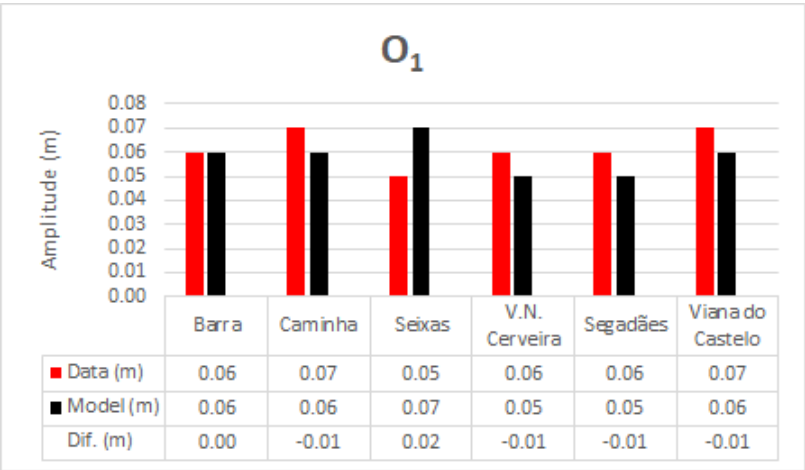

	Barra	Caminha	Seixas	V.N. Cerveira	Segadães	Viana do Castelo
Data (m)	0.06	0.07	0.05	0.06	0.06	0.07
Model (m)	0.06	0.06	0.07	0.05	0.05	0.06
Dif. (m)	0.00	-0.01	0.02	-0.01	-0.01	-0.01

(c) Constituent O_1 - Amplitude (m)

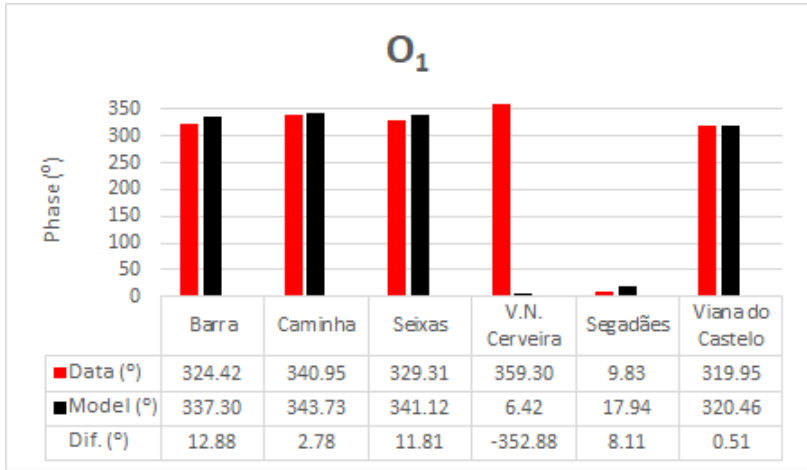

	Barra	Caminha	Seixas	V.N. Cerveira	Segadães	Viana do Castelo
Data (°)	324.42	340.95	329.31	359.30	9.83	319.95
Model (°)	337.30	343.73	341.12	6.42	17.94	320.46
Dif. (°)	12.88	2.78	11.81	-352.88	8.11	0.51

(d) Constituent O_1 - Phase (°)

Figure 15: Harmonic comparison between predicted and observed diurnal constituents (K_1 and O_1) for six tidal stations spatially distributed in the Minho and Lima estuaries and differences between model predictions and observations.

6.2 Salt and heat transport model calibration results

Once the hydrodynamic model was calibrated, it was possible to proceed to the calibration of the salt and heat transport model.

For salinity and water temperature calibration, a comparison was made between the model predictions and the observed data collected by Vieira et al. [2015], in the same period of time (1 February 2012 to 1 February 2013).

Once the observations are punctual data (Tables 13, 14, 15 and 16, in Appendix) over a given period of time, it will only be possible to identify patterns and seasonal evolutions in each estuary.

The comparison between the predicted and observed water temperature and salinity can be observed in Figures 16 to 19 (only Transects 1, 3, 5 and 7 will be presented, as referred to in Section 5.2.2).

When analysing the water temperature results (Figures 16 and 17), it is verified that the model is representing this variable well in both estuaries, observing maximum differences between predictions and observations around 2 °C. Regarding salinity (Figures 18 and 19), the model represents the observed data reasonably, presenting in some months high differences. However, some of the observed points are inside the error bar (representing the uncertainty of sampling time).

After performing this analysis, the RMSE (Equation 35) was calculated to quantify the model accuracy in each transept (transects shown in Figure 7). Results obtained for the RMSE calculation are presented in Tables 8 and 9.

Table 8: Error values for water temperature and salinity for Minho estuary.

Estuary	Site	RMSE for water temperature (°C)	RMSE for salinity (ppt)
Minho	Transept 1	1.549	7.037
	Transept 2	1.295	6.202
	Transept 3	1.151	3.756
	Transept 4	1.310	5.879
	Transept 5	1.084	5.451
	Transept 6	1.308	5.470
	Transept 7	1.647	6.105

Table 9: Error values for water temperature and salinity for Lima estuary.

Estuary	Site	RMSE for water temperature (°C)	RMSE for salinity (ppt)
Lima	Transept 1	0.706	1.824
	Transept 2	0.839	2.742
	Transept 3	0.624	3.152
	Transept 4	0.729	3.789
	Transept 5	0.689	4.714
	Transept 6	0.820	5.780
	Transept 7	1.005	4.687

Through the analysis of Tables 8 and 9, the same conclusions are obtained, since the maximum differences between predictions and observations in the water temperature are around 1.65 °C and in the salinity can reach 7 ppt (usually, the Minho estuary presents higher errors, due mainly to the fact that this river has higher flows discharges).

The differences found between predictions and observations for salinity and water temperature may be due to several factors:

- Simulations performed with a 2D model can cause differences between predictions and observations, since the water samples collected by Vieira et al. [2015] were measured at various depths and the two-dimensional model integrates the data vertically, only considering an average value for the entire water column;
- The existence of dams in both estuaries cause uncertainties in the freshwater inflows imposed, since the river discharges are controlled and depends on the climatic conditions of the region (e.g.: if the period is dry, there will be a lower river discharges);
- The exact time at which the sampling was done was registered, which may also cause some deviations between predictions and observations (e.g.: in just over 10 minutes, the salinity at a location within the estuary can range from 30 ppt to 20 ppt, especially when there are large river discharges from dams);
- Some small tributaries of freshwater along the rivers were not considered (e.g.: Louro river, Tea river, Coura river, ...), and may lead to small changes in the estuarine dynamics and in the values of salinity and water temperature, since with higher freshwater inputs the water will present a lower salinity;
- Groundwater outcrops are not being considered, and these can introduce colder and saline waters inside the estuaries, causing slight deviations in the values of water temperature and salinity;
- Small sand bars existing along the estuary were not considered, and may cause minor changes in local currents;
- Coastal defence works, harbour areas and coastal banks have not been represented in detail (due to the resolution of the grid), and may cause changes in estuarine circulation patterns.

From the results is concluded that although there are some differences between model predictions and observations, in some months of the year, the model demonstrates a good representation of real salt and heat transport.

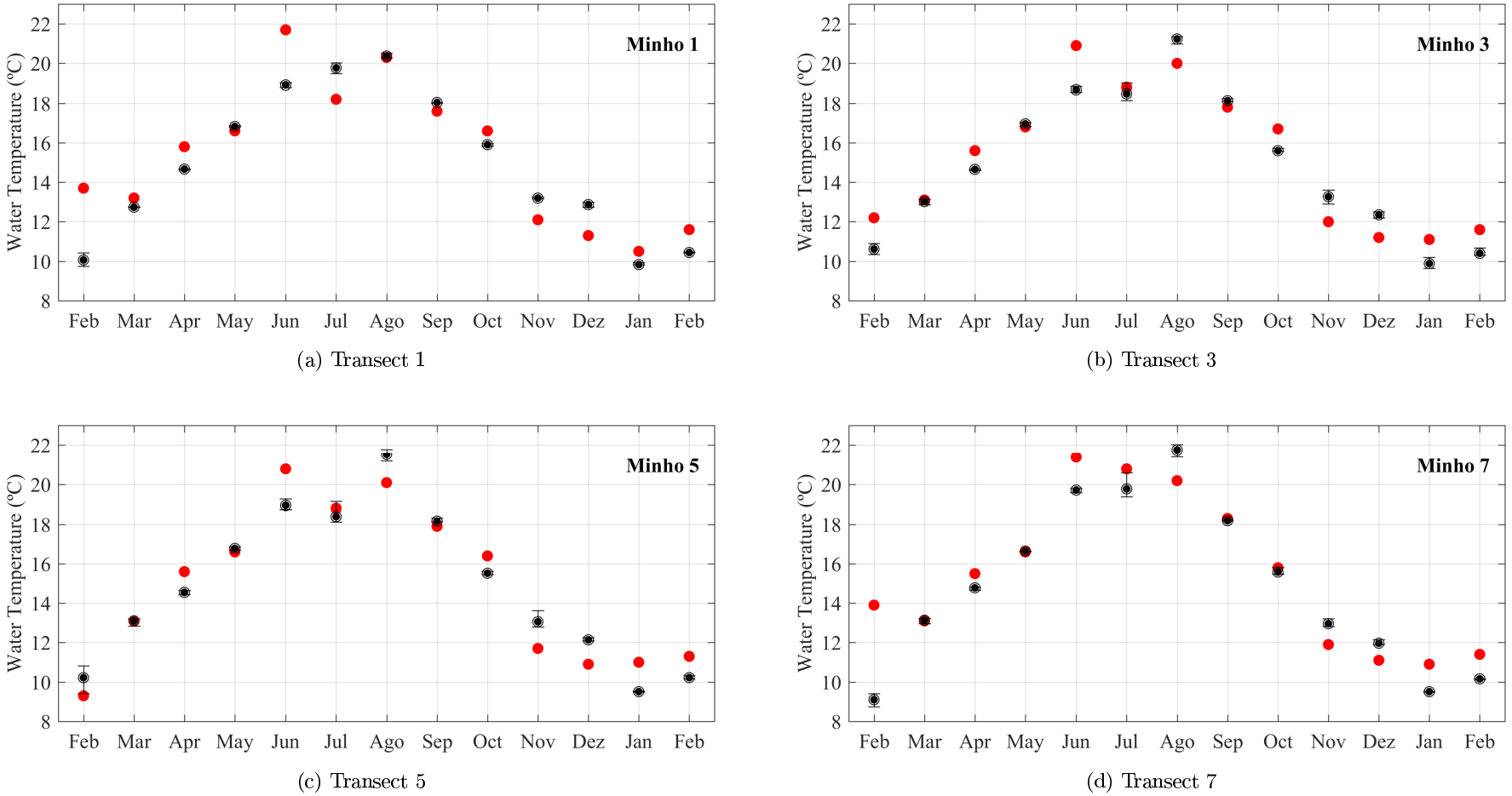

(a) Transect 1

(b) Transect 3

(c) Transect 5

(d) Transect 7

Figure 16: Comparison between predicted (black colour) and observed (red colour) water temperature in transects 1, 3, 5 and 7 of the Minho river.

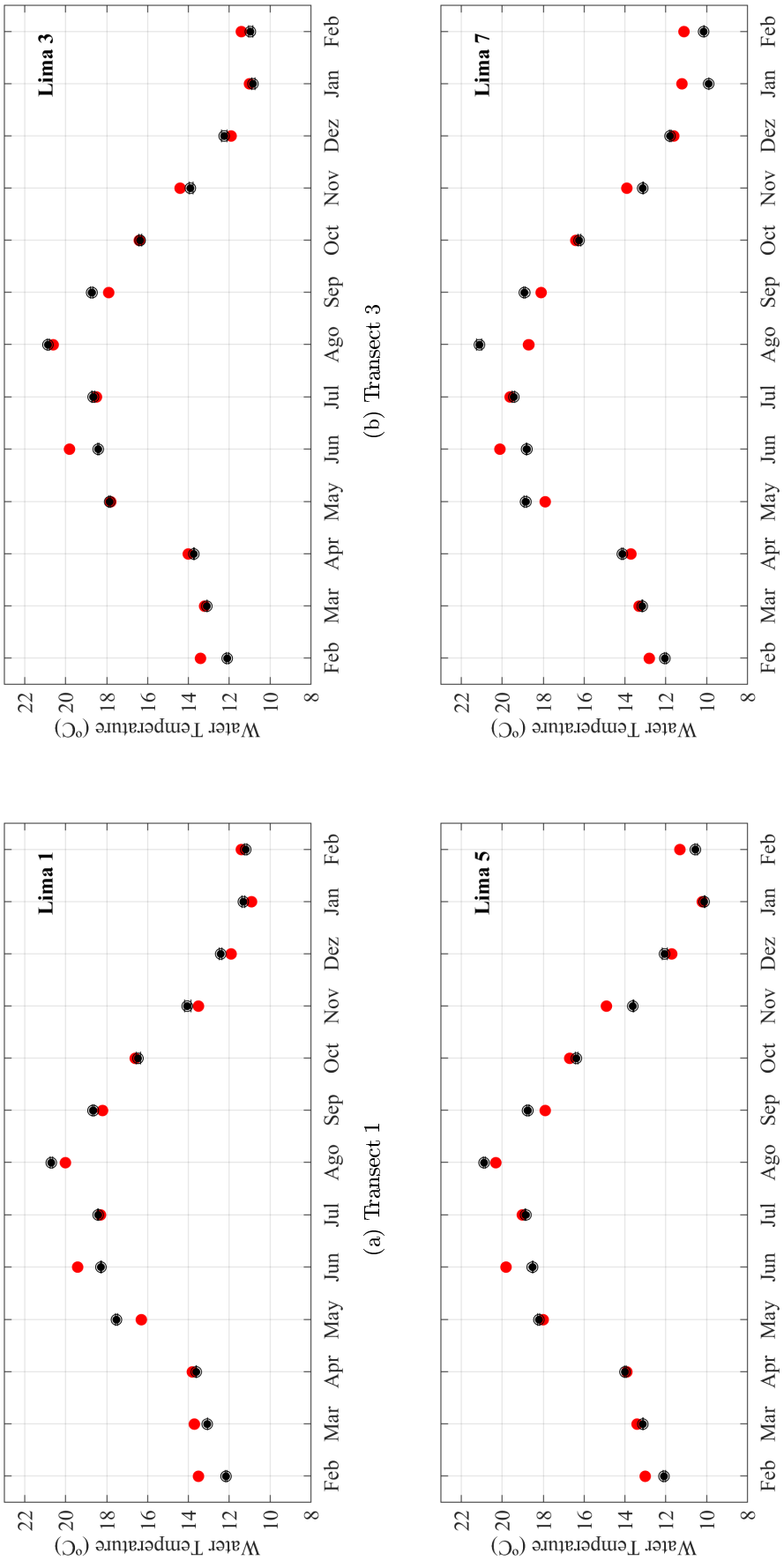

(a) Transect 1 (b) Transect 3

(c) Transect 5 (d) Transect 7

Figure 17: Comparison between predicted (black colour) and observed (red colour) water temperature in transects 1, 3, 5 and 7 of the Lima river.

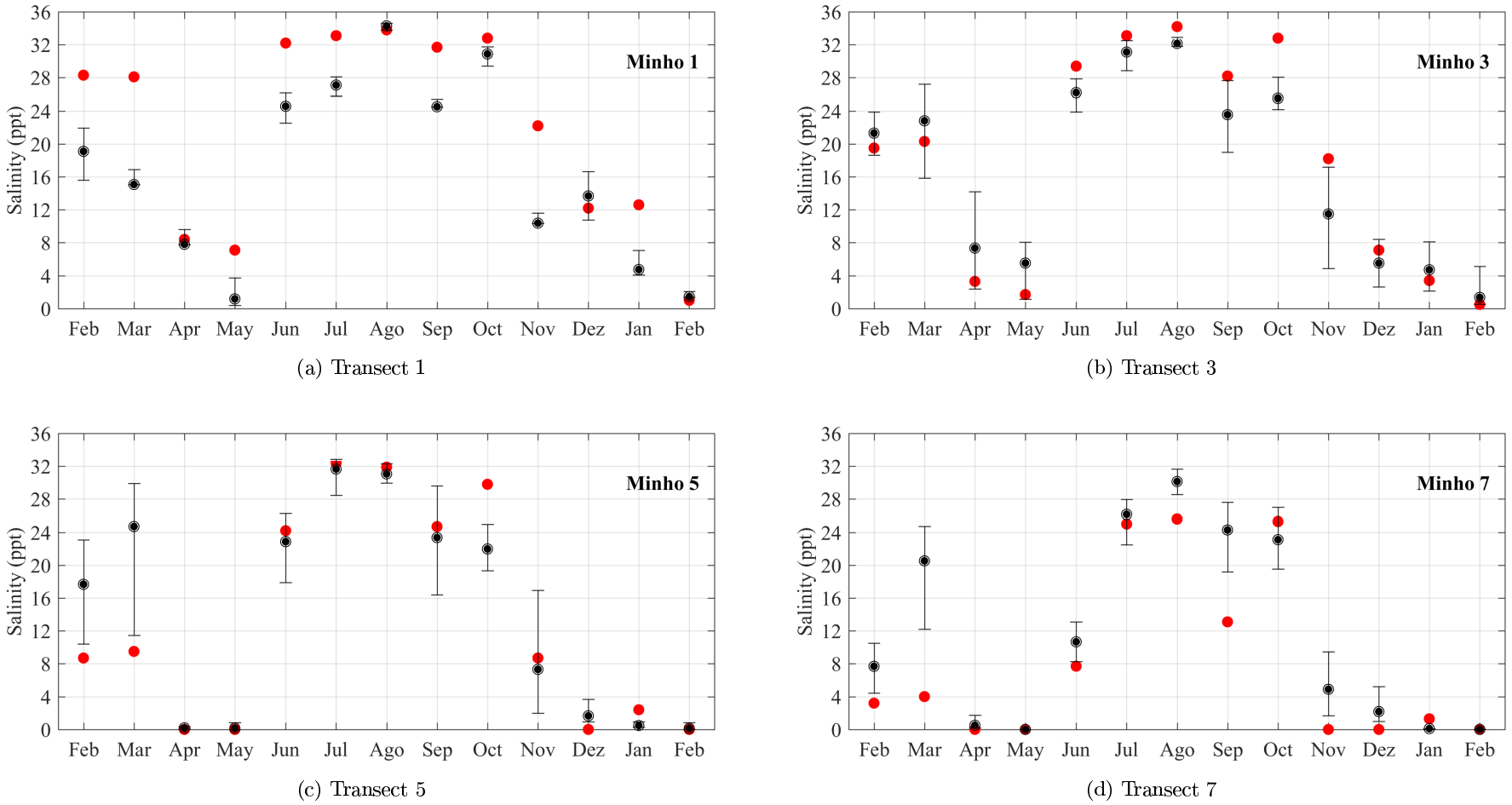

(a) Transect 1

(b) Transect 3

(c) Transect 5

(d) Transect 7

Figure 18: Comparison between predicted (black colour) and observed (red colour) salinity in transects 1, 3, 5 and 7 of the Minho river.

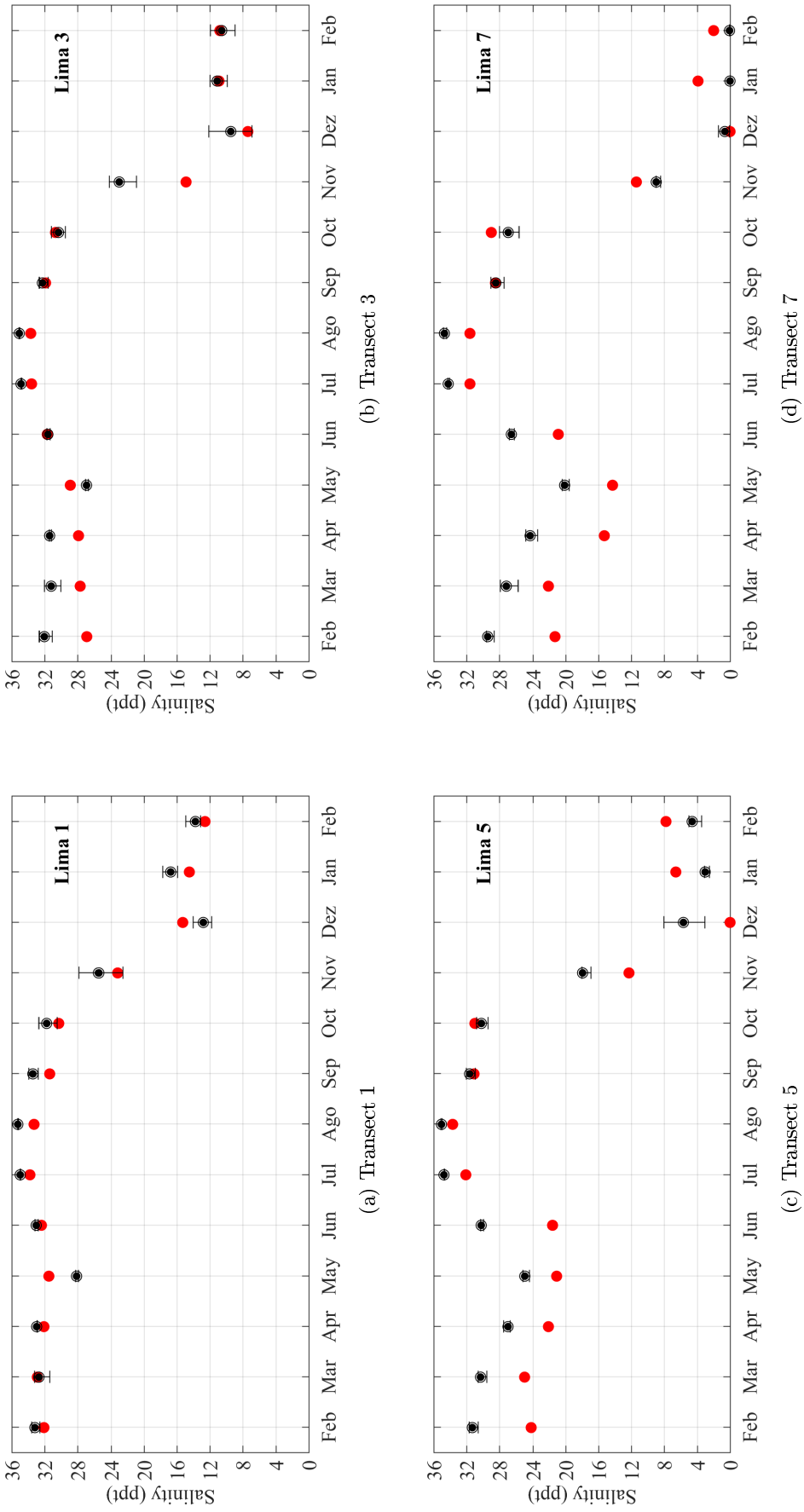

(a) Transect 1 (b) Transect 3

(c) Transect 5 (d) Transect 7

Figure 19: Comparison between predicted (black colour) and observed (red colour) salinity in transects 1, 3, 5 and 7 of the Lima river.

6.3 Water quality model calibration results

Once the hydrodynamic modulus (hydrodynamic model and salt and heat transport model) are calibrated, it is possible to calibrate the water quality model.

To achieve this task, several simulations (as referred in Section 5.2.3) were made to improve the fit between predictions and observations and for this, the total respiration flux was changed accordingly.

Given that in theory the concentration of dissolved oxygen in winter is high (there is more production rate than respiration), the total respiration flux was considered to be about 50% lower than that of total net primary production. For the summer months, there is more consumption than production and it was considered that the rate was about 50% higher than the total net primary production.

The best results obtained are presented in Table 10.

Table 10: Ratios used to obtain the values of total respiration flux.

Dissolved oxygen (mg O2/L)	Ratios
$12 \leq O2 < 13$	0.5
$11 \leq O2 < 12$	0.7
$10 \leq O2 < 11$	0.9
$9 \leq O2 < 10$	1.1
$8 \leq O2 < 9$	1.3
$7 \leq O2 < 8$	1.5

After defining the total respiration flux, simulations were performed to assess the model accuracy in repreducing nutrients dynamics.

For the calibration of nutrients (ammonia, nitrates and orthophosphates) and dissolved oxygen, a comparison was made between model predictions and the observed data collected by Vieira et al. [2015].

The comparison between predicted and observed ammonia, as well as nitrates, orthophosphates and dissolved oxygen, can be observed in Figures 20 to 27.

Comparing the predictions with observations, it is found that the largest differences between predicted (black colour) and observed (red colour) nitrate occur in the winter months (December, January and February) in both estuaries. This can be due to the fact that these periods are very rainy and the river discharges are relatively high, providing transport of large amounts of nutrients (nutrients from human activities, agricultural field runoff, industrial effluents and sewage from urban areas). For the remaining months, the model tends to underestimate concentrations.

Regarding to orthophosphate, is observed that predictions follow the pattern of the observations in some transepts, but the model cannot represent a few months, because the data observed presents very high concentrations. These high concentrations indicate the possibility of discharges of domestic effluents, industrial effluents and sewage existing along the estuaries [Santos et al., 2013], and these point sources are not accounted for in the numerical simulations performed.

For ammonium, it is observed that the model cannot simulate accurately the observed concentrations in the two estuaries under study. These differences between predicted and observed data can be further justified by the fact that there are illegal discharges of domestic and industrial effluents throughout the study area [Santos et al., 2013], leading to an increase in ammonium values. Another possibility is that the model may assume a rate of nitrification faster than observed, leading to total nitrification of the ammonium (ammonium is fully

converted to nitrate).

Finally, in spite of the observed differences between predicted and observed data of dissolved oxygen, the model reproduces the theoretical annual standard of dissolved oxygen, since in the summer months there are lower concentrations of dissolved oxygen (higher consumption of oxygen than production) while in winter there are higher concentrations of dissolved oxygen [higher production of oxygen than respiration (consumption)]. Another justification for this theoretical standard is that the higher the water temperature and salinity, the lower the concentration of oxygen, so in the summer months, where the water is warmer and more saline, it will be observed lower O_2 concentrations, which cannot be found in the observations.

After performing this analysis, the RMSE (Equation 35) and CF (Equation 37) were calculated for all months of the year under study, in order to quantify the accuracy of the model in each transept (transects shown in Figure 7). The results obtained with the RMSE and CF calculations are presented in Tables 11 and 12.

Table 11: RMSE for nitrates (NITR), orthophosphates (PHOS) and dissolved oxygen (OXY).

	RMSE					
	Minho			Lima		
	OXY	NITR	PHOS	OXY	NITR	PHOS
Mar	0.58	0.77	0.06	1.16	0.86	0.05
Apr	0.94	1.02	0.13	1.48	0.99	0.08
May	1.13	0.89	0.11	0.94	0.48	0.42
Jun	2.09	0.47	0.04	1.23	0.48	0.05
Jul	1.12	0.35	0.09	1.41	0.68	0.09
Aug	2.48	0.54	0.06	2.45	0.77	0.08
Sep	1.68	0.96	0.09	1.29	0.57	0.27
Oct	2.84	0.66	0.20	3.19	1.21	0.30
Nov	2.79	1.83	0.29	2.72	0.96	0.36
Dez	1.09	2.15	0.17	1.75	2.01	0.03
Jan	2.47	2.77	0.21	1.29	2.15	0.05
Feb	0.27	2.39	0.17	0.79	2.09	0.16

From the analysis of Table 11 is verified that on average the highest RMSE values are found in the winter months in both estuaries. These differences are mainly due to the fact that there are large river discharges at this time and considering that in the open water boundary was not imposed a continuous temporary series for the period under study, but rather climatologic data. In relation to CF, is found that the model is on average in the "good" data category (values between 1 and 2), showing a good level of adjustment between the two data sets in both estuaries. However, in the winter months there are minor adjustments (values > 3). The high CF values for dissolved oxygen in August, September and November may be due to problems in the field measurements, since the values of dissolved oxygen concentration observed are very high for the values of measured salinity and water temperature.

The differences found between predictions and observations may be due to several factors:

- The model only considers algae as primary producers (e.g.: Cyano-bacteria and Microphytobenthos were not considered). If the activity of the remaining primary producers were also modelled, there could be some improvement in the adjustment between predicted and observed nutrient and dissolved oxygen concentrations, since there would be higher nutrient consumption and higher photosynthesis;

Table 12: CF for nitrates (NITR), orthophosphates (PHOS) and dissolved oxygen (OXY).

	CF					
	Minho			Lima		
	OXY	NITR	PHOS	OXY	NITR	PHOS
Mar	0.50	0.86	0.72	0.70	0.80	0.52
Apr	0.69	0.53	0.63	0.76	0.62	1.52
May	0.56	0.62	0.66	0.43	0.93	0.77
Jun	1.94	0.55	0.74	1.04	0.98	0.65
Jul	0.98	0.38	0.48	1.26	0.46	0.72
Aug	5.15	0.66	0.61	1.48	0.98	0.68
Sep	4.78	1.21	2.74	9.46	0.38	0.51
Oct	3.13	0.62	0.40	3.50	0.36	0.36
Nov	10.26	2.58	0.43	8.65	1.64	0.30
Dez	13.54	6.50	0.44	31.21	18.33	0.76
Jan	2.06	6.62	2.34	0.80	8.20	1.72
Feb	5.03	6.06	4.64	6.84	4.17	0.34

- The conversion described in the following articles EPA [2007] and Kacikoc and Beyhan [2014] may not be the best for estuaries under study.
- Point discharges of pollutants along estuaries have not been inserted and may cause local changes in nutrient concentration and dissolved oxygen;
- Geochemical processes and substances were not considered in the model, having these large impacts on nutrient concentrations in the water column and in the mineralization processes.

It is important to note that some of the factors mentioned in Section 6.2 may also have impact on the accuracy of the water quality model.

After this analysis, it can be assumed that the results of the model are reliable and in general terms the model represents well the expected annual standards of the substances under study, with the exception of ammonium. Since ammonia does not show a good adjustment between predictions and observations, this parameter was not analysed hereafter.

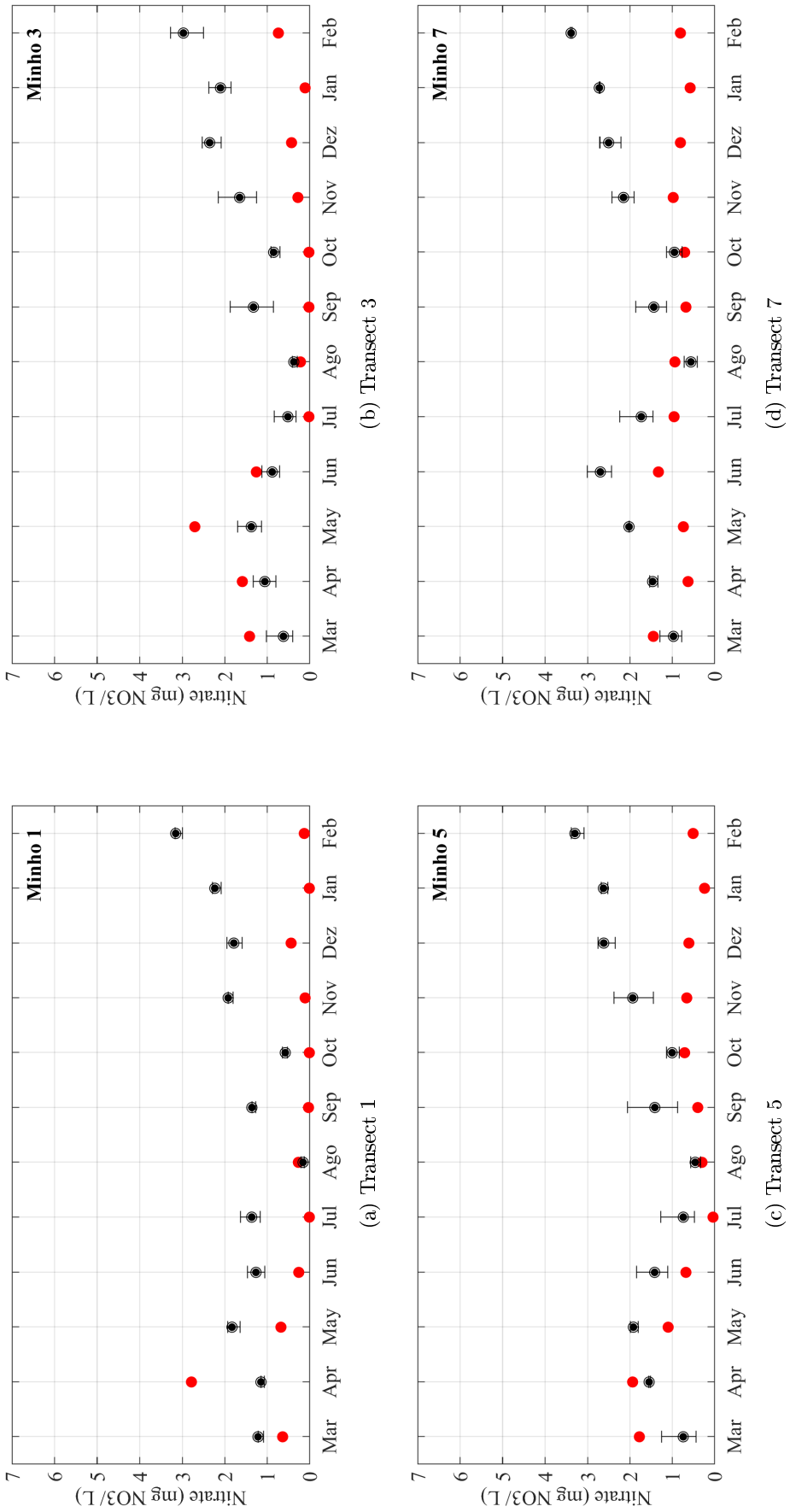

(a) Transect 1 (b) Transect 3

(c) Transect 5 (d) Transect 7

Figure 20: Comparison between predicted (black colour) and observed (red colour) nitrate in transects 1, 3, 5 and 7 of the Minho river.

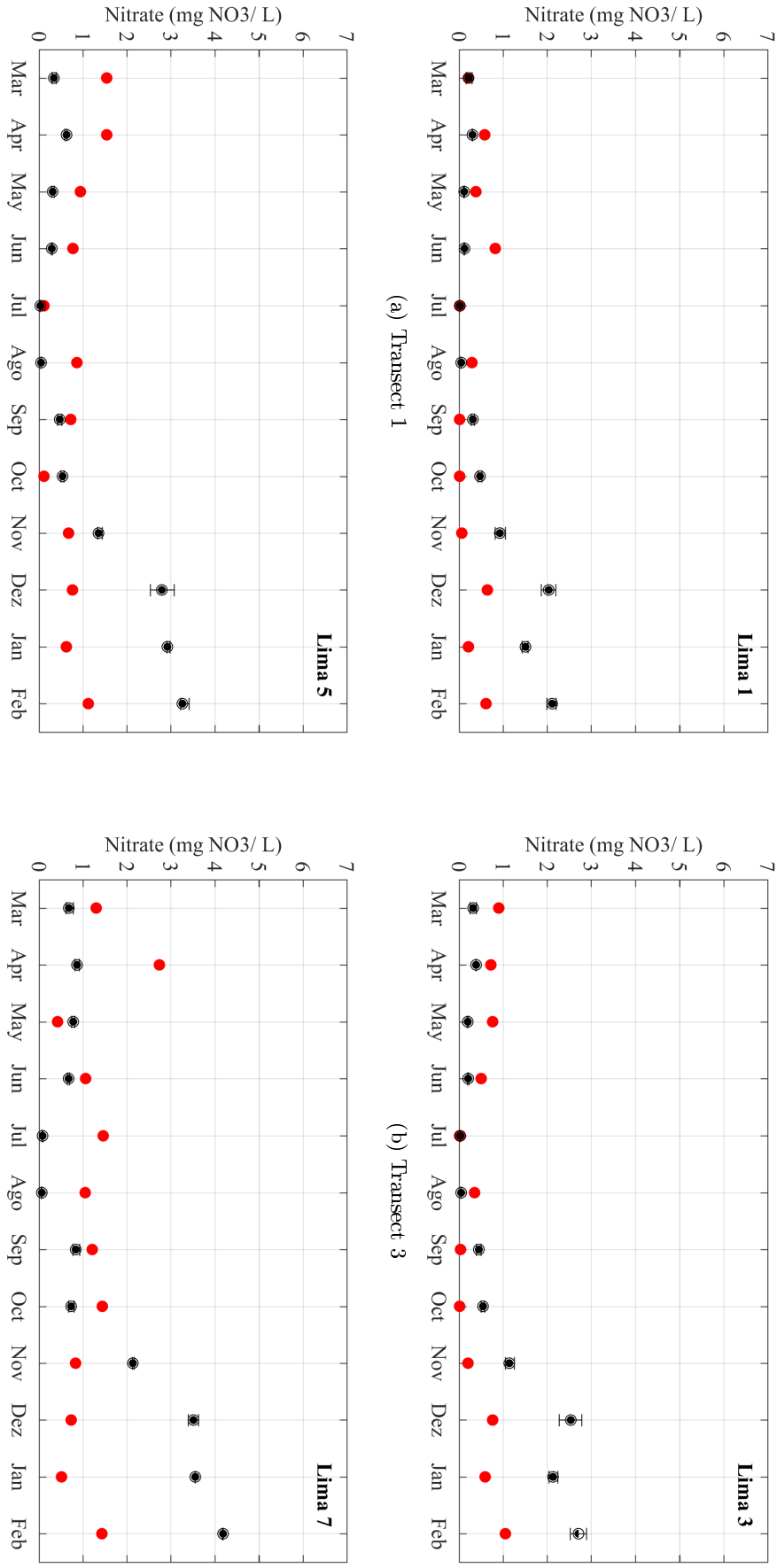

(a) Transect 1 (b) Transect 3

(c) Transect 5 (d) Transect 7

Figure 21: Comparison between predicted (black colour) and observed (red colour) nitrate in transects 1, 3, 5 and 7 of the Lima river.

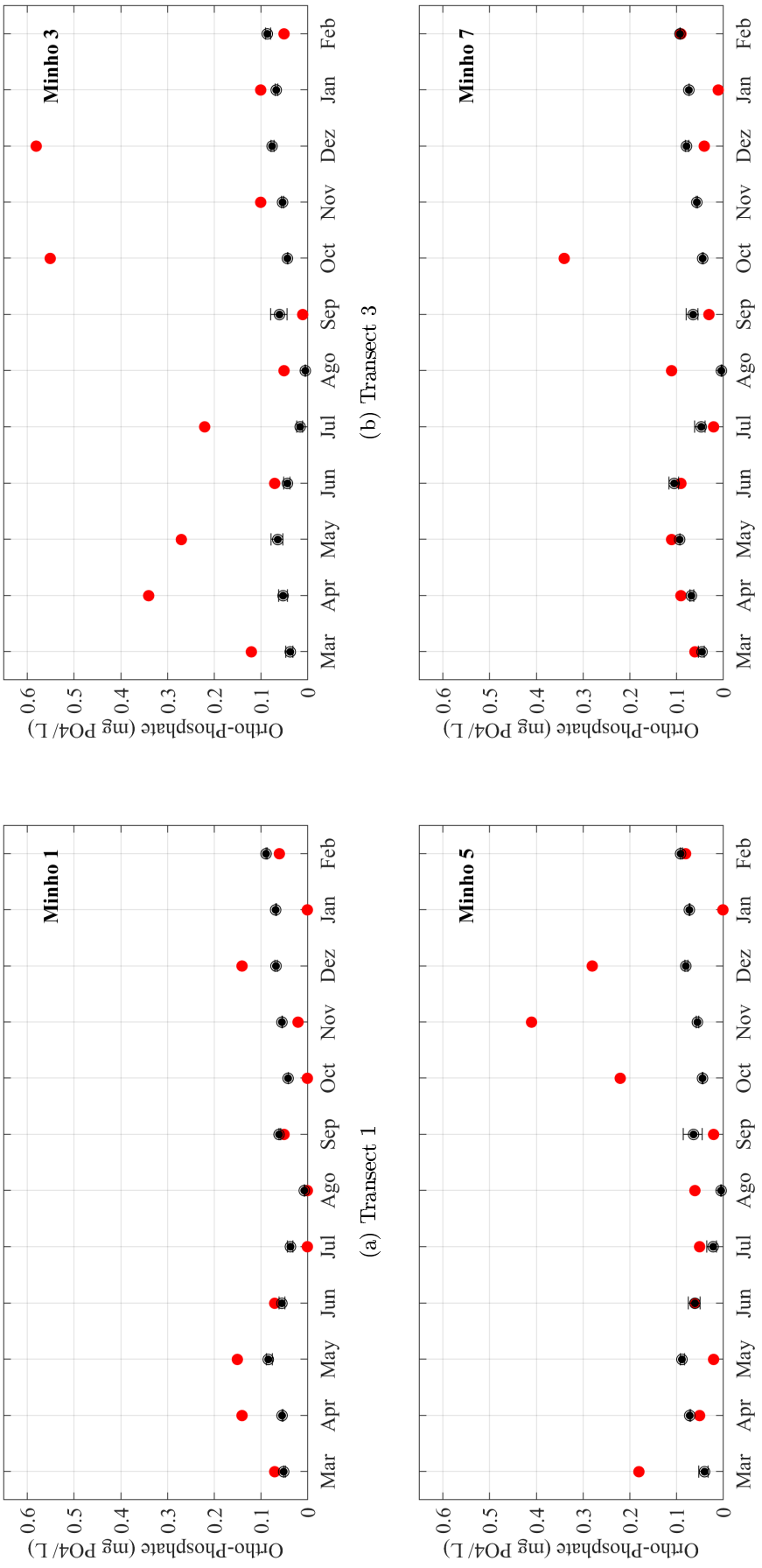

(a) Transect 1 (b) Transect 3 (c) Transect 5 (d) Transect 7

Figure 22: Comparison between predicted (black colour) and observed (red colour) orthophosphates in transects 1, 3, 5 and 7 of the Minho river.

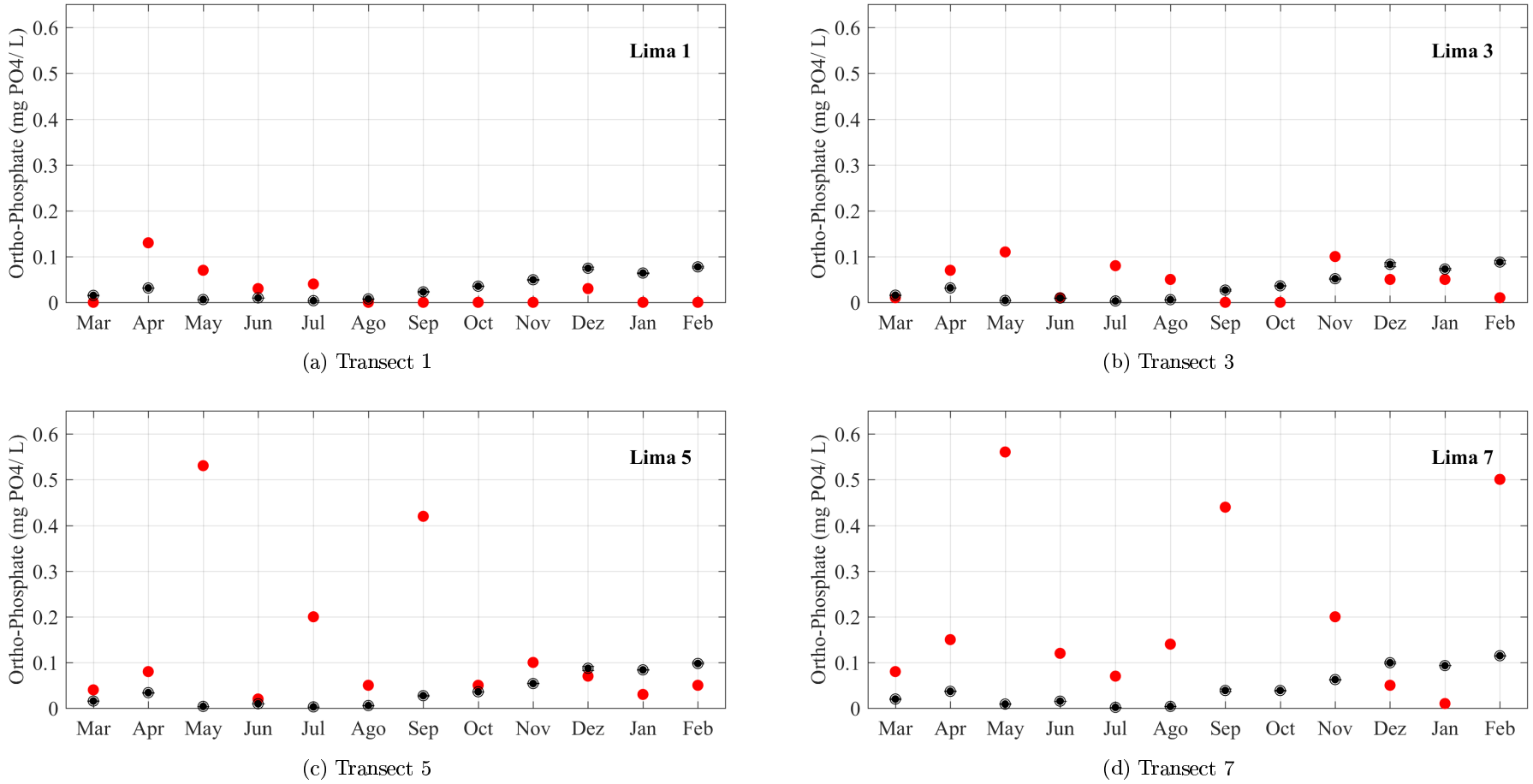

(a) Transect 1

(b) Transect 3

(c) Transect 5

(d) Transect 7

Figure 23: Comparison between predicted (black colour) and observed (red colour) orthophosphates in transects 1, 3, 5 and 7 of the Lima river.

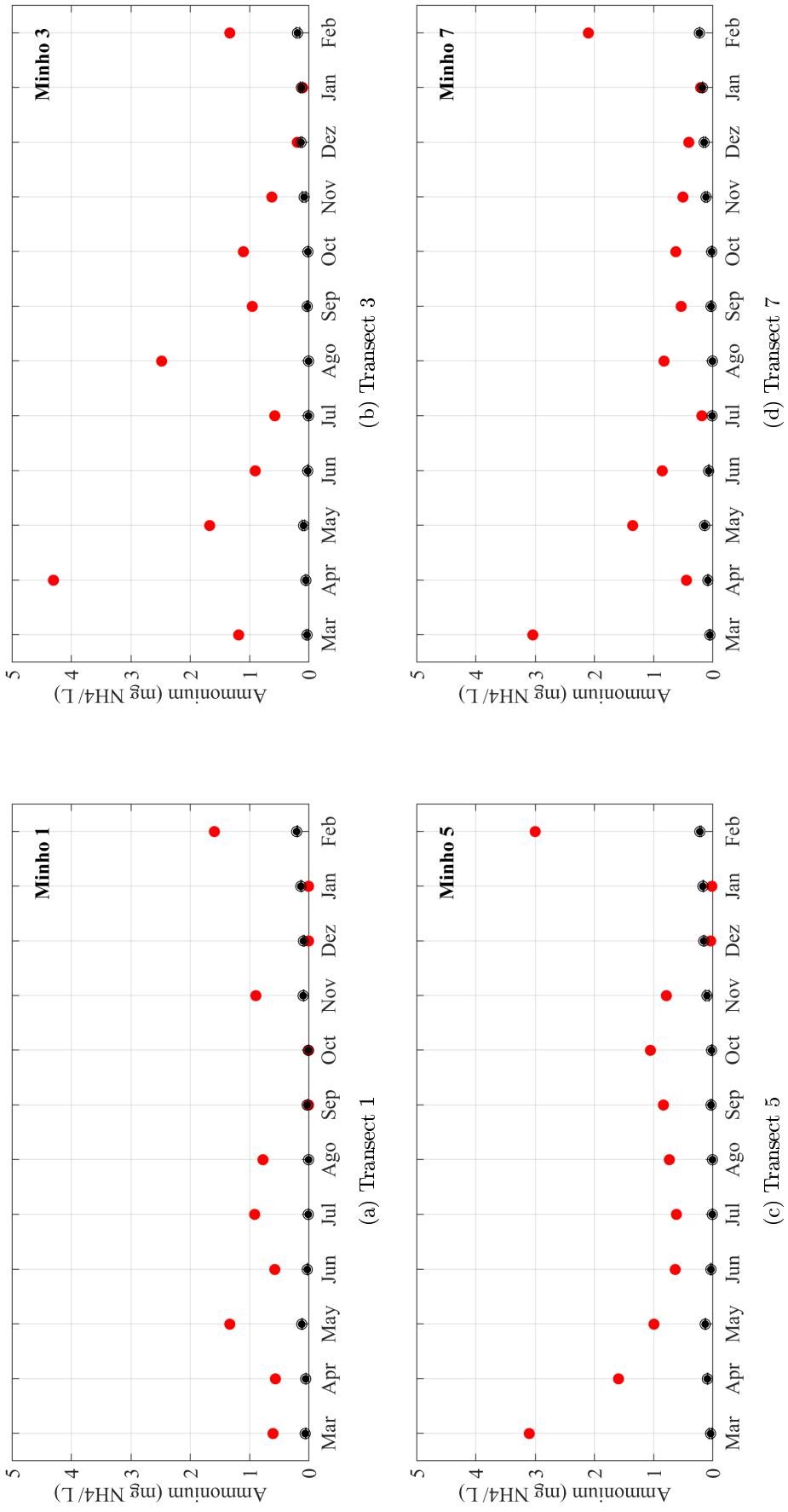

(a) Transect 1 (b) Transect 3

(c) Transect 5 (d) Transect 7

Figure 24: Comparison between predicted (black colour) and observed (red colour) ammonium in transects 1, 3, 5 and 7 of the Minho river.

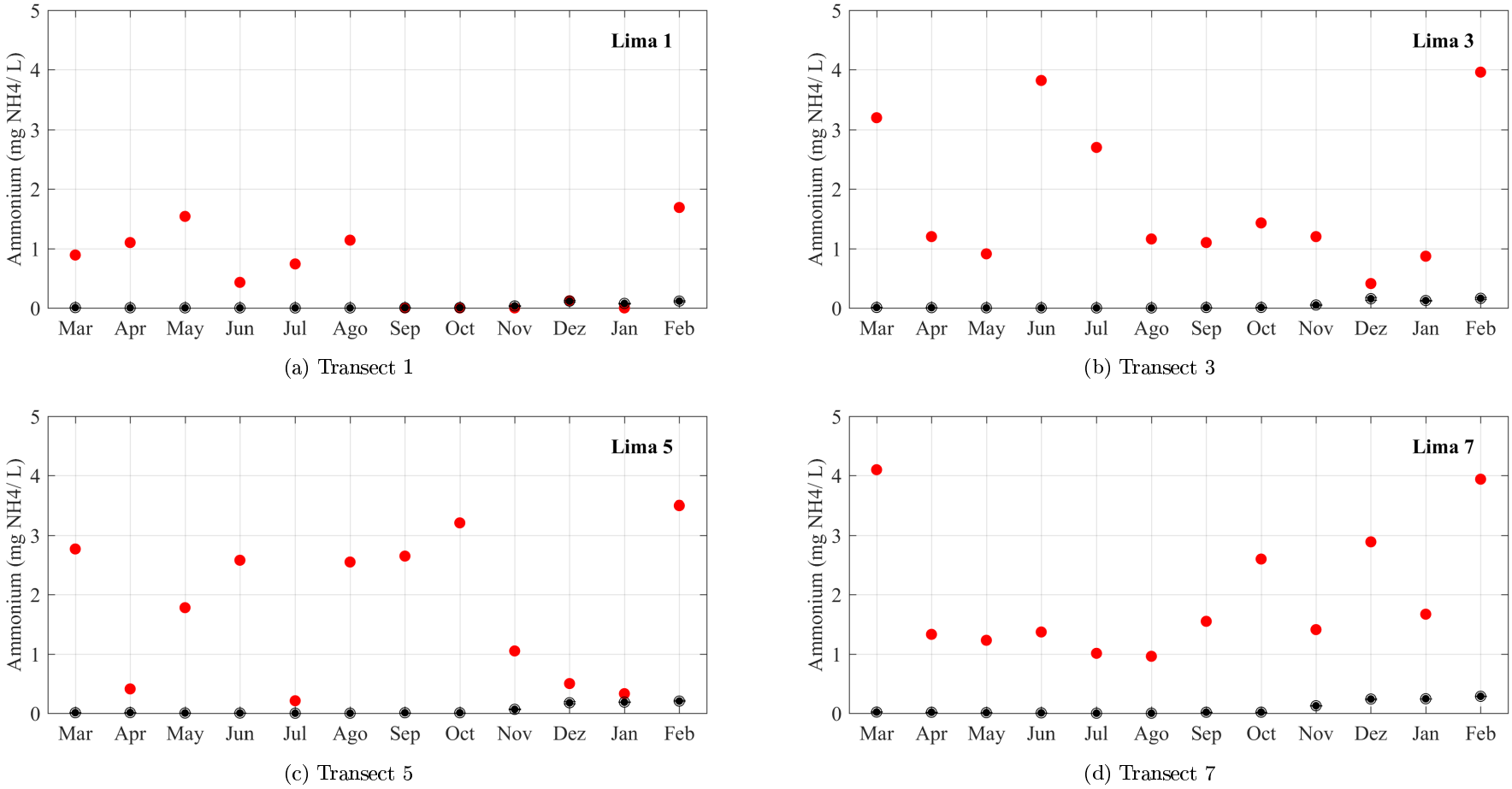

(a) Transect 1

(b) Transect 3

(c) Transect 5

(d) Transect 7

Figure 25: Comparison between predicted (black colour) and observed (red colour) ammonium in transects 1, 3, 5 and 7 of the Lima river.

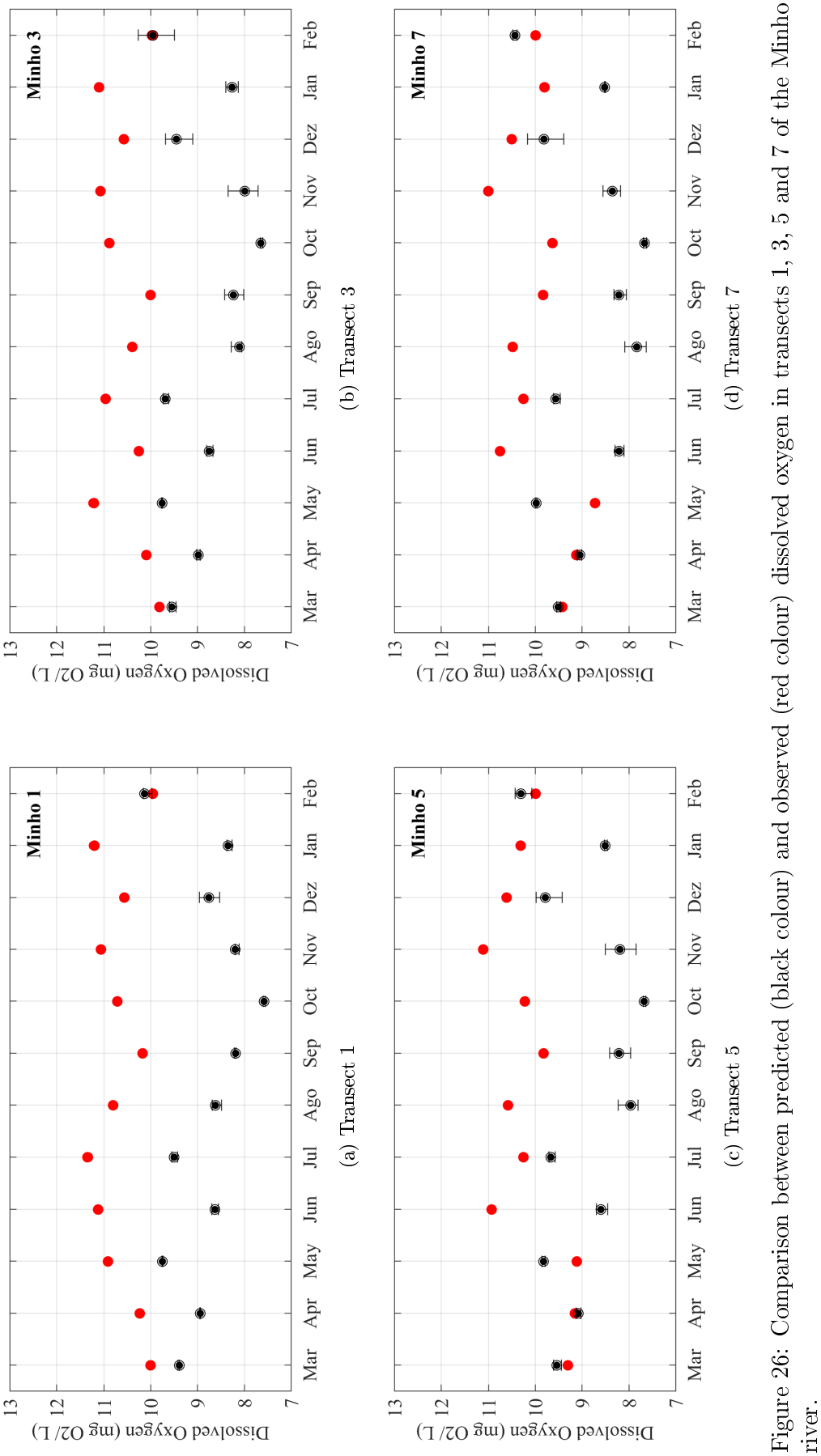

(a) Transect 1 (b) Transect 3

(c) Transect 5 (d) Transect 7

Figure 26: Comparison between predicted (black colour) and observed (red colour) dissolved oxygen in transects 1, 3, 5 and 7 of the Minho river.

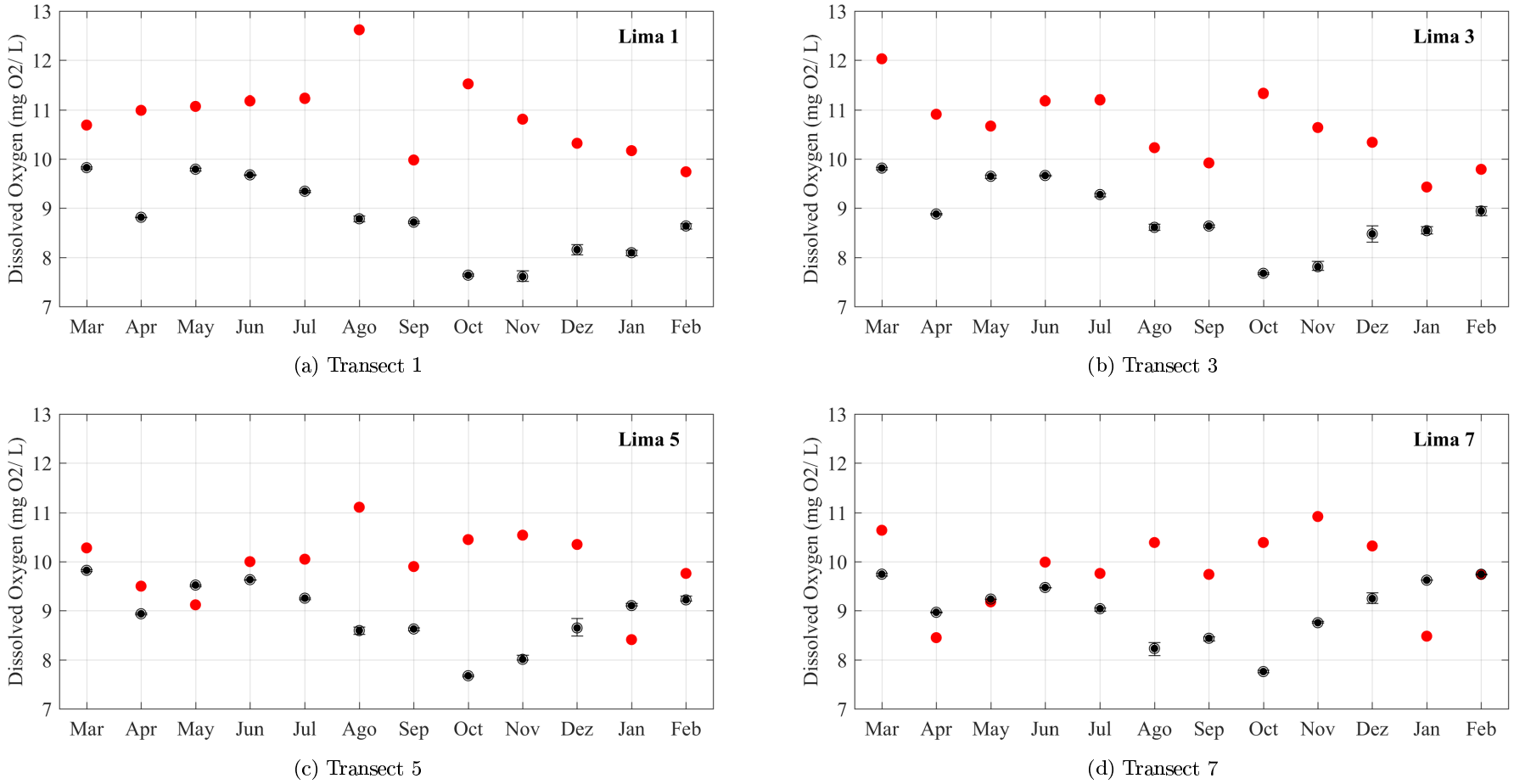

(a) Transect 1

(b) Transect 3

(c) Transect 5

(d) Transect 7

Figure 27: Comparison between predicted (black colour) and observed (red colour) dissolved oxygen in transects 1, 3, 5 and 7 of the Lima river.

7 Results and Discussion

Once calibrated, the numerical model may be applied to predict how salinity, water temperature, nutrients and dissolved oxygen will response to different inputs. Below, the results and discussion of the study of the intrusion and dynamics of estuarine plumes in the two estuaries, the impact of extreme river discharge events on the nutrient dynamics and the response time of the Minho estuary to a point discharge of pollutants will be presented (methodologies referred in Sections 5.3.1, 5.3.2 and 5.3.3).

7.1 Intrusion and dynamics of estuarine plumes of Minho and Lima estuaries

To study the intrusion of the Minho estuarine plume in the Lima estuary and vice versa, as well as the dynamics of the plumes, transepts along the mouths of the estuaries and cross-transepts to the coast were performed. As mentioned in Section 5.3.1, to fulfil these objectives the summer and winter season were studied. Two passive conservative tracers were used, one for Lima estuary outflows and the other for Minho estuary outflows.

7.1.1 Intrusion of the estuarine plumes

To investigate the interaction and exchanges betwen estuaries, the cumulative advective transport of tracers in Transepts 1 and 2 (Figure 11), in the winter and summer season, are analysed. Through the analysis of cumulative advective transport, it is possible to draw the following conclusions: 1) increase in cumulative advective transport occurs when tracer input into the estuary is higher than the tracer output; 2) decrease occurs under inverse conditions, when the tracer output is higher than the input; and 3) constant cumulative advective transport indicates that the amount of tracer entering is equal to that which exits, remaing that there is no intrusion of the estuarine plume.

For winter season [Figure 28 a), b) and c)], in general the Minho estuary presents higher cumulative advective transport than the Lima estuary. This pattern is due to the differences in the river discharges, since the Minho presents, in average, fluvial discharges much higher than those of the Lima.

Between 21 December 2012 and 20 January 2013, the Minho tracer rarely enters the Lima estuary (constant cumulative advective transport), but the Lima tracer enters the Minho estuary. This intrusion is observed because in this period there is predominantly southern winds and the river discharges of the Lima river are around 170 m^3/s, resulting in a plume with predominant direction to the north. Due to this fact, it is expected that the estuarine plume of Minho also heads north, as observed by Sousa et al. [2014a].

After this period, there is a reversal of the direction of the wind (north wind), and since the Minho river discharges from 20 to 28 January are high (reaching 580 m^3/s), there is a large intrusion of the estuarine plume of Minho in Transept 2 (Lima estuary), being observed an increase in cumulative advective transport of 0.8×10^8 km/m^3.

From 28 January to 2 February, it is again observed that the cumulative advective transport of the Minho is practically constant, while in the case of the Lima tracer is observed a large intrusion in Minho. This pattern derives once again from the high Lima discharges and from the north direction wind.

Regarding the last days (2 February to 1 March), there is an abrupt decrease in the cumulative advective transportate of Lima on 2 February, due to the high discharges of the Minho river, which induce an exportation of the Lima tracers out of the Minho estuary. On the other days, cumulative advective transport of the Lima remains constant, indicating that

there is no intrusion of the Lima estuarine plume in Minho estuary. Finally, analysing the same period for the Minho tracer, it is verified that there is a great intrusion of the Minho estuary plume in the Lima estuary, since an increase of 2×10^8 kg/m^3 of tracer is observed. This increase is due to high river discharges from Minho in this period (average 500 m^3/s).

In summary, it can concluded that in the winter season there are interactions between these estuaries, which strongly depends on river discharges and wind direction.

The cumulative advective transport, direction and intensity of wind and river discharges to the summer season are presented in Figure 29. From its analysis is found that the cumulative advective transport for both tracers is low comparing to the winter season, since the Minho and Lima river discharges are also lower in this period. It is important to note that in the summer season, the wind is predominant to the south [Figure 29 b)], inducing a higher intrusion of the Minho estuarine plume in the Lima estuary. However in certain periods there is inversion of the wind direction , inducing intrusion of the Lima plume in the Minho estuary (highlight the 6 of July and the period between 13 to 20 August).

In general, the numerical results indicate that under certain conditions, in summer there is also an intrusion of the Lima estuarine plume in the Minho (south wind) and vice versa (north wind).

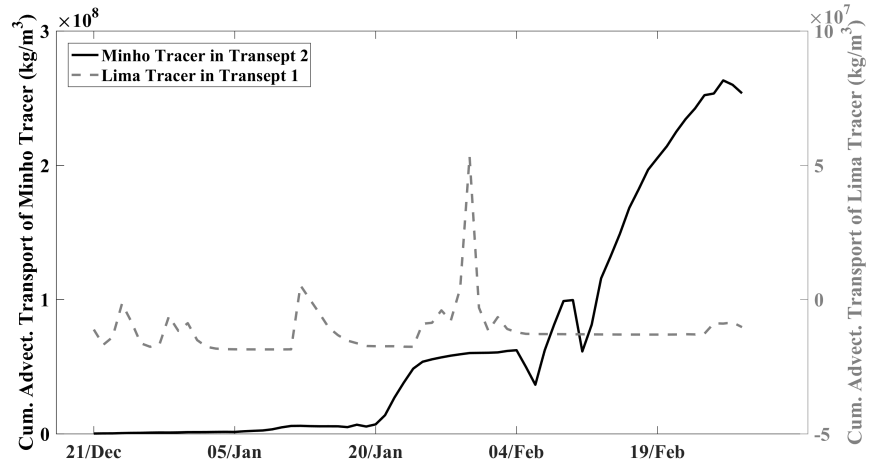

(a)

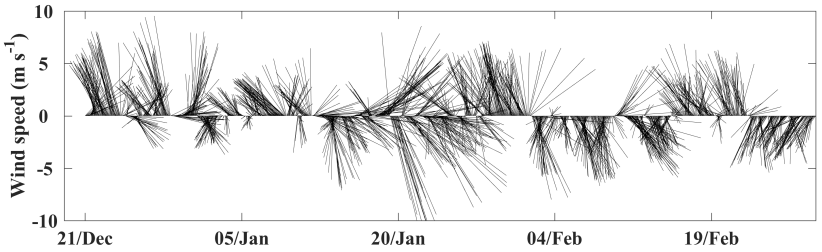

(b)

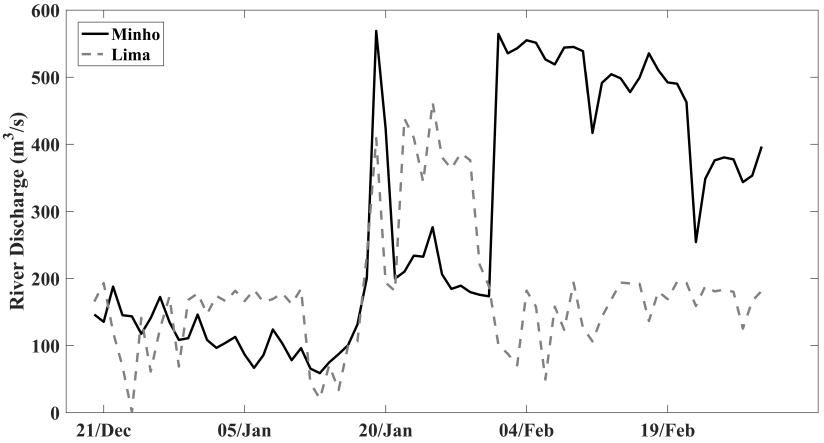

(c)

Figure 28: Cumulative advective transport (a), direction and intensity of wind (b) and Minho and Lima river discharges (c) in winter season.

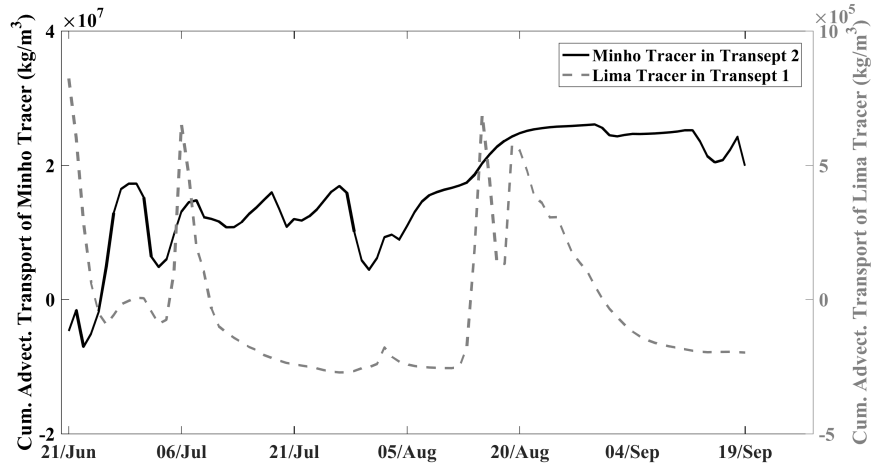

(a)

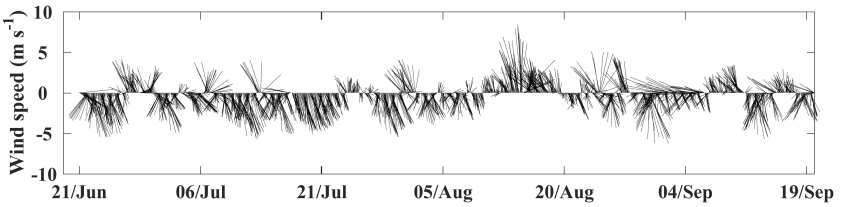

(b)

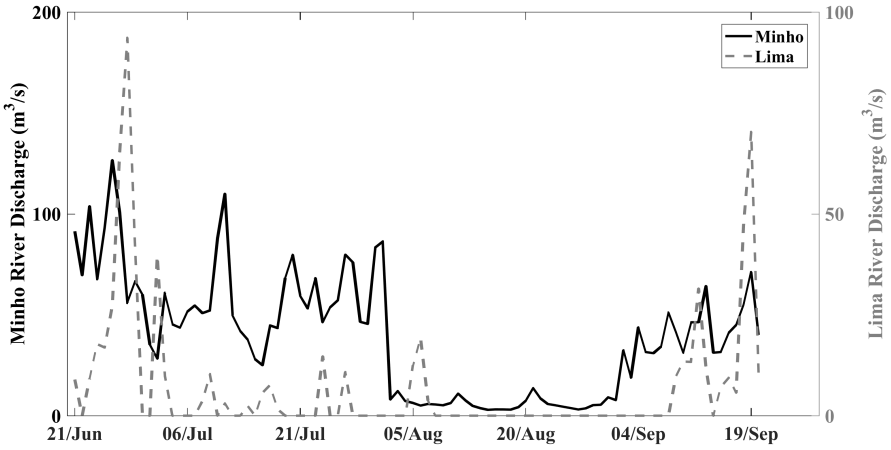

(c)

Figure 29: Cumulative advective transport (a), direction and intensity of wind (b) and Minho and Lima river discharges (c) in summer season.

7.1.2 Dynamics of the estuarine plumes

For the study of the dynamics of the estuarine plumes, the concentrations of the two tracers and the advective transport for 5 transepts (Figure 11) were computed.

With respect to Transept 1 (mouth of the Minho estuary), it can be observed a very high concentration of Lima tracer in the south margin of the Minho estuary for both seasons [Figure 30 a)]. Analysing the order of magnitude of the concentrations it is verified that in the winter season there is a higher tracer concentration than in the summer season. These higher concentrations of tracer in winter result from the high fluvial discharges observed during this period [Figure 28 c)].

The advective transport in Transept 1 [Figure 30 c)] was analysed, being observed the same tracer pattern for winter and summer seasons.

Analysing the Transept 1 from the south margin (left side of the figure) to the north margin (right side of the figure), it is observed a predominance of tracer entering along the south margin (between coordinates 41.865° and 41.866°) and north of the island that is located at the mouth of the Minho river (between coordinates 41.868° to 41.8688°), while the tracer output occurs predominantly along the northern shore of the Minho estuary (between coordinates 41.8688° and 41.872°) and south of the island (between coordinates 41.866° and 41.868°).

When analysing the concentration for Transept 2 (mouth of the Lima estuary), the patterns in winter and summer are different [Figure 30 b)]. In winter, are observed higher concentrations in the south margin of the Lima estuary comparing to the north margin, however in the summer season the opposite is observed (higher concentrations in the north margin than in the south margin). The patterns inversion is observed due to differences in the river discharges and wind direction. Since in summer the Lima river discharges are very low (practically non-existent at certain periods) and the wind is predominantly from the north, the Minho estuary plume tends to propagate to the south, reaching the entrance of the Lima estuary, being possible to observe higher concentrations to the north, since this region is closer to the Minho estuary.

To better understand the Lima estuarine circulation, the advective transport [Figure 30 d)] was computed. The numerical results show that in the summer season there is only a narrow section to the north of the Lima estuary where the tracer exit (between 41.6820° and 41.6825°), being observed the entry of the tracer in the rest of the transept. Analysing the advective transport in winter, it can be observed that the entrance area of the tracer has decreased substantially comparing to the summer season, with a larger exit section now being observed (between 41.6808° and 41.6825°), while the section entrance is reduced (between 41.6795° and 41.6805°). This enlargement of the exit section in the winter occurs because the Lima river discharge is higher (average 250 m^3/s), being expelled from the estuary along the north side (normal circulation of the estuaries, due to the Coriolis effect).

The transepts perpendicular to the coast were also analysed [Transepts 3 (Figure 31), 4 (Figure 32) and 5 (Figure 33)].

In Transept 3, it is verified that the concentration of the Lima tracer in summer is about zero, while for the Minho tracer the opposite patter is observed. The fact that the Minho tracer in summer has a higher concentration than that of Lima in this transept is due to predominant wind direction from north during this season [as observed in Figure 29 b)], spreading the estuarine plumes to the south.

Regarding the winter season, the concentration of the Lima tracer in this transept is significant (2 kg/m^3), presenting the same order of magnitude as the Minho tracer. This significant increase of the Lima tracer in the winter season is due to predominant south wind during this period [as observed in Figure 28 b)], transporting the estuarine plumes to the north. Although there is a significant increase in the concentration of the Lima tracer from

summer to winter, it can be verified that the Minho tracer still has higher concentrations than Lima along this transept. This is observed because the Minho river discharges are much higher, causing a greater dispersion of the estuarine plume. It is important to note that in both tracers the concentration tends to decrease offshore.

Considering the advective transport of the Lima tracer [Figure 31 c)], it can be observed that when the Lima plume moves northward, it propagates very close to the coastline, both in winter and summer seasons. Analysing both seasons in detail, it verified that in winter season this plume is wider than in summer, which is mainly due to the increase in Lima river discharges.

Regarding the advective transport of the Minho tracer [Figure 31 d)], it is observed that the transport of the Minho estuarine plume goes further away from the coast, comparing to the Lima plume. This occurs because when Minho estuarine plume moves southward is advected to the right due to the Coriolis effect, transporting the mass of water further offshore. It is also verified that the advective transport is more intense in the winter season, because of the higher Minho river discharges.

In Transept 4 (transept south of the Lima estuary), higher tracers concentration were observed close to the coast, however decreasing offshore.

Comparing the Minho and Lima tracer concentrations [Figure 32 a) and b)], it was observed that Transept 4 presents a higher concentration of the Lima tracer than Minho in the winter, however in the summer season the opposite patter is observed. This difference is due to the river discharges, since in summer the Lima river discharges are low, trapping the plume within the estuary. In relation to the advective transport [Figure 32 c) and d)], it is verified once again that the plumes in winter are retained closer to the coast and the advective transport is more intense for the Lima tracer, while in summer the plumes tend to move farther away from the coast and the advective transport is more intense for the Minho tracer, since the Minho river presents higher discharges than the Lima river.

Finally, when analysing tracer concentration in Transept 5 (north of the Minho estuary) [Figure 33 a) and b)], it is verified that the concentrations of the Lima tracer in this transept are practically null. Concerning the Minho tracer [Figure 33 b)], it presents higher concentrations (average maximum concentration tracer of 0.20 kg/m^3 in winter and 0.08 kg/m^3 in the summer).

It is also verified in Transept 5 that in winter there are higher concentrations of the Minho tracer than of the Lima tracer, since south winds promote the movement of both estuarine plume to the north. It is important to note that this northern movement of the estuarine plume of the Minho had previously been observed by Sousa et al. [2014a] and that this Minho estuarine plume has influence in the estuarine circulation of the Rias Baixas. In addition to this previously mentioned study, Ribeiro [2015] and Mendes et al. [2016] also verified the movement of estuarine plumes to the north on the Portuguese coast, when the wind is predominant from the south.

According to the results, the river discharges and wind direction play an important role in the estuarine plumes dynamics.

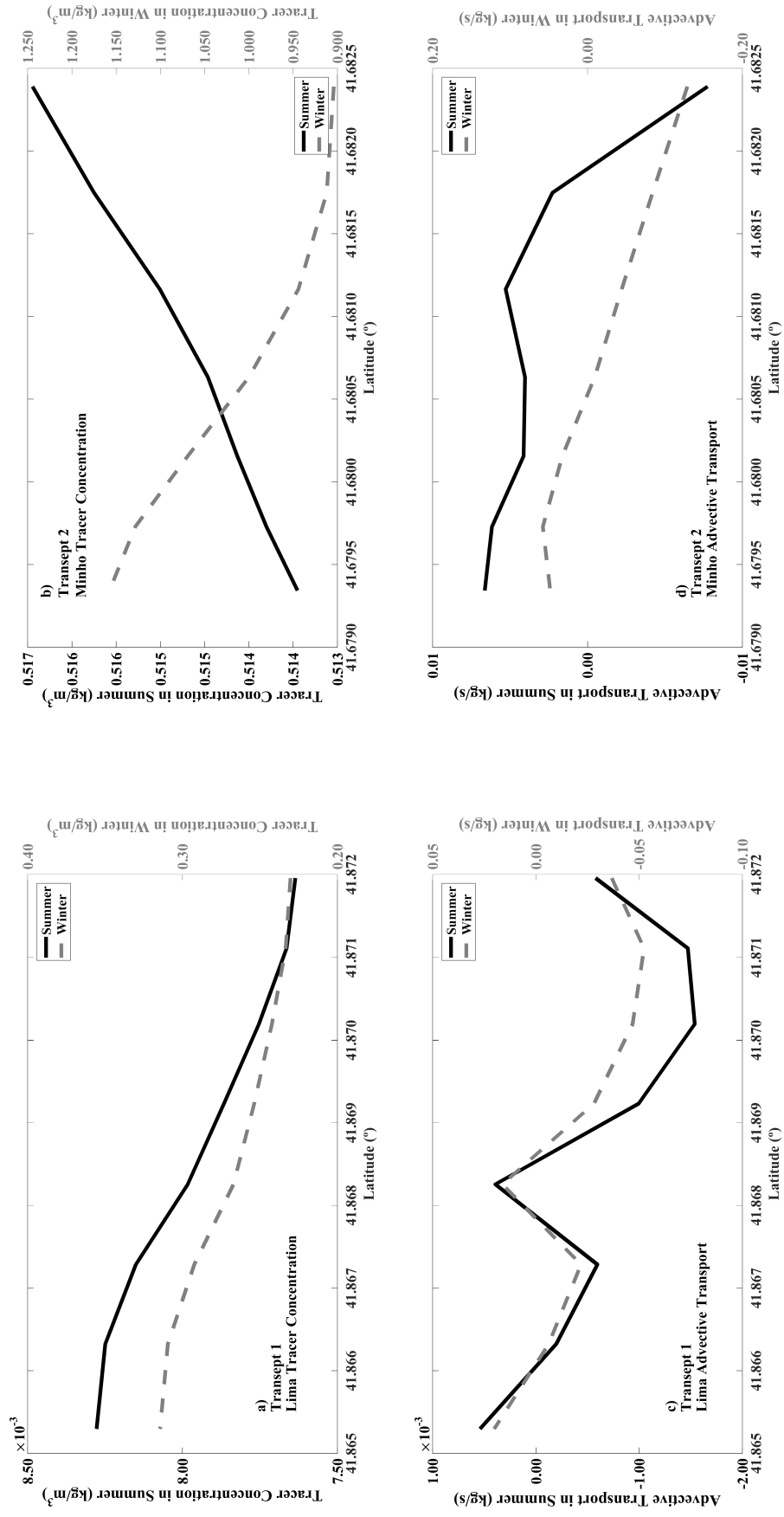

Figure 30: Concentration and advective transport for Lima and Minho tracers in Transepts 1 and 2. Positive (negative) tracer transport means tracer transport into (out of) the domain.

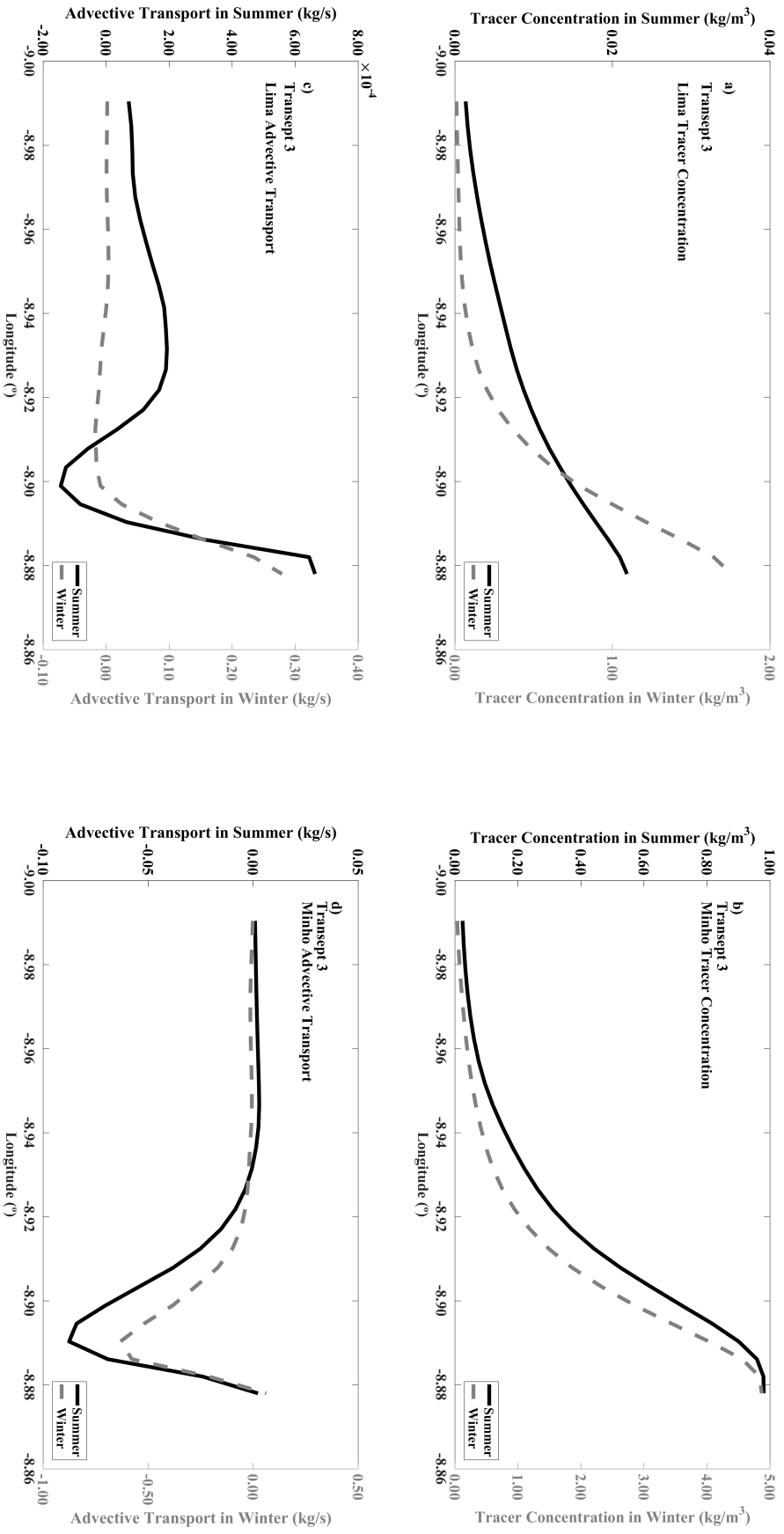

Figure 31: Concentration and advective transport for Lima and Minho tracers in Transept 3. Positive (negative) tracer transport means tracer transport to the north (south) the domain.

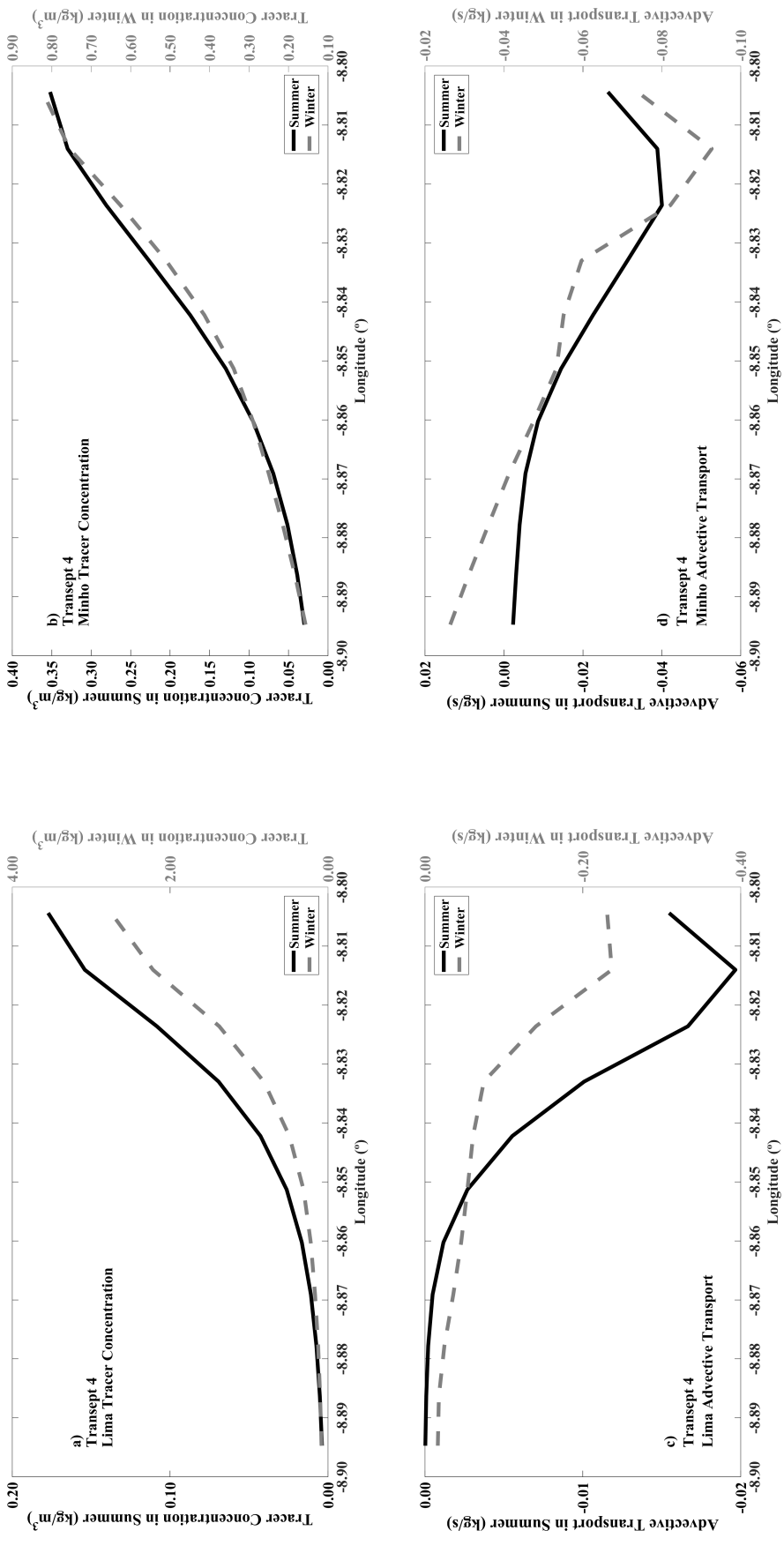

Figure 32: Concentration and advective transport for Lima and Minho tracers in Transept 4. Positive (negative) tracer transport means tracer transport to the north (south) the domain.

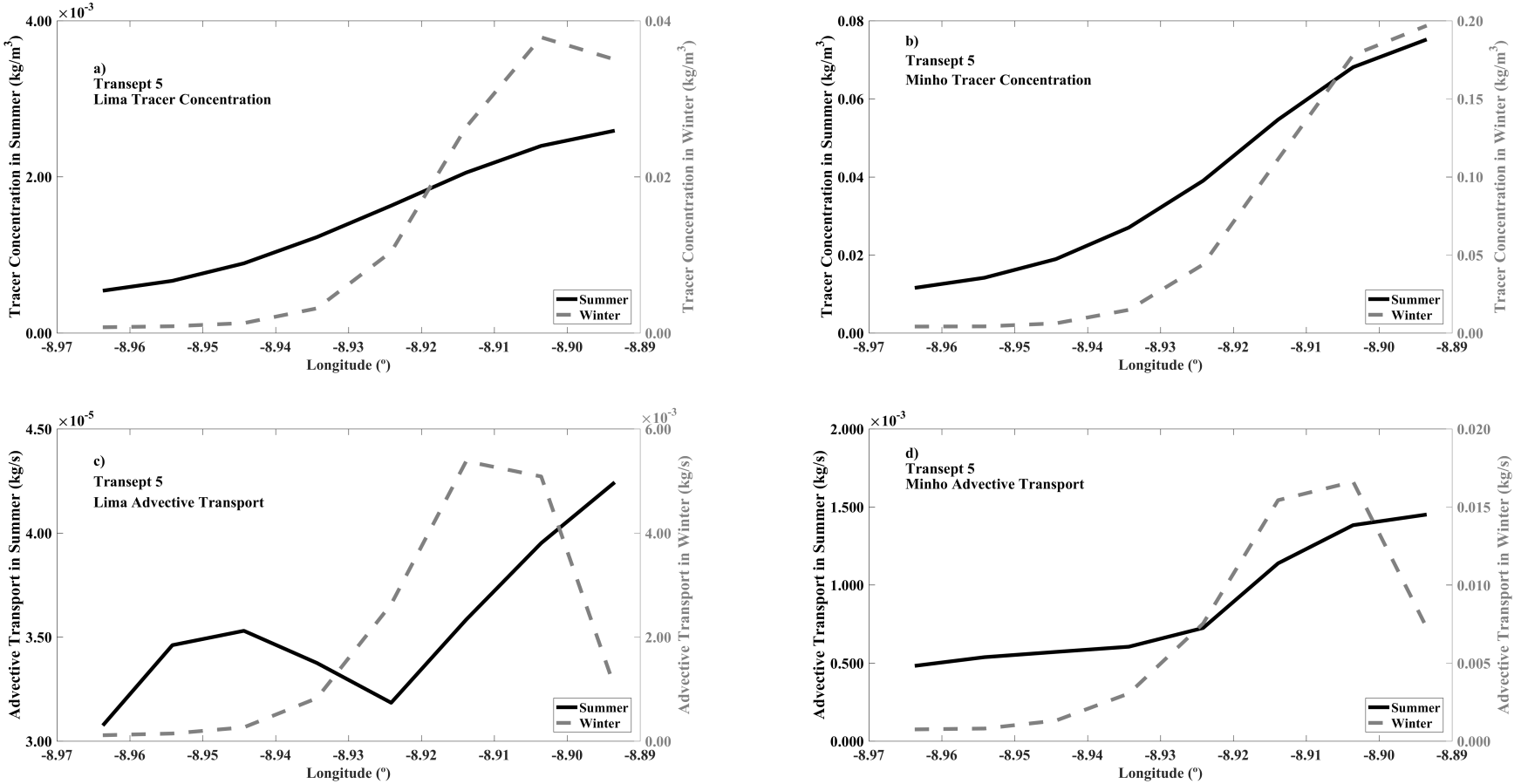

Figure 33: Concentration and advective transport for Lima and Minho tracers in Transept 5. Positive (negative) tracer transport means tracer transport to the north (south) the domain.

7.2 Impact of extreme events on the nutrient dynamics in Minho and Lima estuaries

After analysing the intrusion and dynamics of estuarine plumes of Minho and Lima estuaries, the impact of extreme events on the nutrient dynamics in the two estuaries were studied. For this, 3 scenarios were developed (Section 5.3.2). After performing the numerical simulations for each scenario, were analysed and discussed the results (first to the summer season and then to winter season).

In the following Sections (7.2.1 and 7.2.2), maps of the horizontal fields of salinity, water temperature, nitrates, orthophosphates and dissolved oxygen obtained by numerical model simulations will be presented. The values presented in these horizontal fields correspond to the average of all model data in the respective study period [summer (21 June 2012 to 20 September 2012) and winter (21 December 2012 to 1 March 2013)].

The first column represents the simulation referring to scenario 0 (baseline simulation), the second the difference between scenario 1 and scenario 0 (SCEN 1 - SCEN 0) and finally the third the difference between scenario 2 and scenario 0 (SCEN 2 - SCEN 0), with the aim of quantifying the alterations in the two estuaries.

Given that the impacts of extreme events of river discharge occur more intensely within the estuaries and that some resolution in terms of graphical information was lost if making a single figure with both estuaries, was decided to zoom in the figure to the areas of greater interest (Minho and Lima estuary), in order to carry out a better analysis. This analysis was performed separately (first to the Minho estuary and then to Lima estuary), however, the possible interactions between them (as verified in Section 7.1) were always present.

7.2.1 Summer season

Analysing the first column of Figures 34 to 39, representative of the average of the study variables for the summer season, in the baseline scenario it is verified that the model represents an increasing longitudinal water temperature gradient (in the ocean it is possible to observe a mean water temperature of 18°C and upstream of the rivers of 23°C). This pattern had previously been observed by Pereira [2016], through the analysis of vertical sections along the estuaries.

Regarding salinity [Figure 34 D) and Figure 37 D)], it is observed a longitudinal gradient, with higher values of salinity in the oceanic area and lower in the rivers headwaters.

Regarding nitrates [Figure 35 G) and Figure 38 G)] and orthophosphates [Figure 35 J) and Figure 38 J)], it is observed that, in the oceanic area, the nutrients (nitrates and orthophosphates) are very close to 0, since these are mainly from terrestrial sources and river discharges, being absorbed and degraded as the masses of water coming from the rivers are directed towards the coast.

Finally, analysing the average horizontal field of dissolved oxygen in both estuaries [Figure 36 M) and Figure 39 M)], it is observed that the highest concentrations are found in the coastal zones and near the estuaries mouth, since these areas are propitious for the development and growth of primary producers (e.g.: phytoplankton). The concentrations are around 9.5 mg O_2/L at the mouth and 7.5 mg O_2/L near to river discharge. The limited range of values found is justified considering that the nutrients concentration in the estuarine areas in the summer season are relatively low, being a limiting factor for phytoplankton growth.

The second column of Figures 34 to 39 represents the difference between a scenario of extreme discharges and scenario 0 (baseline). In Figure 34 B, it is observed that water temperature in the Minho estuary increased about 0.3°C near the mouth, but decreased about 0.6°C in the upstream areas, whereas in the Lima estuary [Figure 37 B)] the differences

are very close to zero, since the river discharges are lower than those of the Minho river and the depth of the channel is larger, presenting less impact.

Regarding salinity [Figure 34 E) and Figure 37 E)], it was found that both estuaries tend to become less saline due to the increase of river discharges, being the middle estuarine areas the most affected. This increase in river discharges and decrease of salinity in estuarine areas may have an impact on primary production, since it is expected that there will be a higher transport of nitrates and orthophosphates by rivers [shown in maps H) and K) in Figures 35 and 38]. Furthermore, assuming that nutrients are not a limiting factor, a slight increase in primary production is expected, since the lower the water temperature and the salinity, the higher the oxygen production by primary producers. However, since it is expected higher oxygen consumption in summer months than oxygen production, there will be a slight decrease in oxygen concentrations within the estuaries (decrease of 0.3 mg O_2/L in the Minho estuary and decrease of 0.1 mg O_2/L in the Lima estuary).

Finally, analysing the maps in the third column, representing the difference between the ecological flow scenario and the baseline scenario, it was found an increase of 0.2°C in the interior of the Minho estuary [Figure 34 C)], while in the Lima estuary differences are very close to 0 [Figure 37 C)].

A detailed analysis of the differences between the salinity for scenario 2 and scenario 0, show an unexpected salinity pattern in the Minho estuary [Figure 34 F)], since with ecological flows it was expected that there would be a higher saline intrusion. This is not observed because the values of the ecological flows used for the summer season have fluvial discharges higher than those used in scenario 0 (baseline scenario).

Due to the aforementioned, a higher concentration of nutrients was observed in the ecological flow scenario (SCEN 2) than in the baseline scenario (SCEN 0).

Regarding the Lima estuary, the salinity maps [map F) of Figure 37] show a larger saline intrusion, since the river discharges for scenario 2 are lower than those for the baseline scenario. Since there are lower river discharges, the concentration of nitrates and orthophosphates in the Lima estuary is lower [maps I) and L) of Figure 38)], leading to a decrease in the dissolved oxygen concentration [Figure 39 O)] inside the estuary (decrease of 0.2 mg O_2/L).

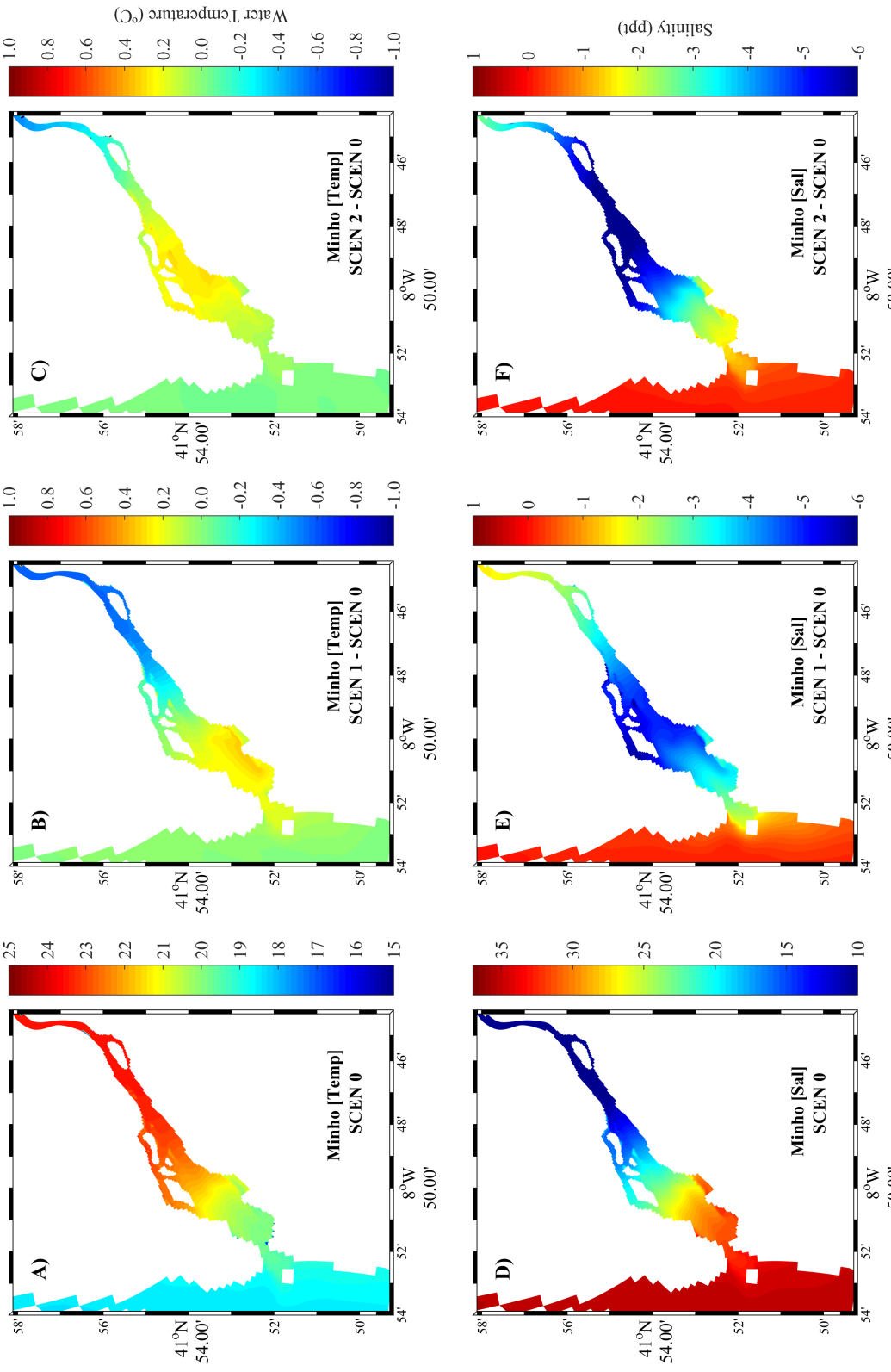

Figure 34: Mean water temperature and salinity for Minho estuary in the summer. From left to right columns: baseline scenario (SCEN 0); differences between scenario 1 and scenario 0 (SCEN 1 - SCEN 0); and difference between scenario 2 and scenario 0 (SCEN 2 - SCEN 0).

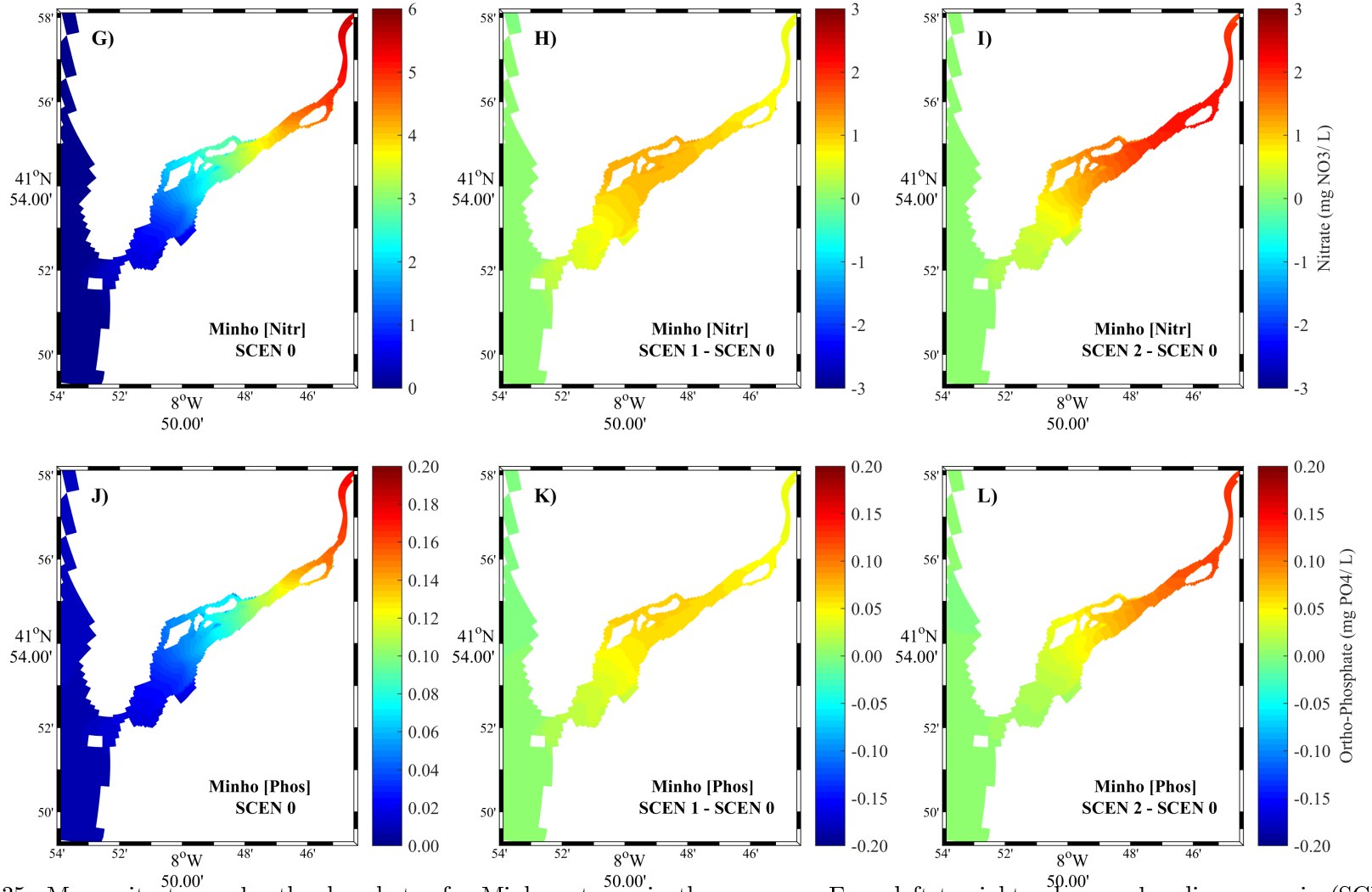

Figure 35: Mean nitrates and orthophosphates for Minho estuary in the summer. From left to right columns: baseline scenario (SCEN 0); differences between scenario 1 and scenario 0 (SCEN 1 - SCEN 0); and difference between scenario 2 and scenario 0 (SCEN 2 - SCEN 0).

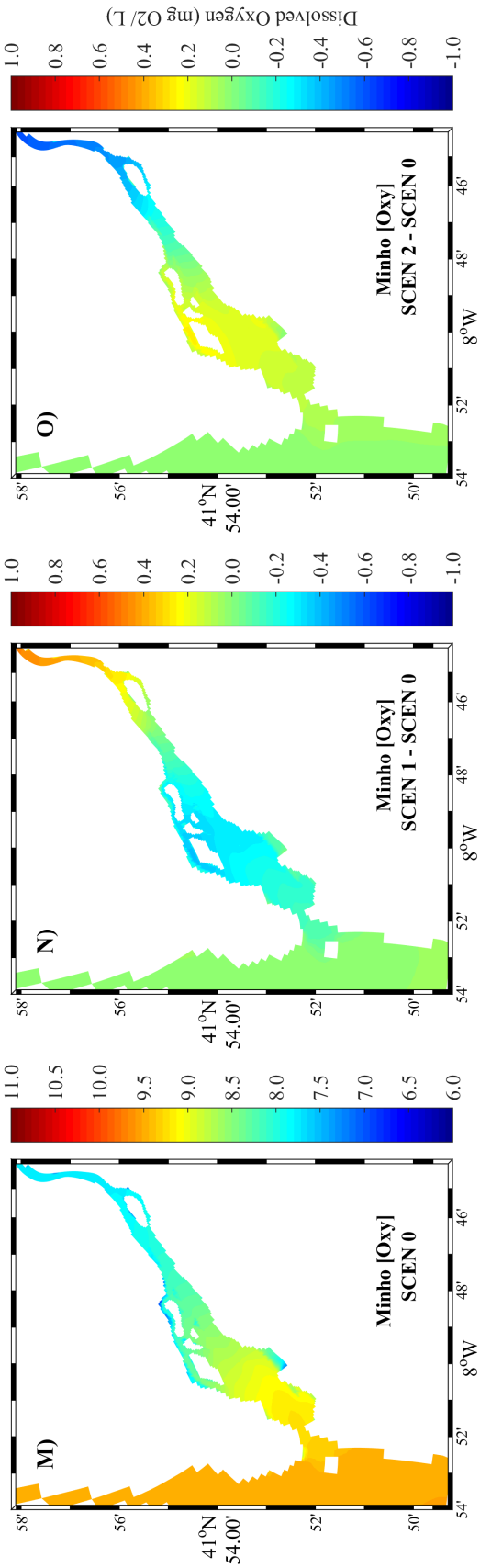

Figure 36: Mean dissolved oxygen for Minho estuary in the summer. From left to right columns: baseline scenario (SCEN 0); differences between scenario 1 and scenario 0 (SCEN 1 - SCEN 0); and difference between scenario 2 and scenario 0 (SCEN 2 - SCEN 0).

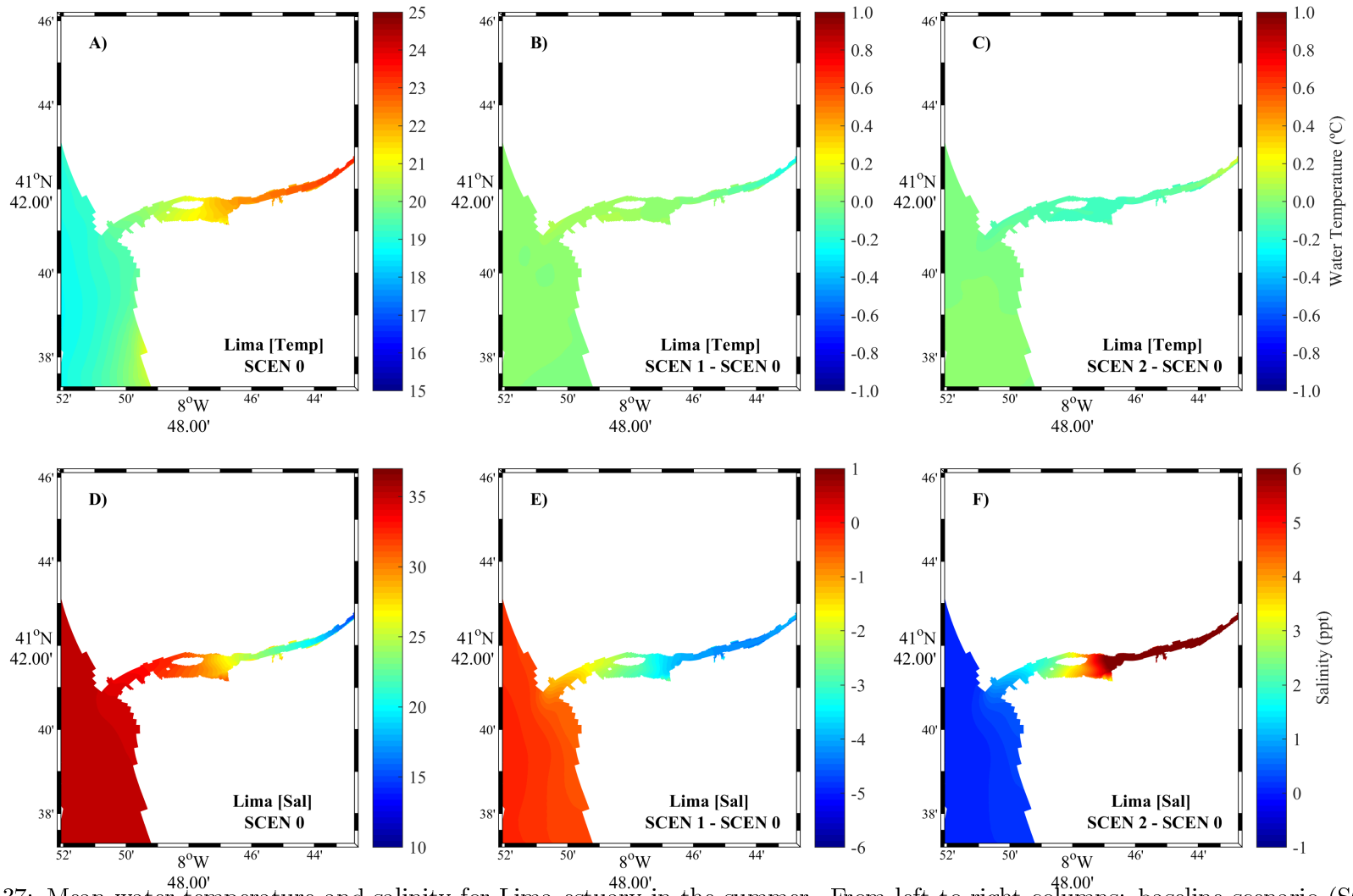

Figure 37: Mean water temperature and salinity for Lima estuary in the summer. From left to right columns: baseline scenario (SCEN 0); differences between scenario 1 and scenario 0 (SCEN 1 - SCEN 0); and difference between scenario 2 and scenario 0 (SCEN 2 - SCEN 0).

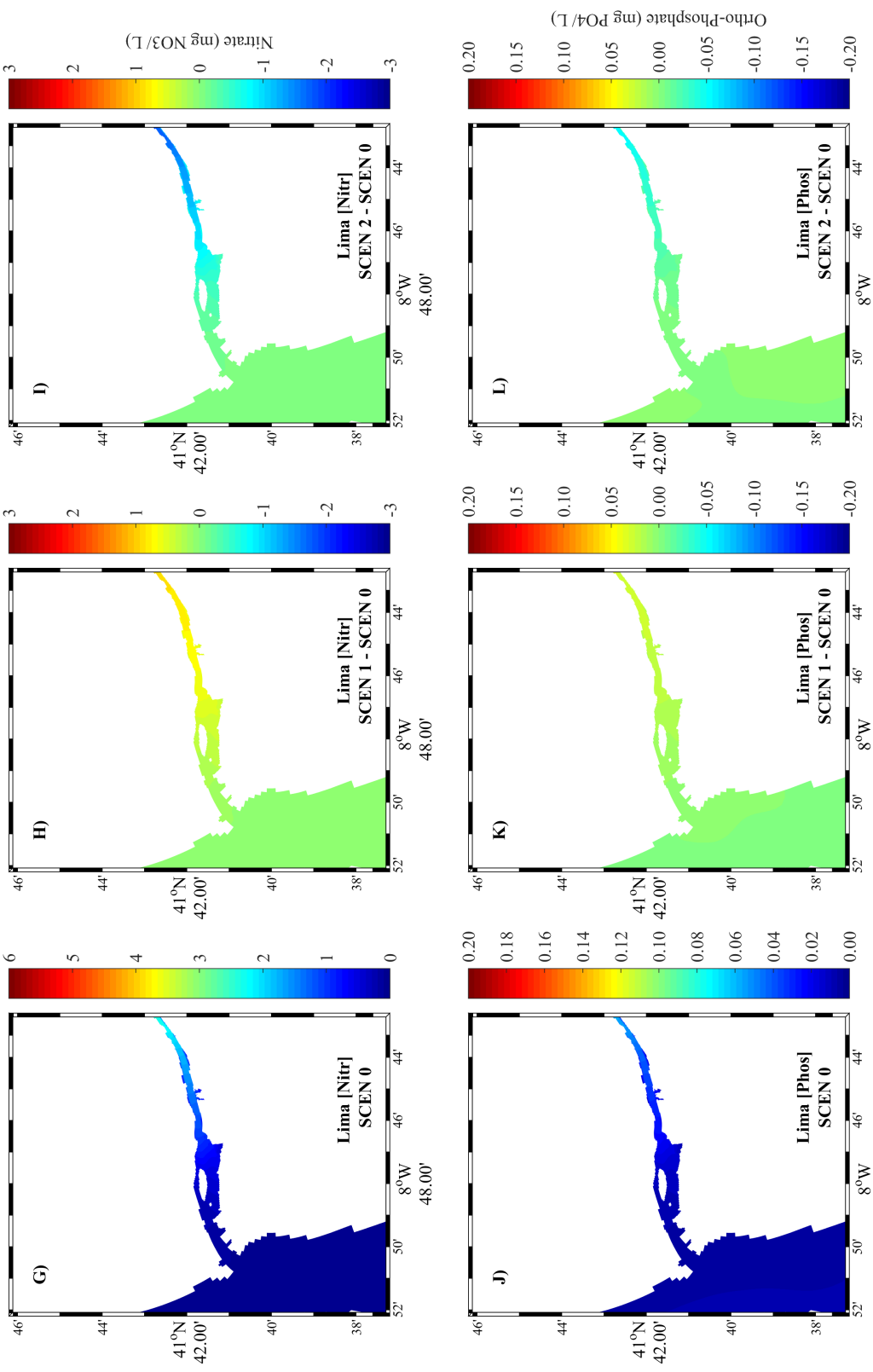

Figure 38: Mean nitrates and orthophosphates for Lima estuary in the summer. From left to right columns: baseline scenario (SCEN 0); differences between scenario 1 and scenario 0 (SCEN 1 - SCEN 0); and difference between scenario 2 and scenario 0 (SCEN 2 - SCEN 0).

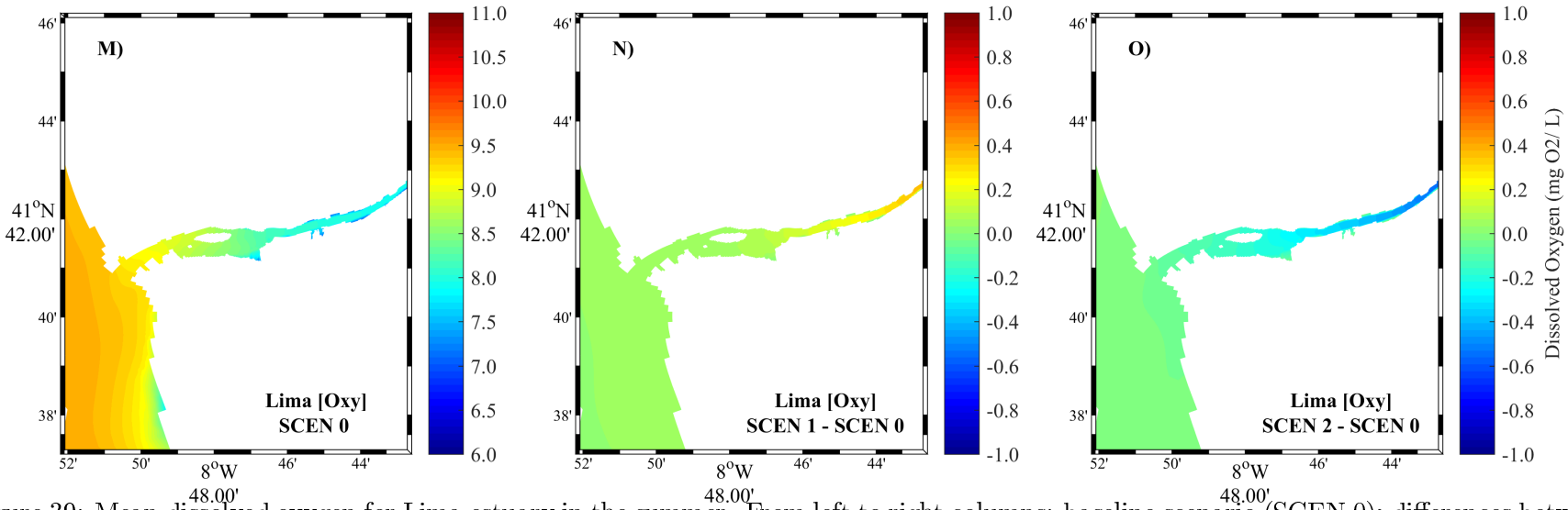

Figure 39: Mean dissolved oxygen for Lima estuary in the summer. From left to right columns: baseline scenario (SCEN 0); differences between scenario 1 and scenario 0 (SCEN 1 - SCEN 0); and difference between scenario 2 and scenario 0 (SCEN 2 - SCEN 0).

7.2.2 Winter season

From the analysis of results for the winter season (Figures 40 to 45), it was found that the variations are more drastic and the impact of changes in river discharges is higher.

Analysing the maps in the first column of Figures 40 to 45, is observed once again that the model represents a longitudinal gradient of water temperature, but this gradient in the winter season is negative (temperature of ocean water higher than near the river mouth, for both estuaries).

Regarding salinity [Figure 40 D) and Figure 43 D)], it was found that the highest values occur in the oceanic areas and decrease upstream, however, with a lower amount of salt water inside the estuaries than in the summer season. This decrease in salinity within the estuaries may bring an increase in the production of dissolved oxygen, as explained before.

When analysing the maps for nitrates and orthophosphates for both estuaries [maps G) and J) in Figures 41 and 44], it can be detected that, in the oceanic area, the nutrients no longer present zero concentrations. The nitrate concentration is around 1 mg NO_3/L and the orthophosphate concentration is about 0.04 mg PO_4/L. These concentrations are observed in the coastal zones because there is a large transport of nutrients by the rivers in this case.

Given that nutrient concentrations are relatively higher than in summer season, it is observed an increase in oxygen concentration in both estuaries [Figure 42 M) and Figure 45 M)]. This increase in concentration, comparing to the summer season, is mainly due to the fact that the water temperature and estuarine salinity are lower and nutrient concentration are higher. In addition to the above mentioned, higher concentrations of dissolved oxygen are expected to exist, since the rate of oxygen production is higher than the consumption.

Analysing the second column, representing the difference between a scenario of extreme discharges and scenario 0 (baseline), is found that the water temperature in both estuaries [Figure 40 B) and Figure 43 B)] decreases about 0.5°C near the mouth, maintaining the temperature almost constant in the areas upstream.

Regarding salinity, in the maps representing the difference between scenario 1 and scenario 0 [Figure 40 E) and Figure 43 E)], it was observed that both estuaries tend to become less saline due to the increase of river discharges, with the area near the mouth of the estuary having the highest differences. As mentioned before, this decrease in salinity and water temperature, as well as increased concentrations of nitrates and orthophosphates (increase of 0.9 mg NO_3/L and 0.01 mg PO_4/L in both estuaries), will lead to an increase of dissolved oxygen in estuarine waters (increase 0.5 mg O_2/L in the Minho estuary [Figure 42 N)] and 0.7 mg O_2/L in the Lima estuary [Figure 45 N)]).

Finally, analysing the maps in the third column, representing the difference between the ecological flow scenario and the baseline scenario, it is noted that if ecological flows are discharged, there will be an increase in the water temperature of 2°C in the Lima estuary [Figure 43 C)] and of 0.5°C in the Minho estuary [Figure 40 C)].

Regarding salinity [Figure 40 F) and Figure 43 F)], it is observed once again a larger saline intrusion, since the river discharges are very low.

Given that river discharges of ecological flows are smaller comparing to scenario 0, it is checked a lower nutrient concentration [maps I) and L) of Figures 41 and 44], causing a huge impact on the concentration of oxygen dissolved in both estuaries. In the Lima estuary, there is a mean decrease of 2 mg O_2/L [Figure 45 O)], while in the Minho estuary [Figure 42 O)], only a decrease of 0.3 mg O_2/L is observed.

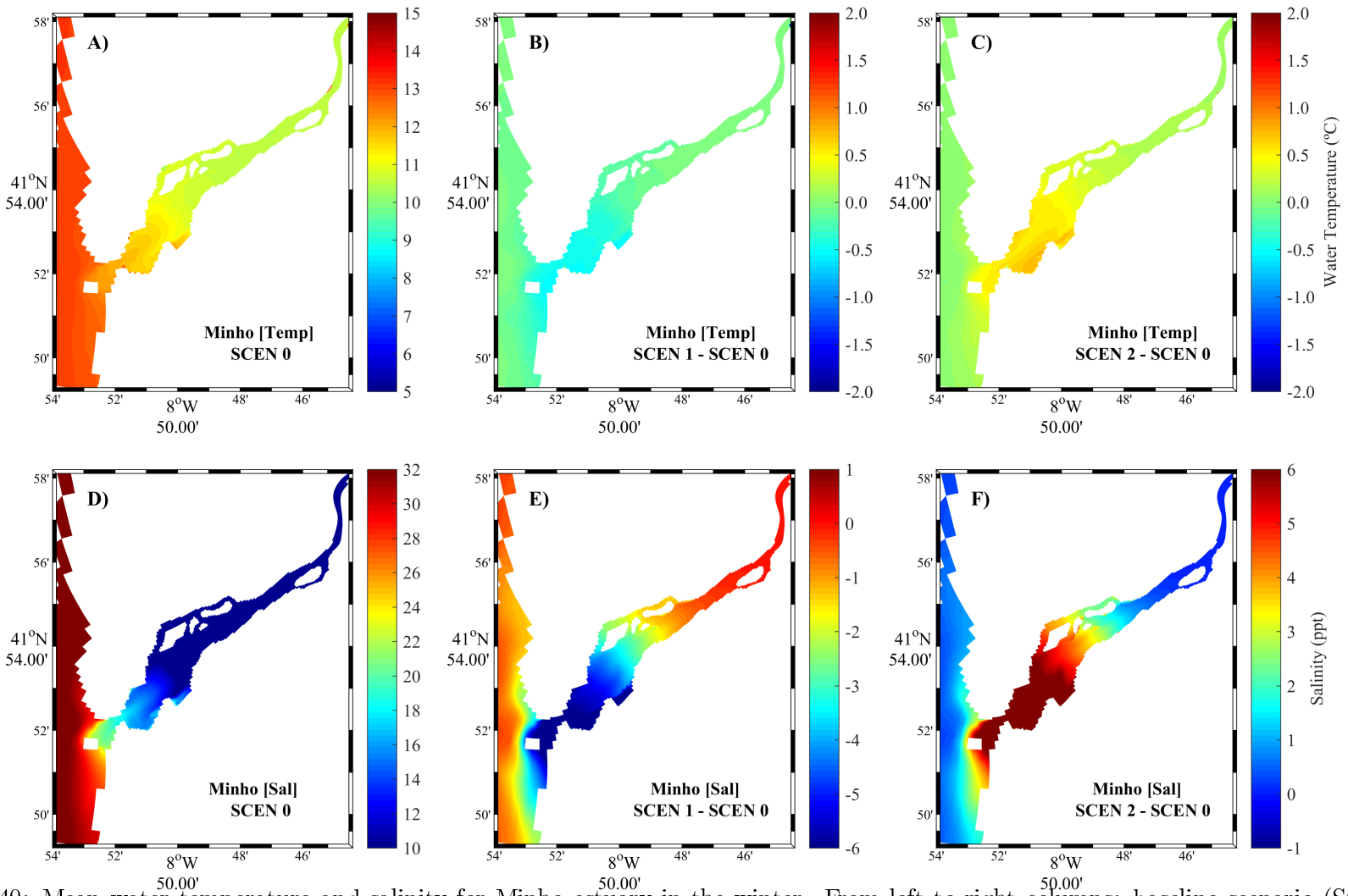

Figure 40: Mean water temperature and salinity for Minho estuary in the winter. From left to right columns: baseline scenario (SCEN 0); differences between scenario 1 and scenario 0 (SCEN 1 - SCEN 0); and difference between scenario 2 and scenario 0 (SCEN 2 - SCEN 0).

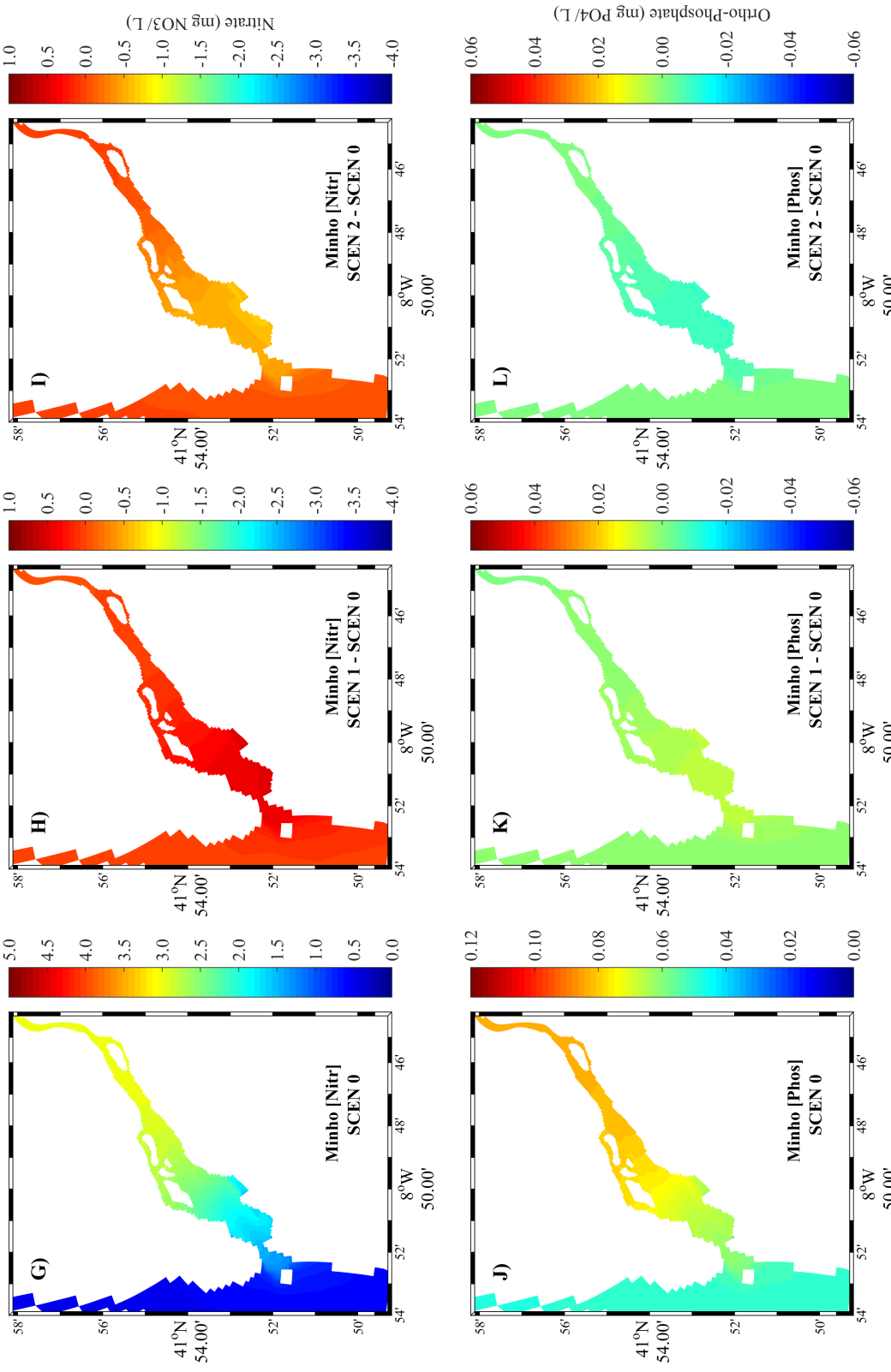

Figure 41: Mean nitrates and orthophosphates for Minho estuary in the winter. From left to right columns: baseline scenario (SCEN 0); differences between scenario 1 and scenario 0 (SCEN 1 - SCEN 0); and difference between scenario 2 and scenario 0 (SCEN 2 - SCEN 0).

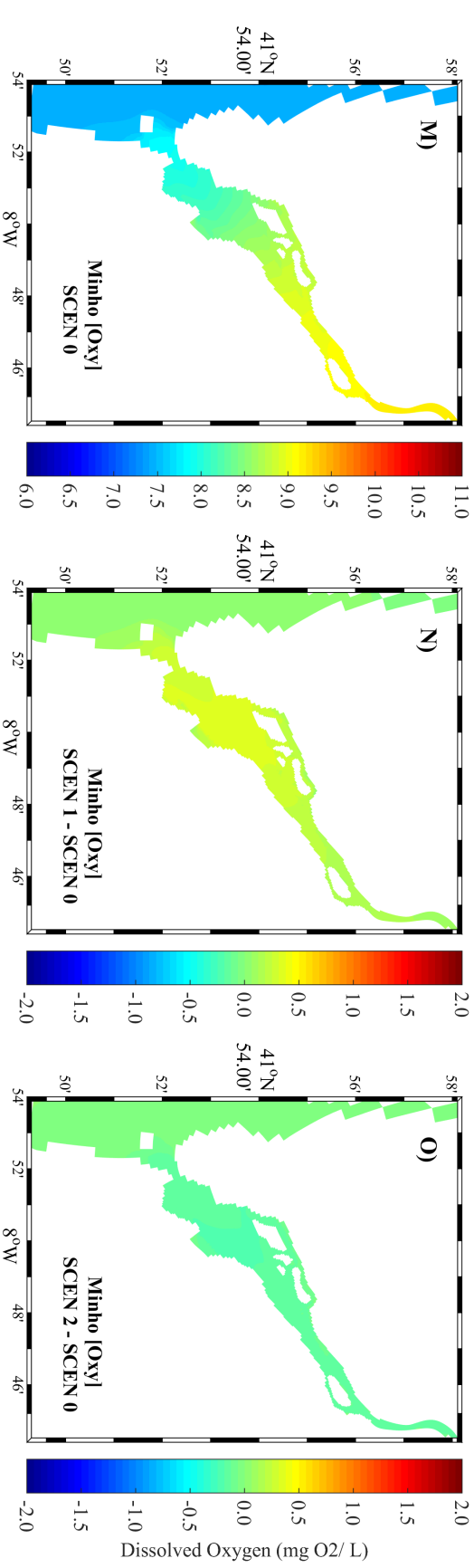

Figure 42: Mean dissolved oxygen for Minho estuary in the winter. From left to right columns: baseline scenario (SCEN 0); differences between scenario 1 and scenario 0 (SCEN 1 - SCEN 0); and difference between scenario 2 and scenario 0 (SCEN 2 - SCEN 0).

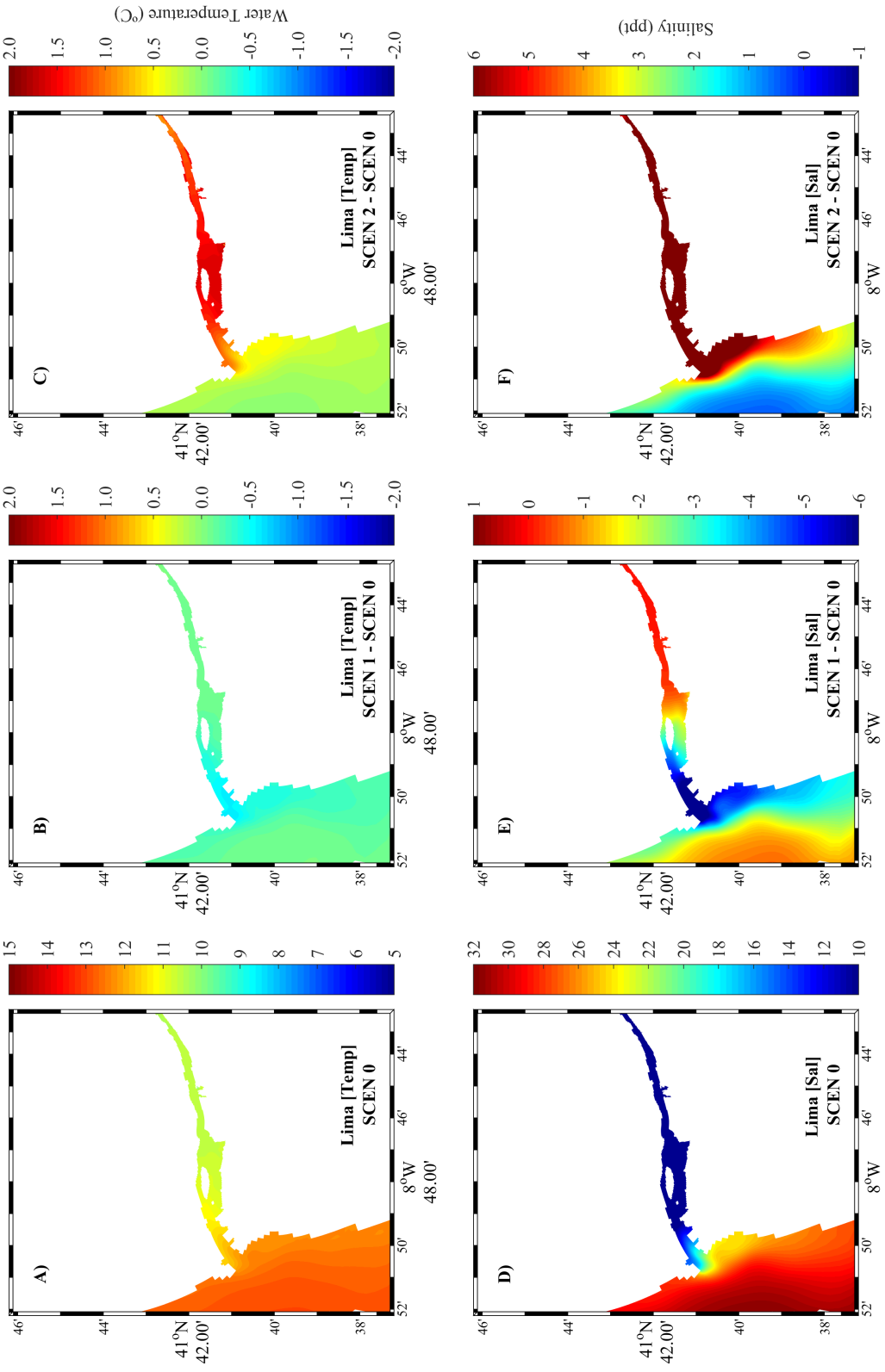

Figure 43: Mean water temperature and salinity for Lima estuary in the winter. From left to right columns: baseline scenario (SCEN 0); differences between scenario 1 and scenario 0 (SCEN 1 - SCEN 0); and difference between scenario 2 and scenario 0 (SCEN 2 - SCEN 0).

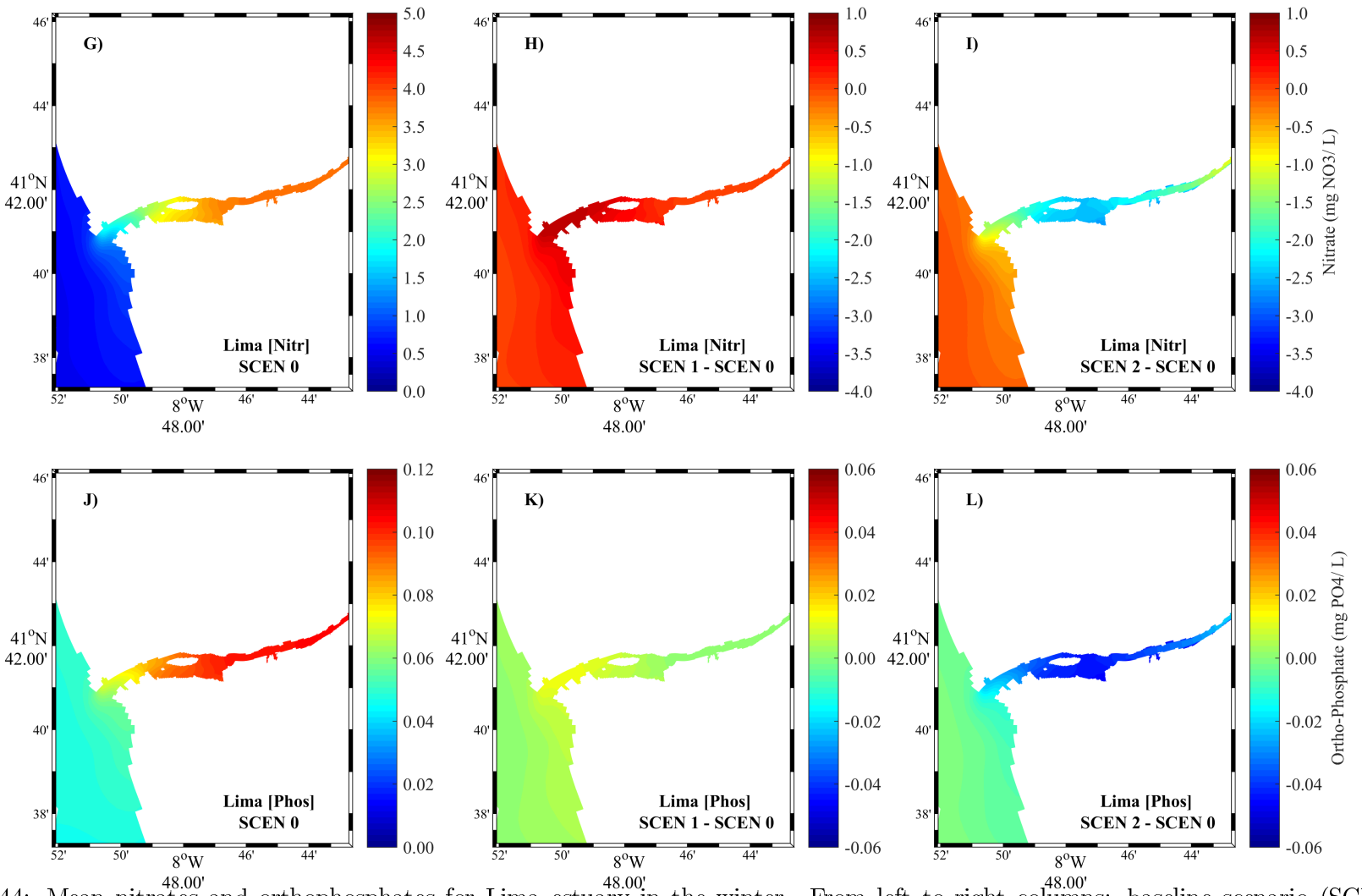

Figure 44: Mean nitrates and orthophosphates for Lima estuary in the winter. From left to right columns: baseline scenario (SCEN 0); differences between scenario 1 and scenario 0 (SCEN 1 - SCEN 0); and difference between scenario 2 and scenario 0 (SCEN 2 - SCEN 0).

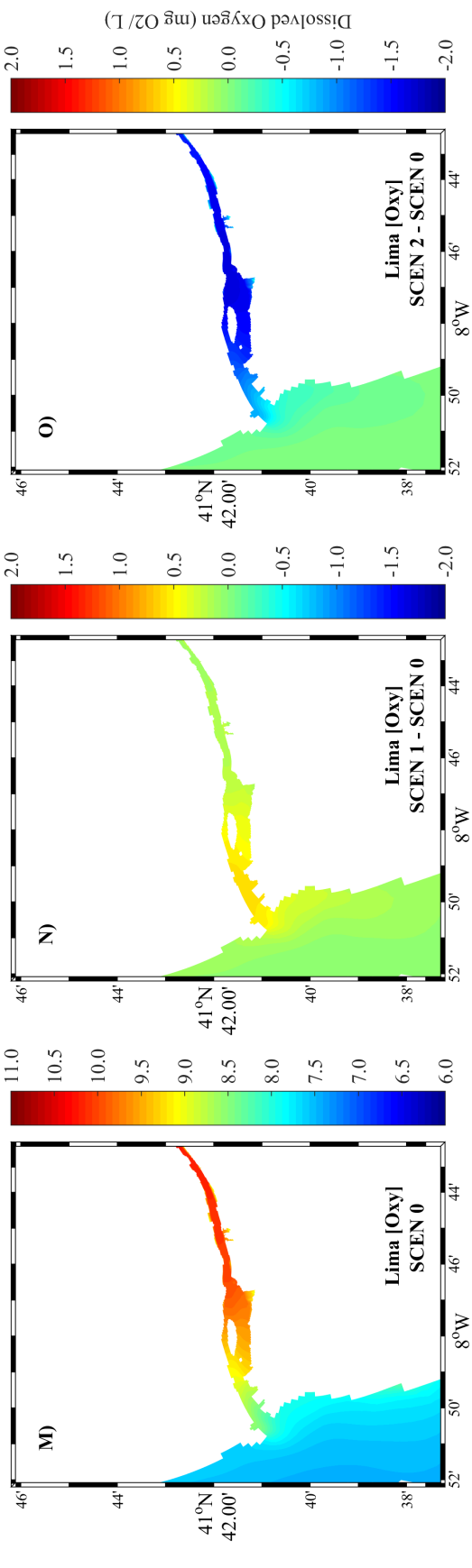

Figure 45: Mean dissolved oxygen for Lima estuary in the winter. From left to right columns: baseline scenario (SCEN 0); differences between scenario 1 and scenario 0 (SCEN 1 - SCEN 0); and difference between scenario 2 and scenario 0 (SCEN 2 - SCEN 0).

7.3 Response time of the Minho estuary to a point discharge of pollutants

After studying the intrusion and dynamics of Minho and Lima estuarine plumes and the impact of extreme events on the nutrient dynamics in Minho and Lima estuaries, the response time of the Minho estuary to a point discharge of pollutants (nitrates and orthophosphates) was studied. As mentioned in Section 5.3.3, for this study another fluvial boundary (simulating the Coura river) was implemented in the Minho estuary and two numerical simulations were carried out (one on the 10 August 2012 and the other on 19 August 2012).

In the next Section (7.3.1), horizontal fields of nitrates and orthophosphates will be represented. The maps presented in Figures 46, 47, 48 and 49 were obtained for low tide conditions. Given that in the case of nitrates the response time of the estuary is relatively large, the results in 10 August will be presented every 4 low tides and in 19 August will be presented every 2 low tides, until the estuary return to normal state.

The maps represent the percentage differences between the scenario with points discharges of pollutants and the baseline scenario, in order to quantify the response time that this estuary has to a point discharge of pollutants.

To quantify the response time, it was considered that when the difference between the 2 scenarios was lower than 5%, the estuary had already returned to its normal state.

7.3.1 Response time results

Through the analysis of Figures 46, 47, 48 and 49, it can be concluded that the response time of the Minho estuary to a point discharge of pollutants highly depends on the stage of the tide and the currents within the estuary.

Regarding the discharge carried out on 10 August (neap tide), it is found that the estuary takes about 41 low tides (approximately 21 days) in the case of nitrates and 7 low tides (approximately 4 days) in the case of orthophosphates until returning to its normal state. The discharge carried out on August 19 (spring tide) only takes 10 low tides (approximately 5 days) in the case of nitrates and 1 low tide (approximately 12 hours) in the case of orthophosphates to return to the normal state.

Although both concentrations of nitrates and orthophosphates are 100 times higher than the average, concentrations of orthophosphates within the estuary quickly return to normal because they have lower concentrations than nitrates.

Comparing and analysing the concentrations of the oceanic area with the estuarine area, it was found that as time progresses, there is an exponential decrease in nutrients concentration near the estuary mouth and near the coast. This decrease may be due to the fact that the primary producers (algae imposed on the model) are predominantly in these zones and use the available nutrients in the protein synthesis and in their cell walls, thereby reducing the concentrations in the water column.

Finally, the intertidal areas are those that takes longer to return to normal state, since they present lower tidal currents (it is noteworthy that in this numerical model benthic plants and bacteria were not considered, being possible to obtain results different from the current ones if these are introduced into the model).

It is important to note that the response time may be directly related to tidal currents intensiry, water temperature, salinity, river discharges and the number of organisms in the estuary. If new organisms (e.g.: benthic plants and cyanobacteria) and processes are implemented in the numerical model, it is expected that this response time will decrease.

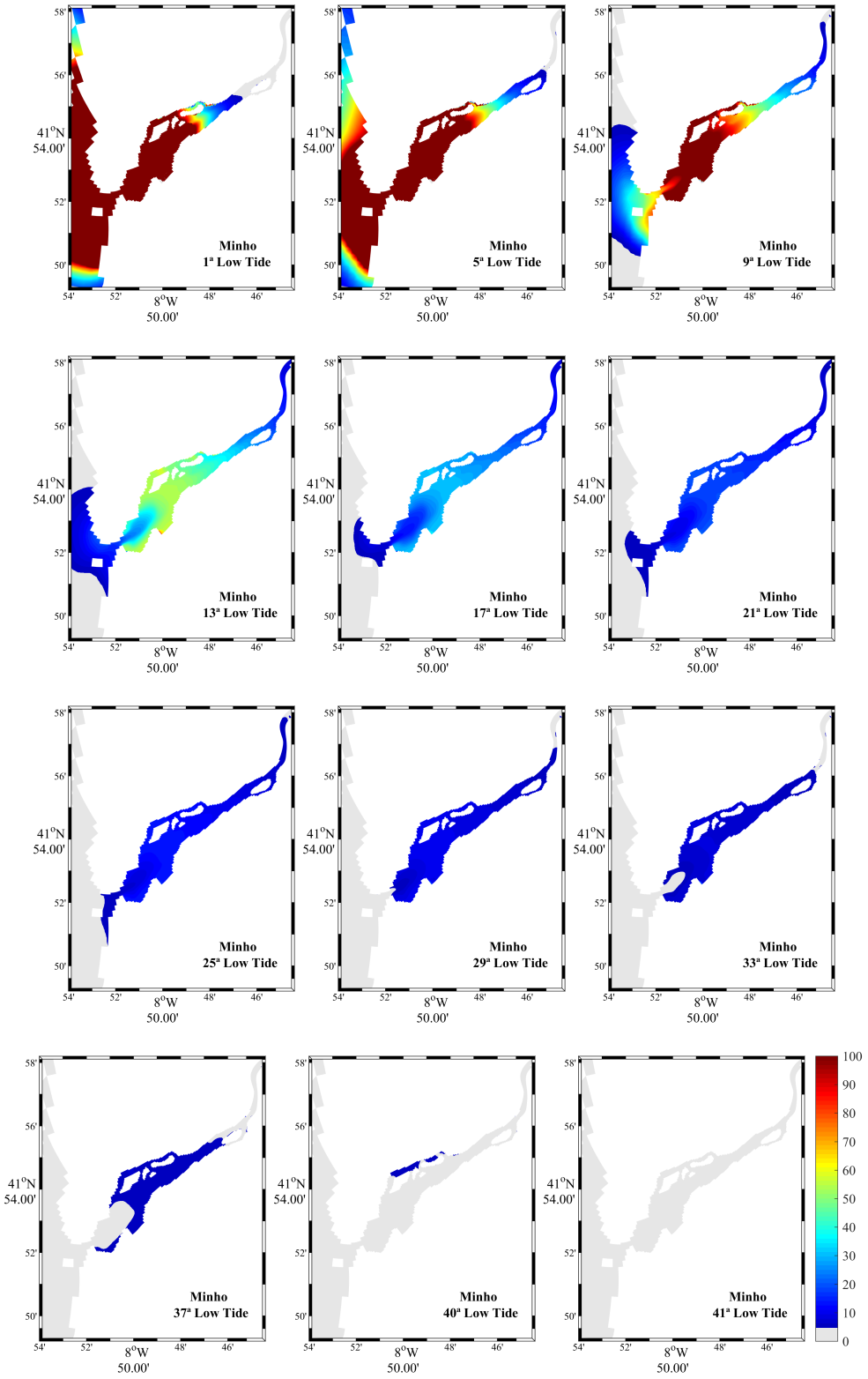

Figure 46: Percentage differences of nitrates between the point discharge of pollutants scenario and the baseline scenario, on August 10.

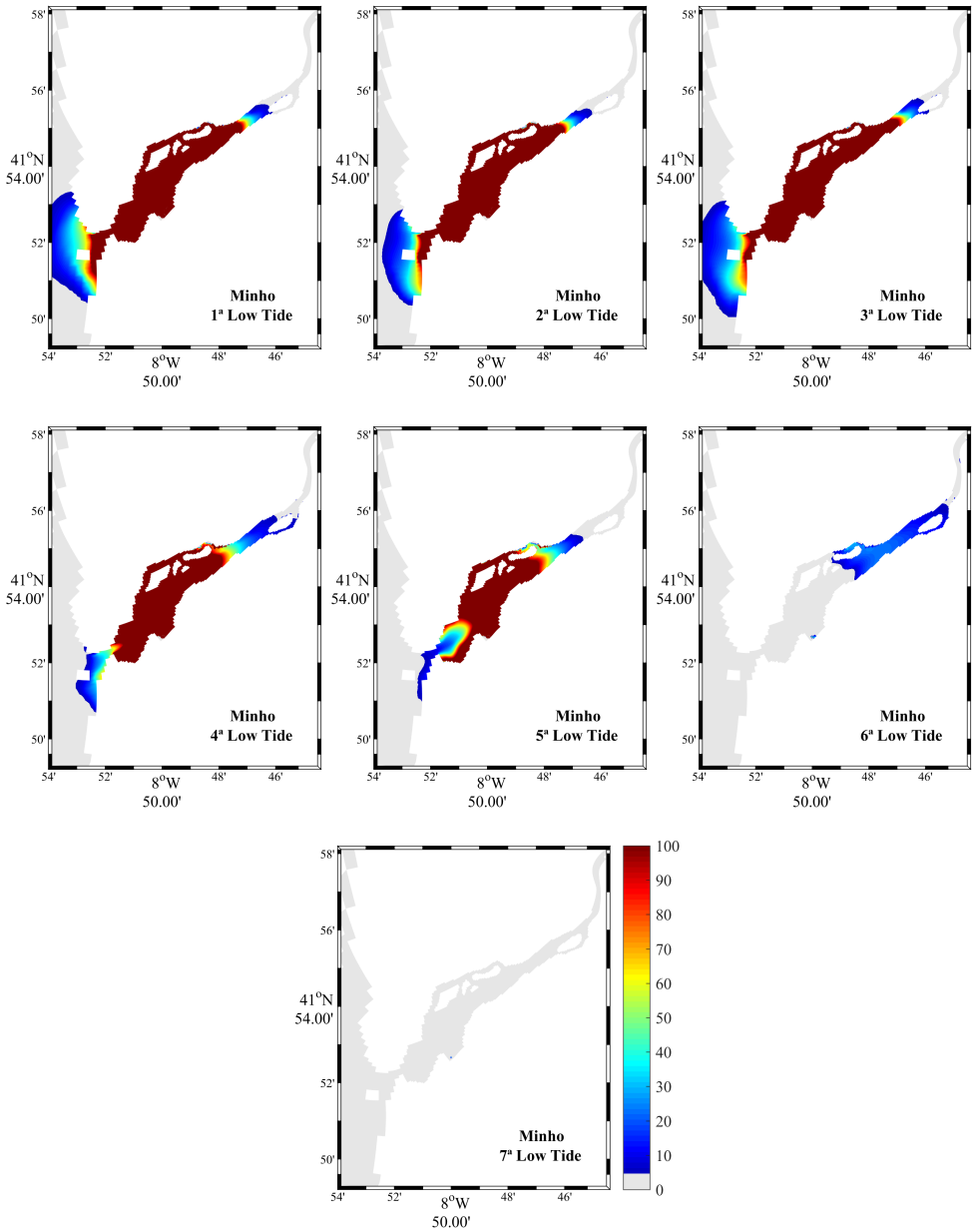

Figure 47: Percentage differences of orthophosphates between the point discharge of pollutants scenario and the baseline scenario, on August 10.

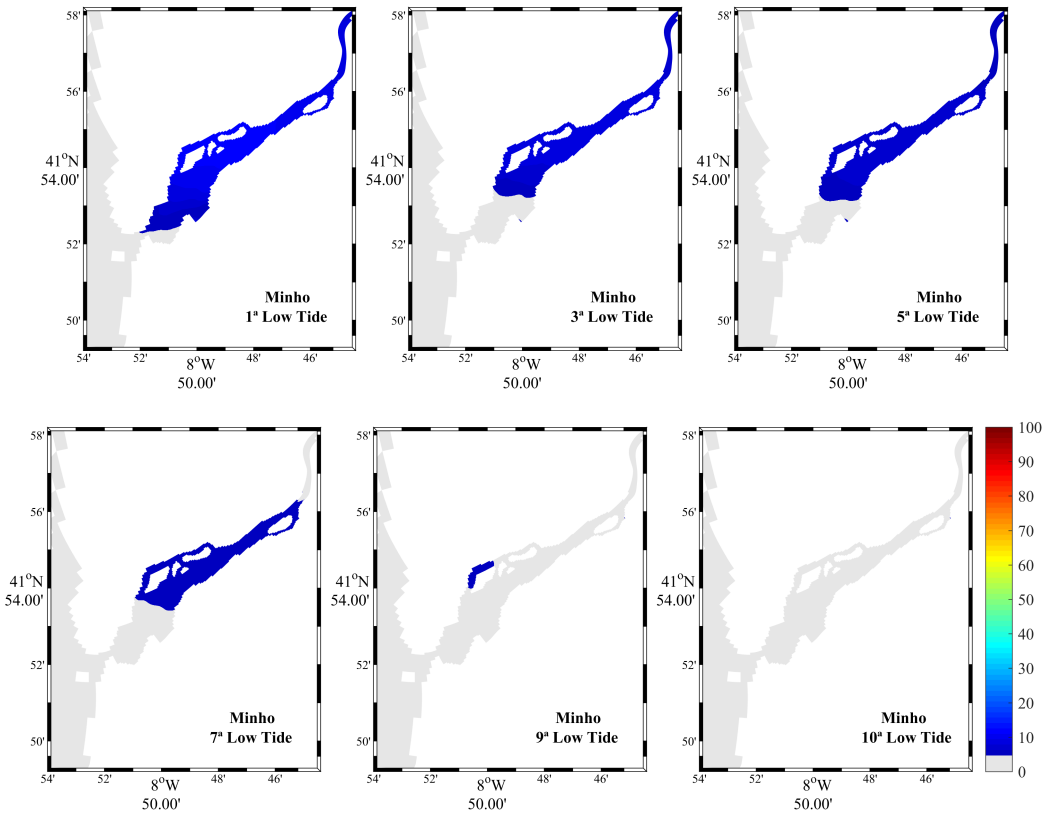

Figure 48: Percentage differences of nitrates between the point discharge of pollutants scenario and the baseline scenario, on August 19.

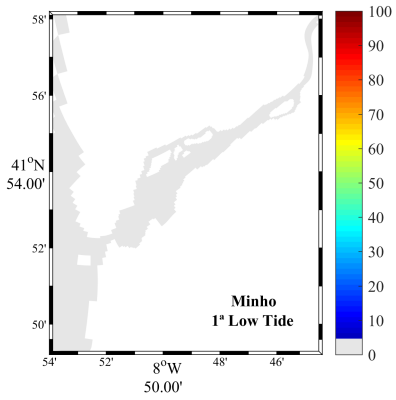

Figure 49: Percentage differences of orthophosphates between the point discharge of pollutants scenario and the baseline scenario, on August 19.

8 Conclusions

The main objectives of this dissertation were to study the intrusion and dynamics of the estuarine plumes of the Minho and Lima estuary, the impact of extreme river discharge events on the nutrient dynamics, as well as the response time of the Minho estuary to a point discharge of pollutants by the Coura river.

To reach these objectives, a numerical model was developed and explored, in which the two estuaries under study were coupled in a single numerical grid. This methodology allows the study of the interaction between them, since the estuaries are relatively close, allowing the exchange of properties (e.g.: nutrients). This procedure of coupling both estuaries had already been done previously by Pereira [2016], but only to study the hydrographic variables (salinity and water temperature).

The calibration of the model was successfully performed for the water temperature, salinity, nitrates, orthophosphates and dissolved oxygen, through the comparison between model predictions and field data. This turns possible to respond to the main objectives of this work.

When studying the intrusion and dynamics of the estuarine plumes of the Minho and Lima estuary, it was concluded that both estuaries interact with each other. Through the analysis of wind direction and intensity, as well as of the fluvial discharges, it can be concluded that the movements of the plumes largely depend on these two factors. In general, in the winter season, as there are large fluvial discharges and the wind is predominant from south, both plumes tend to move northwards, so there will be a higher intrusion of the Lima estuarine plume in the Minho estuary. In the summer season, as the wind is predominant from north, the plumes have a predominant southward direction, with a higher intrusion of the Minho estuarine plume in the Lima estuary.

By observing the plumes movement (through the defined transepts) it was concluded that when the plumes go north, they tend to move very close to the coast, while when moving to the south they are advected offshore.

Regarding the intrusion of the Minho estuarine plume in the Lima estuary and vice versa, it was observed the entrance of the plumes in the south margin of both estuaries, while the exit occurs through the north margin.

Regarding the second objective of this work (to study the impact of extreme river discharge events on nutrient dynamics), it was concluded that with the increase of river discharges the impact on the existing biota inside the estuaries will be impacted (in both seasons), since there will be higher concentrations of dissolved oxygen in winter ($+0.5$ mg O_2/L in the Minho estuary and $+0.7$ mg O_2/L in the Lima estuary), and in summer the decrease of oxygen is low (-0.3 mg O_2/L in the Minho estuary and -0.1 mg O_2/L in the Lima estuary). For nitrate and orthophosphates, an increase in concentrations is observed in both seasons, since river discharges are higher. In conditions of extreme river discharges, the biological communities, mainly beings without locomotion capacity (e.g.: phytoplankton), are more concentrated near the mouth and in the coastal areas. This conclusion can be withdrawn as a slight increase in the concentrations of dissolved oxygen was observed next to these areas.

Regarding the ecological flow scenario, it was concluded that with the reduction of river discharges by upstream dams, there will be a huge impact on the estuarine biota existing in both estuaries. The Lima estuary will be the most affected, since there will be reduced nutrients supplied to the estuary and it will become more anoxic (maximum decrease observed in the winter season of -2 mg O_2/L), which may lead to the death or to migration of some biological species.

Regarding the study of the response time of the Minho estuary to a point discharge of pollutants (nitrates and orthophosphates) by the Coura river, it can be concluded that the

estuary has a relatively long response time when the discharges are carried out in neap tide, but if these are done in spring tide, the response time is considerable lower, since the currents inside the estuary are more intense.

Although two periods were considered, the most critical scenario was observed in neap tide, taking the estuary approximately 21 days to return to the normal state in the case of nitrates and approximately 4 days in the case of orthophosphates, which can cause serious problems to biological communities (e.g.: reduction of some species due to excess of nutrients over a long period of time).

Finally, for future work, it would be important to deeply understand the main biogeochemical processes occurring in both estuaries. For this it would be interesting to add to this biochemical model new substances, such as dissolved silica, alkalinity, sediment oxygen demand, BOD5, inorganic matter, among others, since these processes have great importance in the estuaries. However, it would be necessary to carry out some field campaigns in each estuary, since many parameters necessary (e.g.: denitrification rate in sediments) are unknown.

In addition to adding new processes, it would be interesting to improve the ammonium calibration, since in the present work it was not possible to do it accurately. Finally, it would also be interesting to develop a three-dimensional model, aiming to study the dynamics and the intrusion of the estuarine plumes, as well as the impacts of river discharges on the deeper layers.

9 Appendix

Table 13: Sampling data and sampling period for Transepts 1, 2, 3 and 4 for Lima estuary.

Lima		Transept 1	Transept 2	Transept 3	Transept 4
	Sampling date	Sampling period	Sampling period	Sampling period	Sampling period
Feb	23/02/2012	12 h 40 min - 13 h 40 min	13 h 10 min - 14 h 10 min	13 h 30 min - 14 h 30 min	13 h 50 min - 14 h 50 min
Mar	21/03/2012	10 h 40 min - 11 h 40 min	11 h 10 min - 12 h 10 min	11 h 40 min - 12 h 40 min	12 h 10 min - 13 h 10 min
Apr	23/04/2012	14 h 40 min - 15 h 40 min	15 h 10 min - 16 h 10 min	15 h 30 min - 16 h 30 min	16 h 0 min - 17 h 0 min
May	15/05/2012	8 h 40 min - 9 h 40 min	9 h 10 min - 10 h 10 min	9 h 30 min - 10 h 30 min	9 h 50 min - 10 h 50 min
Jun	12/06/2012	6 h 40 min - 7 h 40 min	7 h 0 min - 8 h 0 min	7 h 30 min - 8 h 30 min	7 h 50 min - 8 h 50 min
Jul	24/07/2012	15 h 10 min - 16 h 10 min	15 h 40 min - 16 h 40 min	16 h 0 min - 17 h 0 min	16 h 20 min - 17 h 20 min
Aug	28/08/2012	7 h 10 min - 8 h 10 min	7 h 20 min - 8 h 20 min	7 h 50 min - 8 h 50 min	8 h 20 min - 9 h 20 min
Set	25/09/2012	6 h 40 min - 7 h 40 min	6 h 40 min - 7 h 40 min	7 h 30 min - 8 h 30 min	8 h 0 min - 9 h 0 min
Oct	30/10/2012	10 h 40 min - 11 h 40 min	10 h 40 min - 11 h 40 min	10 h 40 min - 11 h 40 min	12 h 10 min - 13 h 10 min
Nov	28/11/2012	11 h 40 min - 12 h 40 min	11 h 40 min - 12 h 40 min	12 h 30 min - 13 h 30 min	13 h 10 min - 14 h 10 min
Dez	18/12/2012	14 h 40 min - 15 h 40 min	14 h 40 min - 15 h 40 min	15 h 20 min - 16 h 20 min	15 h 40 min - 16 h 10 min
Jan	21/01/2013	7 h 40 min - 8 h 40 min	7 h 40 min - 8 h 40 min	8 h 20 min - 9 h 20 min	8 h 50 min - 9 h 50 min
Feb	21/02/2013	8 h 40 min - 9 h 40 min	8 h 40 min - 9 h 40 min	9 h 20 min - 10 h 20 min	9 h 40 min - 10 h 40 min

Table 14: Sampling data and sampling period for Transepts 5, 6 and 7 for Lima estuary.

Lima		Transept 5	Transept 6	Transept 7
	Sampling date	Sampling period	Sampling period	Sampling period
Feb	23/02/2012	14 h 10 min - 15 h 10 min	14 h 50 min - 15 h 50 min	15 h 20 min - 16 h 20 min
Mar	21/03/2012	12 h 40 min - 13 h 40 min	13 h 0 min - 14 h 0 min	13 h 30 min - 14 h 30 min
Apr	23/04/2012	16 h 10 min - 17 h 10 min	16 h 30 min - 17 h 30 min	16 h 50 min - 17 h 50 min
May	15/05/2012	10 h 10 min - 11 h 10 min	10 h 30 min - 11 h 30 min	10 h 50 min - 11 h 50 min
Jun	12/06/2012	8 h 20 min - 9 h 20 min	8 h 50 min - 9 h 50 min	9 h 20 min - 10 h 20 min
Jul	24/07/2012	16 h 50 min - 17 h 50 min	17 h 0 min - 18 h 0 min	17 h 20 min - 18 h 20 min
Aug	28/08/2012	8 h 50 min - 9 h 50 min	9 h 10 min - 10 h 10 min	9 h 20 min - 10 h 20 min
Set	25/09/2012	8 h 20 min - 9 h 20 min	9 h 0 min - 10 h 0 min	9 h 30 min - 10 h 30 min
Oct	30/10/2012	12 h 30 min - 13 h 30 min	13 h 0 min - 14 h 0 min	13 h 30 min - 14 h 30 min
Nov	28/11/2012	13 h 20 min - 14 h 20 min	13 h 40 min - 14 h 40 min	14 h 0 min - 15 h 0 min
Dez	18/12/2012	16 h 0 min - 17 h 0 min	16 h 20 min - 17 h 20 min	17 h 20 min - 18 h 20 min
Jan	21/01/2013	9 h 10 min - 10 h 10 min	9 h 50 min - 10 h 50 min	10 h 20 min - 11 h 20 min
Feb	21/02/2013	10 h 10 min - 11 h 10 min	11 h 0 min - 12 h 0 min	11 h 20 min - 12 h 20 min

Table 15: Sampling data and sampling period for Transepts 1, 2, 3 and 4 for Minho estuary.

Minho	Transept 1	Transept 2	Transept 3	Transept 4
Sampling date	Sampling period	Sampling period	Sampling period	Sampling period
Feb 16/02/2012	7 h 10 min - 8 h 10 min	7 h 30 min - 8 h 30 min	7 h 50 min - 8 h 50 min	8 h 20 min - 9 h 20 min
Mar 22/03/2012	11 h 10 min - 12 h 10 min	11 h 40 min - 12 h 40 min	12 h 30 min - 13 h 30 min	12 h 50 min - 13 h 50 min
Apr 12/04/2012	15 h 10 min - 16 h 10 min	15 h 30 min - 16 h 30 min	15 h 50 min - 16 h 50 min	16 h 10 min - 17 h 10 min
May 17/05/2012	9 h 40 min - 10 h 40 min	11 h 0 min - 12 h 0 min	10 h 30 min - 11 h 30 min	10 h 50 min - 11 h 50 min
Jun 13/06/2012	7 h 40 min - 8h 40 min	8 h 0 min - 9 h 0 min	8 h 20 min - 9 h 20 min	8 h 50 min - 9 h 50 min
Jul 29/07/2012	8 h 40 min - 9 h 40 min	9 h 0 min - 10 h 0 min	9 h 20 min - 10 h 20 min	9 h 50 min - 10 h 50 min
Aug 29/08/2012	8 h 10 min - 9 h 10 min	8 h 30 min - 9 h 30 min	9 h 0 min - 10 h 0 min	9 h 20 min - 10 h 20 min
Set 26/09/2012	7 h 40 min - 8 h 40 min	8 h 10 min - 9 h 10 min	8 h 40 min - 9 h 40 min	9 h 10 min - 10 h 10 min
Oct 29/10/2012	9 h 40 min - 10 h 40 min	10 h 10 min - 11 h 10 min	10 h 40 min - 11h 40 min	11 h 0 min - 12 h 0 min
Nov 26/11/2012	9 h 30 min - 10 h 30 min	10 h 10 min - 11 h 10 min	10 h 30 min - 11 h 30 min	11 h 10 min - 12 h 10 min
Dez 19/12/2012	14 h 40 min - 15 h 40 min	15 h 10 min - 16 h 10 min	15 h 30 min - 16 h 30 min	16 h 10 min - 17 h 10 min
Jan 22/01/2013	8 h 40 min - 9 h 40 min	9 h 0 min - 10 h 0 min	9 h 20 min - 10 h 20 min	9 h 50 min - 10 h 50 min
Feb 22/02/2013	9 h 10 min - 10 h 10 min	9 h 40 min - 10 h 40 min	10 h 0 min - 11 h 0 min	10 h 30 min - 11 h 30 min

Table 16: Sampling data and sampling period for Transepts 5, 6 and 7 for Minho estuary.

Minho		Transept 5	Transept 6	Transept 7
	Sampling date	Sampling period	Sampling period	Sampling period
Feb	16/02/2012	8 h 40 min - 9 h 40 min	9 h 10 min - 10 h 10 min	9 h 50 min - 10 h 50 min
Mar	22/03/2012	13 h 20 min - 14 h 20 min	13 h 50 min - 14 h 50 min	14 h 30 min - 15 h 30 min
Apr	12/04/2012	15 h 30 min - 16 h 30 min	17 h 0 min - 18 h 0 min	17 h 50 min - 18 h 50 min
May	17/05/2012	11 h 10 min - 12 h 10 min	11 h 40 min - 12 h 40 min	12 h 50 min - 13 h 50 min
Jun	13/06/2012	9 h 20 min - 10 h 20 min	9 h 40 min - 10 h 40 min	10 h 0 min - 11 h 0 min
Jul	29/07/2012	10 h 20 min - 11 h 20 min	11 h 0 min - 12 h 0 min	11 h 20 min - 12 h 20 min
Aug	29/08/2012	10 h 0 min - 11 h 0 min	10 h 20 min - 11 h 20 min	10 h 50 min - 11 h 50 min
Set	26/09/2012	9 h 50 min - 10 h 50 min	10 h 30 min - 11 h 30 min	11 h 20 min - 12 h 20 min
Oct	29/10/2012	11 h 30 min - 12 h 30 min	11 h 50 min - 12 h 50 min	12 h 50 min - 13 h 50 min
Nov	26/11/2012	11 h 40 min - 12 h 40 min	12 h 10 min - 13 h 10 min	12 h 50 min - 13 h 50 min
Dez	19/12/2012	16 h 50 min - 17 h 50 min	17 h 10 min - 18 h 10 min	17 h 30 min - 18 h 30 min
Jan	22/01/2013	10 h 10 min - 11 h 10 min	10 h 40 min - 11 h 40 min	11 h 20 min - 12 h 20 min
Feb	22/02/2013	11 h 0 min - 12 h 0 min	11 h 30 min - 12 h 30 min	12 h 20 min - 13 h 20 min

References

Almeida, C. M., Mucha, A., and Vasconcelos, M. T. S. D. (2011). Role of different salt marsh plants on metal retention in an urban estuary (Lima estuary, NW Portugal). Estuarine Coastal and Shelf Science, 91:243-249.

Álvarez-Salgado, X. A., Figueiras, F. G., Pérez, F. F., Groom, S., Nogueira, E., Borges, A. V., Chou, L., Castro, C. G., Moncoiffé, G., Ríos, A. F., Miller, A. E. J., Frankignoulle, M., Savidge, G., and Wollast, R. (2003). The Portugal coastal counter current off NW Spain: new insights on its biogeochemical variability. Progress in Oceanography, 56(2):281-321.

Alvarez-Salgado, X. A., Rosón, G., Pérez, F. F., and Pazos, Y. (1993). Hydrographic variability off the Rías Baixas (NW Spain) during the upwelling season. Journal of Geophysical Research: Oceans, 98(C8):14447-14455.

APA (2015). Parte 2 - Caracterização e diagnóstico (anexos) - Plano de gestão da região hidrográfica do Minho e Lima (RH1). Technical report, Agência Portuguesa do Ambiente, 92 pp.

Araújo, M. A. V. C., Mazzolari, A., and Trigo-Teixeira, A. (2011). Wave set-up in the modeling of storm surge at Viana do Castelo (Portugal). Journal of Coastal Research, 971-975.

Ashizawa, D. and Cole, J. J. (1994). Long-term temperature trends of the Hudson river: A study of the historical data. Estuaries, 17(1):166-171.

Atwater, M. A. and Ball, J. T. (1978). Computation of IR sky temperature and comparison with surface temperature. Solar Energy, 21(3):211-216.

Barbosa, A., Lousada, S., and Haie, N. (2004). Análise da qualidade das águas superficiais de Ponte de Lima. Technical report, Universidade do Minho, 14 pp.

Berdeal, I. G., Hickey, B. M., and Kawase, M. (2002). Influence of wind stress and ambient flow on a high discharge river plume. Journal of Geophysical Research: Oceans, 107(C9):13-24.

Bettencourt, A., B. Bricker, S., G. Ferreira, J., Franco, A., Marques, J., de Melo, J., Nobre, A., Ramos, L., S. Reis, C., Salas, F., Silva, M., Simas, T., and Wolff, W. (2003). Typology and reference conditions for portuguese transitional and coastal waters, development of guidelines for the application of the European Union water framework directive. TICOR, 120 pp.

BOE (2009). Anexo III. Plan hidrológico de la parte española de la DH del MIÑO-Sil (2015-2021). Technical report, Boletín oficial del Estado, 28 pp.

Caetano, M., Raimundo, J., Nogueira, M., Santos, M., Mil-Homens, M., Prego, R., and Vale, C. (2016). Defining benchmark values for nutrients under the water framework directive: Application in twelve portuguese estuaries. Marine Chemistry, 185:27-37.

Cameron, W. M. and Pritchard, D. W. (1963). The sea. In Estuaries, chapter 2, 306-324 pp. New York.

Carbonel, C. A. A. and Valentin, J. L. (1999). Numerical modelling of phytoplankton bloom in the upwelling ecosystem of Cabo Frio (Brazil). Ecological Modelling, 116(2):135-148.

Cardoso, R., Araújo, M., Freitas, M., and Fatela, F. (2008). Geochemical characterisation of sediments from marginal environments of Lima estuary (NW Portugal). Geosciences On-line Journal, 5:1-11.

Cardoso, R., Araújo, M. F., Freitas, M. C., and Fatela, F. (2006). Geochemical characterisation of sediments from salt marsh environments of the Lima estuary. In VI Congresso Ibérico de Geoquímica, 305-308.

CMEMS (2018). Copernicus Marine Environment Monitoring Service (www.marine.copernicus.eu).

Day, J. H., Chadwick, H., Day, J. W., Hall, C. A. S., Kemp, W. M., and Yáñez-Arancibia, A. (1989). Estuarine ecology. John Wiley & Sons, New York, Chichester, Brisbane, Toronto, Singapore, 558 pp.

De la Rosa, J. M., Araújo, M. F., González-Pérez, J. A., González-Vila, F. J., Soares, A. M., Martins, J. M., Leorri, E., Corbett, R., and Fatela, F. (2012). Organic matter sources for tidal marsh sediment over the past two millennia in the Minho river estuary (NW Iberian Peninsula). Organic Geochemistry, 53:16-24.

DeCastro, M., Gómez-Gesteira, M., Prego, R., Taboada, J. J., Montero, P., Herbello, P., and Pérez-Villar, V. (2000). Wind and tidal influence on water circulation in a Galician Ria (NW Spain). Estuarine, Coastal and Shelf Science, 51(2):161-176.

Delgado, A. (2011). Hydrodynamic and morphodynamic preliminary simulation of river Minho estuary. 6ª Jornadas de Hidráulica, Recursos Hídricos e Ambiente, 113-126.

Deltares (2016a). Generation and manipulation of curvilinear grids for Delft3D-Flow and Delft3D-Wave) [User Manual]. Boussinesqweg 1, Netherlands, 140 pp.

Deltares (2016b). Simulation of multi-dimensional hydrodynamic flows and transport phenomena, including sediments [User Manual]. Boussinesqweg 1, Netherlands, 702 pp.

Deltares (2016c). Water quality and aquatic ecology [User Manual]. Boussinesqweg 1, Netherlands, 394 pp. Deltares, Boussinesqweg 1, Netherlands.

Dias, E. C. (2015). A circulação oceânica costeira de Portugal. MSc. Thesis, Escola Naval, 49 pp.

Dias, J. M., Lopes, J. F., and Dekeyser, I. (1999). Hydrological characterisation of Ria de Aveiro, Portugal, in early summer. Oceanologica Acta, 22(5):473-485.

Dias, J. M., Lopes, J. F., and Dekeyser, I. (2001). Lagrangian transport of particles in Ria de Aveiro lagoon, Portugal. Physics and Chemistry of the Earth, Part B: Hydrology, Oceans and Atmosphere, 26(9):721-727.

Dias, J. M., Sousa, M. C., Bertin, X., Fortunato, A. B., and Oliveira, A. (2009). Numerical modeling of the impact of the Ancão inlet relocation (Ria Formosa, Portugal). Environmental Modelling & Software, 24(6):711-725.

Doney, S. C., Ruckelshaus, M., Duffy, J. E., Barry, J. P., Chan, F., English, C. A., and Talley, L. D. (2002). Climate change impacts on marine ecosystems. In Estuaries, volume 25, 149-164.

ECMWF (2018). European Centre for Medium-Range Weather Forecasts (www.ecmwf.int).

Edwards, C. A., Batchelder, H. P., and Powell, T. M. (2000). Modeling microzooplankton and macrozooplankton dynamics within a coastal upwelling system. Journal of Plankton Research, 22(9):1619-1648.

Elumalai, M., Antunes, C., and Guilhermino, L. (2007). Enzymatic biomarkers in the crab Carcinus maenas from the Minho river estuary (NW Portugal) exposed to zinc and mercury. Chemosphere, 66(7):1249-1255.

EPA (2007). Total maximum daily load (TMDL) for the Noxubee river watershed (Draft). Technical report, Environmental Protection Agency, 38 pp.

Fairbridge, R. W. (1980). The estuary: Its definition and geodynamic cycle. In Chemistry and biogeochemistry of estuaries, 1-35, Chichester.

Fidalgo, M. L. (2000). Qualidade da água na bacia hidrografica do rio Minho: Troço internacional e principais afluentes em território português. Technical report, Faculdade de Ciências da Universidade do Porto, 10 pp.

Fiedler, P. C. and Laurs, R. M. (1990). Variability of the Columbia river plume observed in visible and infrared satellite imagery. International Journal of Remote Sensing, 11(6):999-1010.

Filgueiras, A. V., Lavilla, I., and Bendicho, C. (2004). Evaluation of distribution, mobility and binding behaviour of heavy metals in surficial sediments of Louro river (Galicia, Spain) using chemometric analysis: a case study. Science of The Total Environment, 330(1-3):115-129.

Fitzpatrick, J. J. and Imhoff, J. (2001). Water quality models: A survey and assessment. Project 99 - WSM - 5 by Water Environment Research Foundation, 102 pp.

Fong, D. A. and Geyer, W. R. (2002). The alongshore transport of freshwater in a surface-trapped river plume. Journal of Physical Oceanography, 32(3):957-972.

Freitas, V., Costa-Dias, S., Campos, J., Bio, A., Santos, P., and Antunes, C. (2009). Patterns in abundance and distribution of juvenile flounder, Platichthys flesus, in Minho estuary (NW Iberian Peninsula). Aquatic Ecology, 43(4):1143.

Garvine, R. W. (1974). Physical features of the Connecticut river outflow during high discharge. Journal of Geophysical Research, 79(6):831-846.

Garvine, R. W. (1984). Radial spreading of buoyant, surface plumes in coastal waters. Journal of Geophysical Research: Oceans, 89:1989-1996.

Hayes, M. (1975). Morphology of sand accumulation in estuaries: An introduction to the symposium. Geology and Engineering, 2:3-22. Academic Press.

Hidroprojecto (1992). Plano Geral dos Vales dos Rios Lima, Anha e Âncora: Memória descritiva. Technical report, Ministério do Ambiente e Recursos Naturais.

Kacikoc, M. and Beyhan, M. (2014). Hydrodynamic and water quality modeling of Lake Egirdir. CLEAN - Soil, Air, Water, 42(11):1573-1582.

Kemp, W. M., Brooks, M. T., and Hood, R. R. (2001). Nutrient enrichment, habitat variability and trophic transfer efficiency in simple models of pelagic ecosystems. Marine Ecology Progress Series, 223:73-87.

Kourafalou, V. H. (1999). Process studies on the Po river plume, North Adriatic Sea. Journal of Geophysical Research: Oceans, 104:29963-29985.

Lopes, L. F. G., Do Carmo, J. S. A., Cortes, R. M. V., and Oliveira, D. (2004). Hydrodynamics and water quality modelling in a regulated river segment: Application on the instream flow definition. Ecological Modelling, 173(2-3):197-218.

Macmillan, D. S., Beckley, B. D., and Fang, P. (2004). Monitoring the TOPEX and Jason-1 microwave tadiometers with GPS and VLBI Wet Zenith path delays. Marine Geodesy, 27(3-4):703-716.

Mateus, M., Vaz, N., and Neves, R. (2012). A process-oriented model of pelagic biogeochemistry for marine systems. Part II: Application to a mesotidal estuary. Journal of Marine Systems, 94:90-101.

Mattern, J. P., Song, H., Edwards, C. A., Moore, A. M., and Fiechter, J. (2017). Data assimilation of physical and chlorophyll a observations in the California current system using two biogeochemical models. Ocean Modelling, 109:55-71.

Mazé, J. P., Arhan, M., and Mercier, H. (1997). Volume budget of the eastern boundary layer off the Iberian Peninsula. Deep-Sea Research I, 44(9):1543-1574.

Mendes, R., DeCastro, M., Sousa, M. C., Gómez-Gesteira, M., and Dias, J. M. (2016). New insights into the Western Iberian Buoyant Plume: Interaction between the Douro and Minho river plumes under winter conditions. Progress in Oceanography, 141:30-43.

Mendes, R., Saldías, G. S., DeCastro, M., Gómez-Gesteira, M., Vaz, N., and Dias, J. M. (2017). Seasonal and interannual variability of the Douro turbid river plume, northwestern Iberian Peninsula. *Remote Sensing of Environment*, 194:401–411.

Miranda, L., Castro, B., and Kjerfve, B. (2002). Principios de oceanografia física de estuários. Technical report, Universidade de São Paulo, 427 pp.

Neves, R. (2007). Numerical models as decision support tools in coastal areas. In Assessment of the Fate and Effects of Toxic Agents on Water Resources, 171-195, Dordrecht. Springer Netherlands.

O'Connor, D. J. (1961). Oxygen balance of an estuary. Transactions of the American Society of Civil Engineers, 126(3):556-575.

O'Connor, D. J. (1967). The temporal and spatial distribution of dissolved oxygen in streams. Water Resources Research, 3(1):65-79.

Otero, P., Ruiz-Villarreal, M., García-García, L., González-Nuevo, G., and Cabanas, J. M. (2013). Coastal dynamics off Northwest Iberia during a stormy winter period. Ocean Dynamics, 63(1):115-129.

Otero, P., Ruiz-Villarreal, M., and Peliz, A. (2008). Variability of river plumes off Northwest Iberia in response to wind events. Journal of Marine Systems, 72(1):238-255.

Pan, G., Chai, F., Tang, D., and Wang, D. (2017). Marine phytoplankton biomass responses to typhoon events in the South China Sea based on physical-biogeochemical model. Ecological Modelling, 356:38-47.

Pawlowicz, R., Beardsley, B., and Lentz, S. (2002). Classical tidal harmonic analysis including error estimates in MATLAB using T_TIDE. Computers & Geosciences, 28(8):929-937.

PBH (2001). Plano de Bacia Hidrográfica do Rio Minho - Relatório final. . Technical report, Ministério do Ambiente e do Ordenamento do Território, Instituto da Água, Instituto Português, 1704 pp.

Peliz, A., Dubert, J., Santos, A. M. P., Oliveira, P. B., and Cann, B. (2005). Winter upper ocean circulation in the Western Iberian Basin fronts, eddies and poleward flows: An overview. Deep Sea Research Part I: Oceanographic Research Papers. Oceanographic Research Papers, 52(4):621-646.

Peliz, A., Rosa, T. L., Santos, A. M. P., and Pissarra, J. L. (2002). Fronts, jets, and counter-flows in the Western Iberian upwelling system. Journal of Marine Systems, 35(1):61-77.

Pereira, H. (2016). Coupled Modelling of the Minho and Lima Estuaries: Hydrological Response to Climate Changes. MSc. Thesis, Aveiro University, 106 pp.

PGRH1 (2012). Plano de Gestão da Região Hidrográfica do Minho e Lima - RH1 - Relatório técnico - Comissão Europeia. Technical report, Agência Portuguesa do Ambiente, 178 pp.

Picado, A., Dias, J. M., and Fortunato, A. B. (2010). Tidal changes in estuarine systems induced by local geomorphologic modifications. Continental Shelf Research, 30(17):1854-1864.

Pinho, J. L. S. and Vieira, J. M. P. (2007). Mathematical modelling of salt water intrusion in a Northern Portuguese estuary. Iahs Publication, 14 pp.

Pollard, R. T. and Pu, S. (1985). Structure and circulation of the Upper Atlantic Ocean northeast of the Azores. Progress in Oceanography, 14:443-462.

Preston, B. (2004). Observed winter warming of the Chesapeake Bay estuary (1949-2002): Implications for ecosystem management. Environmental management, 34:125-139.

Pritchard, D. W. (1967). What is an estuary: physical viewpoint. In Estuaries, Publication No. 83, 3-5. American Association for the Advancement of Science, Washington D.C.

Radach, G. and Moll, A. (2006). Review of three-dimensional ecological modeling related to the North Sea shelf system. Part II: Model validation and data needs. Oceanography and Marine Biology, 44:1-60.

Rebordão, I. and Trigo-Teixeira, A. (2009). Tidal Propagation in the Lima estuary. Journal of Coastal Research, SI 56:1400-1404.

Reis, J. L., Martinho, A. S., Pires-Silva, A., and Silva, A. J. (2009). Assessing the influence of the river discharge on the Minho estuary tidal regime. Coastal Education & Research Foundation, 1405-1409.

Ribeiro, A. (2015). Coupled modelling of the Tagus and Sado estuaries and their associated mesoscale patterns. MSc. Thesis, Aveiro University, 124 pp.

RTP (2017). Retrato Territorial de Portugal. Technical report, Instituto Nacional de Estatística, 219 pp.

Ruiz-Villarreal, M., Montero, P., Taboada, J. J., Prego, R., Leitão, P. C., and Pérez-Villar, V. (2002). Hydrodynamic model study of the Ria de Pontevedra under estuarine conditions. Coastal and Shelf Science, 54(1):101-113.

Santos, A. I., Balsinha, M. J., Oliveira, A. T., and Silva, A. J. (2006). Tide induced variability in the hydrography and dynamics of the Minho and Douro estuaries during low runoff. 5th Symposium on the Iberian Atlantic Margin, 195-197.

Santos, S., Vilar, V. J. P., Alves, P., Boaventura, R. A. R., and Botelho, C. (2013). Water quality in Minho/Miño River (Portugal/Spain). Environmental Monitoring and Assessment, 185(4):3269-3281.

SNIRH (2018). Sistema Nacional de Informação de Recursos Hídricos (www.snirh.pt).

Sousa, M., Vaz, N., Alvarez, I., Gomez-Gesteira, M., and Dias, J. M. (2014a). Influence of the Minho river plume on the Rias Baixas (NW of the Iberian Peninsula). Journal of Marine Systems, 139:248-260.

Sousa, M. C. (2013). Modelling the Minho river plume intrusion into the Rias Baixas. PhD. Thesis, Aveiro University and Porto University, 166 pp.

Sousa, M. C., Mendes, R., Alvarez, I., Vaz, N., Gomez-Gesteira, M., and Dias, J. M. (2014b). Unusual circulation patterns of the Rias Baixas induced by Minho freshwater intrusion (NW of the Iberian Peninsula). PLOS ONE, 9(11):1-9.

Sousa, R., Guilhermino, L., and Antunes, C. (2005). Molluscan fauna in the freshwater tidal area of the river Minho estuary, NW of Iberian Peninsula. Annales de Limnologie - International Journal of Limnology, 41(2):141-147.

Streeter, H. W. and Phelps, E. B. (1925). Factors concerned in the phenomena of oxidation and reaeration. A Study of Pollution and Natural Purification of the Ohio River, 146:1-69.

Thomann, R. V. (1963). Mathematical model for dissolved oxygen. Journal of the Sanitary Engineering Division, 89(5):1-32.

Vale, L. M. (2008). Estudo Hidrodinâmico do porto de Viana do Castelo. MSc. Thesis, Aveiro University, 164 pp.

Vale, L. M. and Dias, J. M. (2011). The effect of tidal regime and river flow on the hydrodynamics and salinity structure of the Lima estuary: Use of a numerical model to assist on estuary classification. Journal of Coastal Research, SI 64:1604-1608.

Varela, R. A., Rosón, G., Herrera, J. L., Torres-López, S., and Fernández-Romero, A. (2005). A general view of the hydrographic and dynamical patterns of the Rías Baixas adjacent sea area. Journal of Marine Systems, 54(1):97-113.

Vieira, J. M. and Pinho, J. L. (2010). Salt distribution in river Lima estuary for different hydrodynamic regimes. Recursos Hídricos, (31):5-14.

Vieira, L. R., Guilhermino, L., and Morgado, F. (2015). Zooplankton structure and dynamics in two estuaries from the Atlantic coast in relation to multi-stressors exposure. Estuarine, Coastal and Shelf Science, 167:347-367.

Villar, J. C. E., Guyot, J. L., Ronchail, J., Cochonneau, G., Filizola, N., Fraizy, P., Labat, D., de Oliveira, E., Ordoñez, J. J., and Vauchel, P. (2009). Contrasting regional discharge evolutions in the Amazon basin (1974 - 2004). Journal of Hydrology, 375(3):297-311.

Walker, R. G. and James, N. P. (1992). Facies models: Response to sea level change. Geological Association of Canada, 454 pp.

Wang, Y., Zhao, M., Dai, C., and Pan, X. (2014). Nonlinear dynamics of a nutrient-plankton model. Abstract and Applied Analysis, 1-10.

Willmott, C. J. (1981). On the validation of models. Physical Geography, 2(2):184-194.

Wolanski, E. (2007). Estuarine ecohydrology. Elsevier, Amsterdam, 1 edition, 168 pp.

Zacarias, N. (2007). Influência da batimetria e do caudal fluvial na propagação da maré no estuário do rio Minho. Technical report, Universidade de Évora, 81 pp.